THE VOLUMETRIC PROPERTIES OF THE HELIUM-KRYPTON SYSTEM AT MODERATE TEMPERATURES AND PRESSURES

By

DONALD DWAYNE DILLARD

Bachelor of Science in Chemical Engineering
University of Arkansas
Fayetteville, Arkansas
1964

Master of Science
Oklahoma State University
Stillwater, Oklahoma
1966

Submitted to the Faculty of the Graduate College
of the Oklahoma State University
in partial fulfillment of the requirements
for the Degree of
DOCTOR OF PHILOSOPHY
July, 1975

THE VOLUMETRIC PROPERTIES OF THE HELIUM-KRYPTON SYSTEM AT MODERATE TEMPERATURES AND PRESSURES

Thesis Approved:

Robert L. Robinson, Jr.
Thesis Adviser

R. N. Maddox

John H. Erbar

Lionel M. Raff

A. N. Hunter
Dean of the Graduate College

PREFACE

A modern version of the Burnett apparatus was constructed and subsequently employed to experimental determine the pressure-volume-temperature behavior of the helium-krypton system. Measurements were made on the -50, 0 and +50°C isotherms over a pressure range of 7 to 150 atm. The results of this work were compared to previous works and then combined with selected previous values to form an appropriate basis for a study of molecular interactions utilizing the Kihara intermolecular potential function.

I am indebted to many individuals as well as organization for making this study possible. A particular debt of gratitude is owed to my thesis adviser, Dr. R. L. Robinson, Jr., for his patient direction, support and continued interest in this work. A special note of thanks is due Dr. B. L. Crynes for his helpful suggestions on the original draft of this thesis.

Dr. F. B. Canfield supplied valuable information during the design phase of the experimental work. During the data reduction work, K. E. Hall and J. A. Provine, Jr., provided valuable assistance. A note of thanks is extended to H.-M. Lin for his assistance in the calculational aspects of the molecular interaction study.

Financial support and equipment funds for this work were gratefully received from NASA (Grant NGL 37-002-011), an NDEA Fellowship and the School of Chemical Engineering. The United States Bureau of Mines generously donated the high purity helium used in this work.

The experimental and theoretical phases of this work were completed in March 1970. The review of previous work relevent to the present study does not extend beyond this date.

TABLE OF CONTENTS

Chapter Page

LIST OF TABLES

LIST OF FIGURES

NOMENCLATURE

A	- area
B	- second virial coefficient
B,C,D,E---	- constants in density expansion of the virial equation of state
B_P, C_P, D_P, E_P,---	- constants in pressure expansion of the virial equation of state
$B_a, C_a D_a E_a$,---	- constants in virial equation of state with volume expressed in Amagat
B_{11}	- component "1" second virial coefficient
B_{22}	- component "2" second virial coefficient
B_{12}	- interaction second virial coefficient
B_m	- second virial coefficient for a mixture
b_0	- second virial coefficient for rigid spheres
C	- potential term constant
E	- excess virial coefficient
E	- modulus of elasticity
e	- 2.71828---
g	- local acceleration of gravity
g_c	- standard acceleration of gravity
I	- ionization potential
K	- bulk modulus

k	- Boltzmann's constant
M	- molecular weight
m	- number of coefficients used in the virial equation of state
m	- exponent in empirical potential function
N_0	- Avagadro's number
N_j	- cell constant for the j^{th} expansion
N_∞	- cell constant at zero pressure
n	- exponent in empirical potential function
n	- number of moles
P	- pressure
R	- universal gas constant
r	- distance between molecules
T	- temperature
$U(r)$	- intermolecular potential energy
V	- volume
W	- weight
Y	- mole fraction
Z	- compressibility factor

Greek Symbols

α	- a constant
β	- a constant
γ	- constant in the Kihara potential
Δ	- change in a quantity
ϵ	- error in a quantity

ε	- intermolecular potential energy parameter
Π	- series multiplication sign
π	- 3.14159---
ρ	- density
Σ	- summation sign
δ	- deflection of DPI diaphragm
σ	- intermolecular potential distance parameter
σ	- standard error

Subscripts

calc	- calculated value
exp	- experimental value
i	- component i
j	- component j
ij	- interaction parameter
m	- mixture property
p	- refers to pressure
v	- refers to volume

Superscripts

*	- reduced quantity

Miscellaneous

∂	- partial differential operator
$\simeq$	- approximately equal
>	- greater than

$<$	- less than
∞	- infinity
$\| \|$	- absolute value sign
$\int$	- integral sign

CHAPTER I

INTRODUCTION

Statistical mechanics (35) offers a transitional vehicle for relating the macroscopic properties of a fluid to the microscopic potential energy of interaction between the constituent particles of the fluid. Since the converse of this is also true, all transport and equilibrium properties of a system can be determined from an adequate quantitative description of the intermolecular interactions between molecules within a system. As a natural consequence, the scientific community has devoted extensive efforts from both experimental and theoretical viewpoints toward the development and testing of intermolecular potential functions.

Studying molecular interactions via equilibrium properties of gaseous phase systems has been a popular approach in recent years. Such studies are typically characterized by a tremendous emphasis on precision during the data acquisition phase of the work. Also, the systems chosen for such studies should (and normally do) consist of spherically symmetric components. This, of course, reduces the uncertainty involved when reconciling lack of fit between experimental and predicted results since most theoretical descriptions contain assumptions which are valid only for such simple systems.

Despite the good efforts expended to date, much remains to be learned about all phases of studies of molecular interactions via

equilibrium properties of gaseous phase systems. Of significant importance is the need for additional pressure-volume-temperature (PVT) data of known accuracy. Such data can form a logical basis for evaluating the quality of existing data from the literature. Subsequently, data from different laboratories could be combined to yield a data base across a broad temperature range. The wide temperature range data base could then be used to adequately test proposed intermolecular potential functions. This approach will be used in the present study.

Another area where additional work is needed is the prediction of unlike molecular interactions from constituent pure component data. Studies in this area are hindered by lack of data on suitable mixtures. The present study adds to the scarce quantity of appropriate data. Also, the data from this work, combined with data from the literature, is used to test the most commonly used mixing rules for predicting interaction pair potentials from pure component data.

Consistent with the above discussion and stated more specifically, this thesis is a report on the construction of a modern version of the Burnett (14) apparatus and the subsequent use of the apparatus to study the volumetric properties of helium, krypton and three helium-krypton mixtures having nominal compositions of 25, 50 and 75 mole percent krypton. Data were taken along the -50, 0 and +50^{o} C isotherms for pressure up to 150 atm. A non-linear regression method as developed by Hall (30) was used to extract compressibility factors and virial coefficients from the Burnett data. The second virial coefficients from this work were then combined with values from the literature to form the basis for a study of molecular interactions, utilizing the Kihara (43) intermolecular potential function.

CHAPTER II

REVIEW OF PREVIOUS WORK

This chapter offers a brief summary of past work relevant to the present study. The areas of interest include application of the Burnett apparatus, methods for reduction of Burnett data and PVT studies on helium, krypton and helium-krypton mixtures.

Burnett Method

In 1936 E. S. Burnett (14) of the U. S. Bureau of Mines Helium Plant and Cryogenic Laboratory in Amarillo, Texas, reported an experimental method for the determination of compressibility factors of gases which required no direct measurement of volume or mass. Since these variables are often the most difficult to measure experimentally, the Burnett method was welcomed by the scientific and engineering community and has been widely employed. Since the Burnett method was used for the experimental determinations in this work, the method is developed in detail in the following sections of this chapter.

Burnett Relationships

The Burnett apparatus consists of two thermostated volumes, V_a and V_b, interconnected by an expansion valve. The first chamber is equipped with a charge line and pressure tap while the second chamber is equipped with an exhaust line leading to a vacuum system. Auxiliary

equipment is supplied to afford a means for precise determination of the temperature and pressure of the contents of the two chambers.

The necessary measurements are made by charging V_a to the desired pressure with the gas under study and then expanding the gas from V_a to a previously evacuated V_b. After thermal equilibrium is established, the expansion valve is closed and V_b is re-evacuated. A succession of expansions are made in this manner until the pressure has been reduced to some predetermined minimum. The pressure and temperature are precisely determined before the first expansion and then after each of the succeeding expansions.

Before the first expansion, the gas in V_a can be described by

$$P_0(V_a)_0 = n_0 Z_0 R T_0 \tag{1}$$

where the subscripts refer to the number of times the gas has been expanded. After the first expansion, n_0 moles of gas are shared between V_a and V_b. Thus, the equation of state for the gas becomes

$$P_1(V_a + V_b)_1 = n_0 Z_1 R T_1 \tag{2}$$

Dividing Equation (1) by Equation (2) and rearranging slightly yields

$$\frac{P_0/T_0}{P_1/T_1} = \frac{(V_a + V_b)_1}{(V_a)_0} \frac{Z_0}{Z_1} \tag{3}$$

Writing Equation (3) for an arbitrary expansion j and defining the ratio of the volume occupied by the gas after expansion j to that occupied before expansion j as N gives

$$\frac{P_{j-1}/T_{j-1}}{P_j/T_j} = N_j \frac{Z_{j-1}}{Z_j} \tag{4}$$

The apparatus volume ratio, N_j, is not in general a constant due to the slight deformation of the Burnett chambers with pressure. However, the apparatus volume ratio at zero pressure is a constant and is denoted by N_{00}. By Burnett convention, this term is called the cell constant. Thus, the apparatus volume ratio can be expressed as the product of N_{00} and a correction term, X_j, calculated via the theory of elasticity (See Appendix C).

$$N_j = N_{00}\, X_j \tag{5}$$

With this convention, Equation (4) applied to the first expansion, after slight rearrangement, is

$$\frac{Z_1}{P_1/T_1} = N_{00} X_1 \frac{Z_0}{P_0/T_0} \tag{6}$$

For the second expansion,

$$\frac{Z_2}{P_2/T_2} = N_{00} X_2 \frac{Z_1}{P_1/T_1}$$

or (7)

$$\frac{Z_2}{(P_2/T_2)} = N_{00}^{\,2} X_1 X_2 \frac{Z_0}{(P_0/T_0)}$$

In general, the compressibility factor after the k^{th} expansion can be expressed as

$$Z_k = (P_k/T_k) N_{00}^{k} \frac{Z_0}{(P_0/T_0)} \prod_{j=0}^{k} X_j \tag{8}$$

Thus the compressibility after any expansion can be expressed in terms of experimentally measured quantities, the initial compressibility, Z_0, the cell constant, N_{∞}, and calculable correction factors, X_j.

Examination of Equation (4) reveals that in the limit of an infinite number of expansions the cell constant is equal to the pressure-temperature ratio. Thus, if this ratio is expressed as a function of a pressure and extrapolated to zero pressure, either graphically or by regression methods, the value of the cell constant can be determined. The success of this determination is enhanced if a fluid having a linear compressibility as a function of pressure (e.g., helium) is used.

A similar limiting process can be used to evaluate the initial compressibility, Z_0. After establishing the value of the cell constant, the quantity $(P_0/T_0)/Z_0$ is solved for by rearranging Equation (8).

$$\frac{P_0/T_0}{Z_0} = \frac{P_k/T_k}{Z_k} N_{\infty}^{k} \prod_{j=0}^{k} X_j \tag{9}$$

As k becomes very large, Z_k approaches unity. Thus, if $(P_k/T_k)N_{\infty}^{k}\prod_{j=1}^{k} X_j$ is expressed as a function pressure, the limit of this quantity as the pressure approaches zero is equal to the left hand side of Equation (9). That is,

$$\lim_{P\to 0} \left[(P_k/T_k)N_{\infty}^{k} \prod_{j=1}^{k} X_j\right] = \frac{P_0/T_0}{Z_0} \tag{10}$$

Combining the result obtained from Equation (10) with the experimental value of P_0/T_0 yields the value for the initial compressibility factor. The value of the compressibility at all other experimental pressures then follows directly from Equation (8).

A more modern approach to the analysis of Burnett data utilizes non-linear regression. This method requires the selection of a model that will precisely represent the volumetric behavior of the fluid being studied. In general, the model selected is of the form

$$Z = Z(\rho, T, B_i) \tag{11}$$

where the B_i are constants which may or may not be temperature dependent and ρ is molar density. Because of its unique theoretical significance, the model almost universally chosen is the virial equation of state

$$Z = 1 + B(T)\rho + C(T)\rho^2 + \text{---} \tag{12}$$

The importance of this equation stems from the fact that the virial coefficients, through statistical mechanics (35), can be quantitatively expressed in terms of intermolecular potential functions.

After selecting an appropriate model, non-linear regression analysis can be applied such that not only are the optimal values of model parameters found but also the values for the cell constant and the initial compressibility factor. For example, if the objective function chosen (many choices are possible) to be minimized is the difference between the Burnett compressibility factor, Z_b, and the compressibility factor as calculated from the virial equation of state, Z_v, squared and summed over all experimental points, then the regression analysis can be formulated as followed:

$$\text{Minimize} \quad \sum_{k=0}^{\ell} \left[P_k N_{00}^k \left(\frac{Z_0}{P_0}\right) \prod_{j=0}^{k} X_j - \sum_{i=1}^{m+1} B_i \rho_k^{i-1} \right]^2 \tag{13}$$

where regression parameters are N_{00}, (Z_0/P_0) and the B_i's. The first coefficient, B_1, is, by definition, equal to 1.0. This type of analysis can easily be expanded to incorporate multiple runs. However, since the B_i's are intended to approximate temperature-dependent virial coefficients, the Burnett data must be collected under isothermal conditions.

Burnett Applications

Because of the conceptual simplicity of the Burnett apparatus -- two chambers connected by an expansion valve -- the variation in one experimenter's design as compared to another's usually results directly from the restrictions or opportunities offered by the system being studied and/or the conditions of temperature and pressure. For example, when high pressures are of interest, pressure-jacketed Burnett cells (48) are usually employed to reduce the error introduced by pressure distortion. Because of the inherent difficulty in measuring pressure while maintaining constant volume, Burnett cells are usually designed of sufficient size to offset or significantly reduce the error introduced by this factor. However, when expensive fluids such as krypton, xenon, etc. are studied, the cost sometimes becomes an important factor and smaller cells are designed to minimize gas requirements. Another example is the practice of locating the expansion valve outside the temperature bath when extreme temperatures would otherwise jeopardize the necessary leak-tight operation of the valve. In this case, the experimenter must correct carefully for the fact that all the fluid is not at the same temperature. Examples of designs that feature volumes outside the principal bath can be found in the work of Lee (48) as well as that of Witonsky and Miller (93).

Methods employed to measure temperature and pressure are fairly standard. Temperature is usually measured with a calibrated platinum resistance thermometer in conjunction with a precise resistance bridge. The most common device for pressure determination is the dead weight piston gauge. A recent example of this is the work of Rowlinson et al. (18). Rowlinson's work is unique in the method used to separate the Burnett apparatus from the pressure measuring system. A null manometer was constructed from a quartz spiral capsule as supplied by Texas Instruments. Displacement of the quartz spiral from its null position was determined by projecting a beam of light on a plane mirror attached to the spiral and then back to a pair of silicon solar cells. Rowlinson reports that the final sensitivity of the instrument was 3mm deflection per μ-bar of differential pressure. This method is in contrast to the diaphragm type differential pressure null indicator used in most high pressure work.

Lee (48) has reported a list of previous investigations employing the Burnett method. An updated version (through 1970) of this list is presented in Table I.

Helium

Helium has been studied extensively for many years, the first PVT studies being reported before the turn of the century (47). Much of the early study was prompted by general interest in the simplest and lightest of the rare gas atoms. In later years, helium was a favorite with experimenters studying molecular interactions between unlike pairs due to the unique differences (size, ionization potential and reduced temperature) between helium atoms and other gas atoms. This

TABLE I

SUMMARY OF PREVIOUS INVESTIGATIONS USING THE ISOTHERMAL EXPANSION RATIO METHOD OF BURNETT

Temperature Range °C	Pressure Range psia	System	Investigator	Reference
0	to 2,200 to 900	Helium Air	Burnett	(14)
	to 4,000	Apparatus only	Cattel et al	(17)
26 to 93	to 4,000	Natural gas	Stevens and Vance	(75)
0 to 600	to 1,200	Helium	Schneider	(70)
0 to 600	88-1,200	Helium	Schneider and Duffie	(71)
600 to 1,200	88-900	Helium	Yntema and Schneider	(94)
0 to 600	to 735	Carbon dioxide	MacCormack and Schneider	(55)
0 to 400 0 to 250	to 735 to 735	Carbon tetrafluoride Sulfur hexafloride	MacCormack and Schneider	(56)
0 to 600	150-1,200	Argon	Whalley, Lupien and Schneider	(88)
0 to 700	to 1,200	Neon	Nicholson and Schneider	(65)

TABLE I (Continued)

Temperature Range °C	Pressure Range psia	System	Investigator	Reference
-60 to 30	7-37	Carbon dioxide	Cook	(20)
25	to 1,000	Natural gas	Bloomer	(8)
30	to 1,800	He, N_2, CO_2 and their binary mixtures	Pfefferle, Goff and Miller	(66)
30	to 1,910	He, N_2 and mixtures	Kramer and Miller	(46)
100 to 500	45-1,200	He-Ar, He-CF_4	Kalfoglou and Miller	(39)
175 to 475	to 1,500	He-N_2 mixtures	Witonsky and Miller	(93)
500 to 200	to 2,000	Apparatus and data treatment	Silberberg, Kobe and McKetta	(73)
50 to 200	to 1,000	Isopentane	Silberberg, Kobe and McKetta	(74)
10 to 250	15-4,600	Sulfur dioxide	Kang et al	(40)
-30 to 150	15,4,600	Nitrous oxide	Hirth and Kobe	(36)
30 to 200	15-1,000	Neopentane	Heichelheim et al	(34)
-200 to 50	to 7,000	Methane-H_2 mixtures	Mueller, Leland and Kobayashi	(62)

TABLE I (Continued)

Temperature Range °C	Pressure Range psia	System	Investigator	Reference
-163 to -48	to 150	Krypton	Rowlinson	(87)
-50 to 50	to 10,000	He-Ar	Blancett	(7)
-190 to -160	to 10,000	$Ne-N_2$	Hall	(30)
-130 to -90	to 10,000	He-Ar	Provine	(67)
25 to 75	to 12,000	$Ch_4-C_2H_4$	Lee	(48)
0	to 12,000	Helium	Briggs	(12)

interest was coupled with the fact that helium was declared a natural resource in danger of extinction by the Department of Interior which generated many studies by the Bureau of Mines in an effort to coordinate the conservation of helium reserves. In addition to the experimental studies conducted by the Bureau, a complete compilation of all original experimental PVT data on helium for the period 1895 to 1968 was recently published (2). This compilation contains a total of 163 references. Another good source of information on helium is the publication of Cook (21). This book presents a thorough review of helium properties, including PVT and thermodynamics data.

Due to the exhaustive review on helium available in the above references, a complete review of past work will not be repeated here. However, a list of previous work that will be used later for data comparisons is given in Table II. Efforts were made to include high quality data acquired by a cross-section of different experimental methods and by authors from a variety of different laboratories.

Krypton

Scant experimental PVT data are available for krypton, the first work being published as recently as 1952 by Beattie and co-workers (4). Beattie used an experimental apparatus as developed in 1934 (3), which has henceforth become known as the Beattie apparatus, to determine the volumetric properties of krypton for a temperature range of 0^{o} to 300^{o}C and over a density range of 1 to 10 moles per liter. The Beattie method consists of inserting a sample of known mass, which is contained in a thin walled vessel (glass) of known volume, into a high pressure bomb and then pumping mercury into the pressure vessel and releasing

TABLE II

SELECTED HELIUM REFERENCES

Temperature Range °C	Pressure Range atm	Investigator	Reference
-5 to 80	to 800	Briggs	(12)
-50 to 50	to 680	Blancett	(7)
-140 to 0	to 500	Canfield	(16)
-183 to 400	to 100	Holborn	(37)
0 to 150	to 200	Michels	(59)
-253 to 27	1 to 33	White	(90)
0 to 1200	to 80	Schneider	(71)
-70 to 200	to 1,000	Wiebe	(91)
0 to 100	to 200	Miller	(61)
-270 to 300	--	Keesom	(41)

the gas sample. The change in volume of the sample is determined by measuring the amount of mercury pumped into the high pressure vessel from a precalibrated screw pump.

A second paper by Beattie and co-workers (5) was devoted to calculation of second and third virial coefficients and parameters for the Lennard-Jones potential function from their experimental volumetric data for krypton.

Using a Burnett apparatus, Whalley and Schneider (89) studied the krypton system over a temperature range of 0° to $600^{\circ}C$ for pressures of 10 to 80 atm. The design of this apparatus differs modestly from most modern designs in that a mercury U-tube was used as the differential pressure null indicator for pressure measurements as opposed to the commonly used diaphragm type instrument.

A linear regression scheme utilizing the Berlin virial equation of state was employed for data reduction.

Fender and Halsey (29) determined second virial coefficients for krypton over a temperature range of 105° to $140^{\circ}K$. These workers employed an experimental apparatus which was first described by Constabaris and others (19) for use in the determination of rare gas adsorption on highly graphitized carbon black. This same apparatus was later used by Sams and co-workers (69).

Basically, the experimental method employed by Fender and Halsey was to determine a sample mass at a reference temperature by combining the known compressibility of the krypton with pressure and temperature measurement in a calibrated volume. The data of Beattie et al. (4) was used for this purpose. Knowing the sample mass, the second virial coefficient was determined at low temperature by expanding the krypton

from the original volume to a copper vessel maintained at some predetermined temperature. Using the pressure of the total system, the number of moles in the low temperature bomb was calculated as the difference between the total sample and that still remaining in the high temperature portion of the apparatus. The volume of the copper bomb was predetermined at various temperatures by expansion measurements with helium.

Thomaes and Steenwinkel (80) report second virial coefficient data for krypton over a temperature range of 110° to 270°K. The experimental method used is described in a prior publication (79). The method involves measuring the difference between volume expansions at the same temperature and pressure of krypton and hydrogen chosen as a standard of reference. The advantage of this method is that virial coefficients of higher order than second can be neglected. One obvious disadvantage is that any uncertainty in the volumetric properties of the standard will be reflected in the krypton determinations.

Trappeniers et al of the Van der Walls Laboratory (83) studied the volumetric properties of krypton at temperatures between 0° and 150°C for densities up to 620 amagat, corresponding to pressures up to 2900 atm. Second and higher order virial coefficients were reported. The experimental method employed was that developed in 1934 by Michels (60). The experimental apparatus was of the constant volume-constant mass type. The method consists of charging a sample into a high pressure bomb and then varying the temperature. Pressure is measured at each new temperature.

Rowlinson and co-workers (87) report second virial coefficients based on data for krypton over a temperature range of 110° to 225° K.

at low pressure. The authors employed a Burnett type apparatus. The principal features of the apparatus include an absolute mercury manometer, with which pressures up to 1 bar could be measured with an accuracy of $\pm 2 \times 10^{-6}$ bar, and a null manometer constructed from a quartz spiral. Since the measurements were made at low temperature, Rowlinson used double wall construction in order to allow measurements of B to be made with two widely different ratios of volume to surface area. This permits correction for the effect of gas adsorption on the vessel walls.

Staveley et al. (15) report values for the second virial of krypton from 117° to 252° K. The authors employed a differential type apparatus in which the imperfection of a sample gas is compared directly to that of helium for which the second virial coefficient is known over the complete temperature range of the measurements. To evaluate the second virial coefficient of the test gas, its value at one temperature must be known. The authors used the krypton data of Beattie (4) for this purpose. The volumetric properties of helium by White (90) were used to describe the behavior of helium. Therefore, Staveley's data is dependent on the accuracy of data from the above sources.

In a recent study, Theeuwes and Bearman (77) investigated the PVT behavior of liquid and dense gaseous krypton in the temperature range 130° to 240° K. at pressures from the vapor pressure to 280 atm. These workers used a constant volume-constant mass apparatus similar to the type developed by Michels et al. (60). However, the experimental method was slightly modified in the procedure used to determine the sample mass. Instead of starting the measurements for each isochore at a reference temperature where the PVT properties of krypton were

known, the sample mass was calculated directly from measurements made with a gasometer (78) prior to injection of the sample into the isochoric apparatus.

Two data compilation works deserve mention although no new experimental data are reported in these papers. The first is that of Sengers, Klein and Gallagher of the National Bureau of Standards. This work is to appear in the "American Institute of Physics Handbook." The authors used linear and non-linear regression techniques to determine the best m-6 potential to represent the published experimental second virial coefficient data for eight substances, including krypton. The potential functions were then used to generate second virial and other information at even values of temperature.

A second publication, co-authored by Dymond and Smith (28), offers a complete compilation of experimentally determined second virial coefficients for many substances, including krypton and helium. All virial coefficients have been converted to units corresponding to the density series (Leiden) form of the virial equation (cc/mol).

Helium-Krypton Mixtures

Only one PVT study on the helium-krypton system has been published. Using the experimental method developed at the Annes Laboratory (45,84), Brewer and Vaughn (10) measured the interaction second virial coefficients of 10 gas mixtures including helium and krypton. The measurements were conducted over a temperature range of -125 to 50° C in 25° increments. The experimental method consists basically of measuring the pressure change generated when two gases, initially separated in two bulbs at the same temperature and pressure, are mixed at constant

volume and temperature. The pressure change is directly related to the excess second virial coefficient (E), where E is defined by the following equation.

$$E = B_{12} - (B_{11} + B_{22})/2 \tag{14}$$

As indicated by Equation (14), calculation of the interaction second virial, B_{12}, requires a knowledge of pure second virial coefficients B_{11} and B_{22}.

CHAPTER III

EXPERIMENTAL APPARATUS

A schematic representation of the equipment used in this work is shown in Figure 1. The apparatus consisted essentially of a Burnett cell enclosed in a constant temperature bath, auxiliary equipment for measuring temperature and pressure, a gas compressor, and a secondary temperature bath providing the heat sink for the primary bath. This chapter provides a general description of the apparatus. Additional specifications are given in Appendix A.

Burnett Cell and Pressure Measuring System

The Burnett cell consisted of two identical chambers drilled in opposite ends of an 11 inch segment of 3 inch O.D. 303 stainless steel bar stock. The dimensions of the chambers were 0.591 inches in diameter by 4.5 inches deep, corresponding to a volume of approximately 20 cc. The chambers were tapped with 3/8 inch NPT pipe threads and then thoroughly cleaned (with solvent and ultrasonically) before being polished to a mirror finish with crocus cloth. The chambers were given a final application of solvent and ultrasonic cleaning before being assembled. A 303 stainless steel cylinder (9/16 O.D. x 2 1/4 in. long) was inserted into the second, or expansion, chamber in order to achieve the desired volume ratio. The chambers were connected, as

shown schematically in Figure 1, with 15,000 psi 1/8 inch stainless tubing and needle valves. The charge and exhaust valves were connected with the packing side away from the system so that two potential leak sources were isolated from the system. The expansion valve was connected with the packing side toward the expansion chamber. This allowed checking for leaks around the packing simply by noting the ease (or difficulty) in pulling a vacuum on the second chamber after an expansion. Teflon packing was used in all three valves.

The upper chamber of the Burnett cell was connected directly to a cryogenic differential pressure cell. This arrangement is preferable to older methods having the differential pressure cell outside the temperature bath since all test gas is maintained at the same temperature. The differential pressure cell consists of two pressure chambers separated by a thin stainless steel diaphragm. A pressure difference between the two chambers causes a deflection of the diaphragm and a resultant electronic signal. The signal is obtained from a differential transformer whose movable core is attached to the diaphragm. The signal is transferred to an electronic null indicator where any pressure imbalance is indicated on a readout scale. The composite of the cell and electronic readout is usually referred to simply as a differential pressure indicator, or DPI.

The upper chamber of the DPI was connected to an intermediate gas system containing an ambient, or room temperature, DPI as shown in Figure 1. This arrangement was necessary in order to separate the oil system of the dead weight tester from the temperature bath. Otherwise, the temperature range of the bath would be restricted to levels compatible with the physical properties of the oil. Another

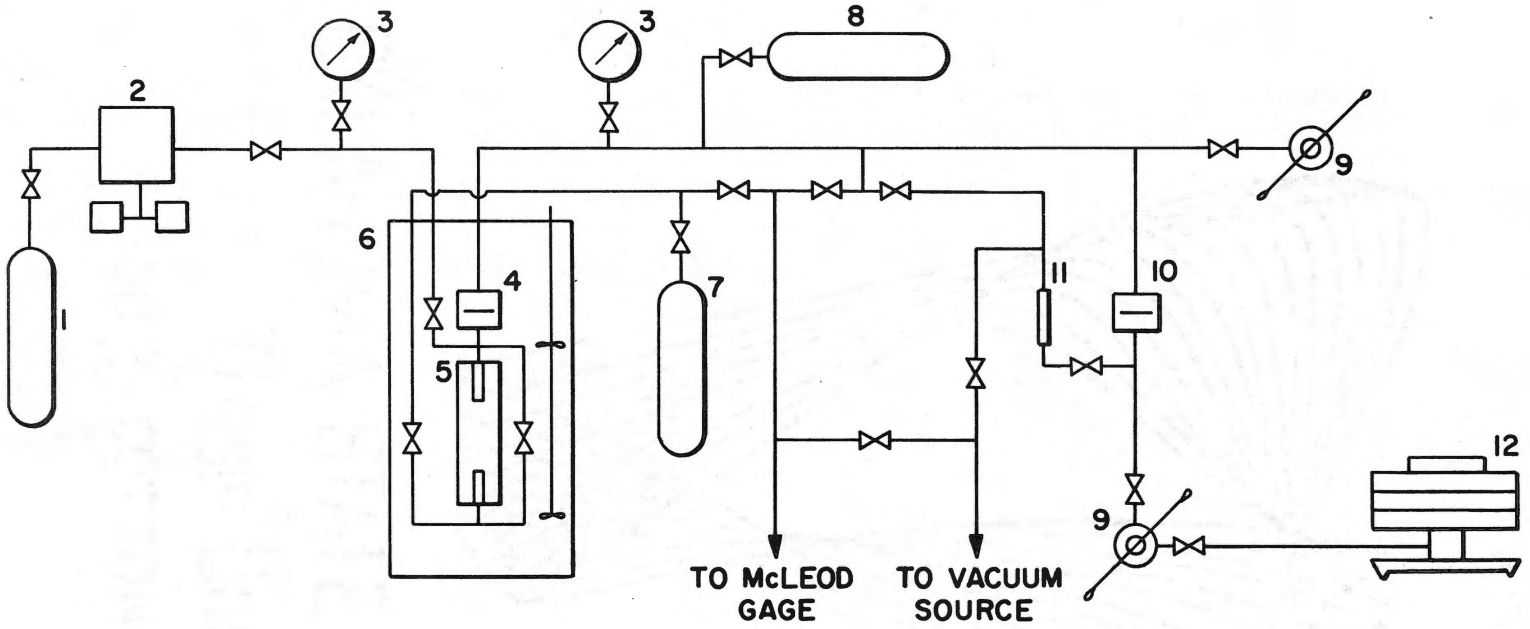

1 - SAMPLE GAS

2 - DIAPHRAGM COMPRESSOR

3 - PRESSURE GAGE

4 - CRYOGENIC DIFFERENTIAL PRESSURE INDICATOR

5 - BURNETT CELL

6 - CONSTANT TEMPERATURE BATH

7 - SAMPLE RECOVERY

8 - HIGH PRESSURE HELIUM

9 - SCREW PUMP

10 - DIFFERENTIAL PRESSURE INDICATOR

11 - OIL MANOMETER

12 - DEAD WEIGHT PISTON GAGE

Figure 1. Schematic Representation of Experimental Equipment

advantage of the arrangement used for this work is that the oil was maintained at a fairly uniform temperature as opposed to having part of the oil at ambient temperature and part at the temperature of the experiment. With the arrangement used in this work, the corrections for the density of the oil as a function of temperature in the pressure calculations are small enough to make any error in the calculations negligible. Of course, the large temperature difference between the temperature bath and the ambient had to be accounted for, but since helium was used between the two DPI cells, the head corrections were very small.

As indicated, the lower chamber of the ambient DPI was connected to the oil system of the dead weight tester. A Ruska Model 2400 was used in this work. Two different testers were actually used during the course of the experimental work, but the two instruments were identical except for age. The newer tester became available during the early stage of the data acquisition, and on the chance that the new instrument might be more precise, it was installed.

Two Ruska pumps, one for oil and one for gas service, were installed for pressure generation between the dead weight tester and the lower chamber of the ambient DPI and between the upper chambers of the two DPI's, respectively. The gas pump was only used for generation of small pressure changes in the intermediate gas system. A cylinder of high pressure helium was used to roughly balance the pressure of the intermediate gas to the pressure of the sample gas in the Burnett cell. Fine balancing in the pressure measuring system was accomplished with needle valves. For rough measurement, 16-inch

calibrated Heise gauges were used in the charge line to the Burnett cell and in the intermediate gas system.

As indicated in the above description of the components of the pressure measuring system, three separate segments of the system (sample gas, intermediate gas and oil) must have accurately balanced pressures in order to make a pressure determination. This balancing technique avoids having to use the DPI's for measurement of differential pressure; they are used strictly as null indicators to indicate pressure balance in the three segments of the system. This makes the determination more precise since a correlation between DPI read-out and differential pressure is only needed at one point (null) rather than for a range. However, a null shift as a function of applied pressure and temperature is an inherent property of these instruments and this, of course, required experimental work to develop the functional relationships describing the effect of pressure on the DPI read-out. This and other corrections such as volume change in the Burnett cells as a function of pressure are presented in Appendices B and C.

The first step toward acquiring a pressure determination is to ascertain that the DPI's indeed read zero when the pressure of the system is perfectly balanced and at some reference pressure. (A nominal pressure of 15 psia was used.) To insure a balanced system, valves and tubing were installed such that all parts of the pressure measuring system could be exposed to the same reference pressure. An oil manometer, scored at the exact height of the diaphragm in the ambient DPI, was used to adjust the oil head such that the diaphragm could be positioned to the height corresponding to an unflexed condition. Thus, with the oil head in the manometer adjusted to the

exact height of the diaphragm of the ambient DPI, the remaining requirements for pressure balance are:

1) The pressure above the oil manometer must be equal to the pressure in the upper chamber of the ambient DPI.

2) The pressure in the upper and lower chambers of the cryogenic DPI must be equal.

3) And, finally, the results are enhanced if the pressure in the upper and lower chambers of the cryogenic DPI, the pressure above the oil manometer, and the pressure in the upper chamber of the ambient DPI are all equal.

These requirements are easily met by sealing the top of the oil manometer, the upper chamber of the ambient DPI, and both chambers of the cryogenic DPI into a common header of tubing.

Since the valving and tubing installed for the balancing service is somewhat difficult to see clearly in Figure 1, the balancing system is schematically depicted in Figure 2. Only components pertaining to the balancing system are shown. Also, valves which would be open during this operation are deleted from the sketch.

Pressure Generation

A diaphragm type compressor was used to compress the gases from the sample containers to the Burnett cell. The primary advantage of this type compressor is, of course, that the sample gas is completely separated from the compressing fluids so that the possibility of contamination is minimized. The particular compressor used in this work was an American Instrument Company Model 46-1435 air-driven compressor. The compressor was a double action type with a compressing

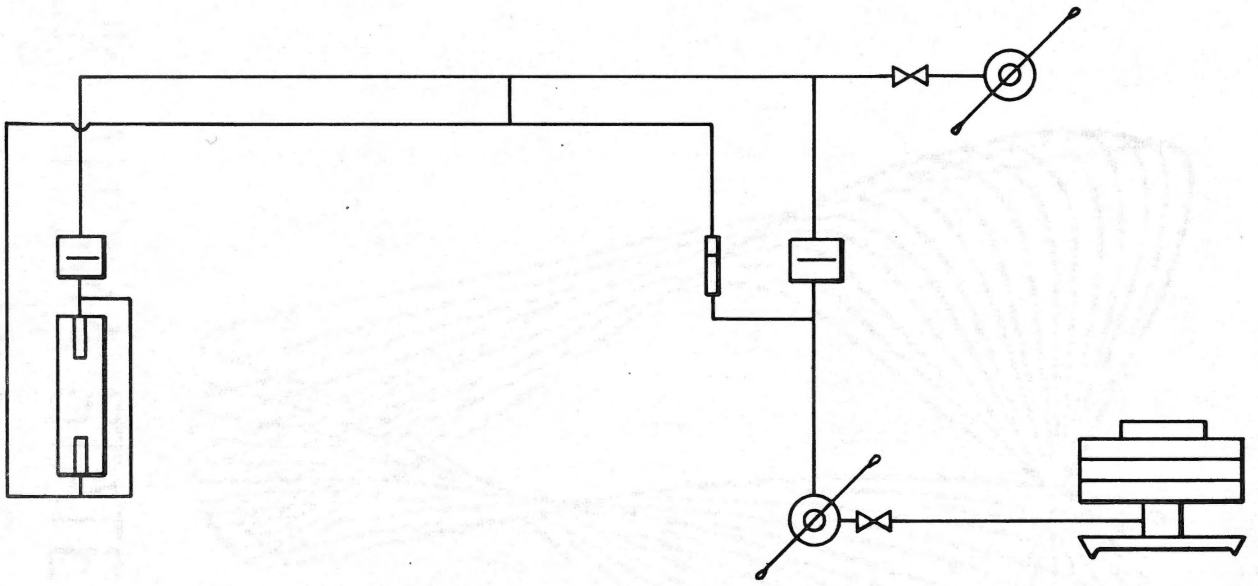

Figure 2. Schematic of Tubing Arrangement for Balancing DPI's

diaphragm at each end of the hydraulic system used to flex the diaphragms. A very desirable feature of this machine was the very small clearances between the diaphragms and the check valves, making compression ratios above 50 possible. Since the compressor was a positive displacement device, care was exercised not to start the machine with too much suction pressure available.

For helium runs, the Burnett cell could be charged directly from the helium storage cylinder since sufficient pressure was available throughout the course of the experimental work.

Vacuum System

The vacuum pump used in this work was a Welch Duo-seal two stage pump. The pump was capable of pulling a vacuum to 0.1 microns of mercury under shut-off conditions. A Model 94151 Cenco McLeod gauge was used to measure the pressure in the vacuum system.

This system served to evacuate the second chamber, V_b, of the Burnett apparatus and was also used as a valuable aid for leak checking. Before each run, the charge valve, expansion valve and associated fittings were checked for leaks by pulling a vacuum on the system. The exhaust valve, of course, could be checked in this manner after each expansion during a run.

A variety of fittings were used in the vacuum system successfully, including common copper tubing flare joints. This is pointed out because other investigators, including Canfield (16), have reported that sweat fittings were the only fittings found to be acceptable for vacuum service even at the modest vacuum levels (0.1 microns Hg) required in this work. This writer found that if the copper tubing

was properly prepared by smoothing the end with a file and then reaming slightly to remove any burrs on the inside diameter of the tube that the flare fittings worked satisfactorily.

High Pressure Valves and Tubing

Since a leak-tight system is the first prerequisite to successful application of the Burnett method, the valves and tubing used in the apparatus were selected with a great deal of care. Based on previous experience of this author, 1/8 inch valves and tubing are usually the best choice when leak-tight service is essential. This gives a minimum surface area to seal at the valve seat and the packing since most manufacturers use the same seat and stem size in their 1/16 inch valves as is used in their 1/8 inch valves. Valves larger than 1/8 inch generally are designed with proportionately larger stems which makes the seals at both the packing and the seat more difficult. Also, if 1/16 inch tubing and valves are used, a debit is incurred since the I.D. of 1/16 inch tubing is so small that much longer time periods must be allowed for any pressure difference between two sections of the equipment to equilibrate. Thus, 1/8 inch tubing and valves were used almost exclusively in this work. Noteable exceptions were the vacuum system where all tubing was 1/4 inch or larger (to avoid undue pressure drop between the vacuum pump and the system) and the oil system between the ambient DPI and the dead weight tester where 3/16 inch tubing and valves were used. Small size tubing in the oil system would very quickly become a limiting factor in the precision of the pressure determinations. This is due to the fact that when a pressure measurement is in progress the weights of the dead weight tester are floating

on the oil system via the piston in the tester and any pressure change on the upper side of the ambient DPI can only be reflected at the tester by a change in the height of the weights. This, of course, can only occur by the flexing of the DPI causing a flow of oil to or from the dead weight tester. Since pressure changes on the order of 0.001 psi need to be discernible, any pressure drop between the DPI and the tester must be minimized.

The most critical service in the apparatus is the tubing and three valves connected directly to the Burnett cell. If a leak developes in this part of the system and repairs and/or replacements are necessary, the volume of the Burnett cell will be altered slightly. For the data to be useful at all, the volume ratio of the Burnett cell must be constant for a complete series of expansions which constitutes a run. Furthermore, the variation in the cell constant as a function of composition, time and temperature is a very useful parameter in assessing the precision of the data acquisition and data reduction methods. Thus, if the volume ratio is altered frequently during the experimental work, an important source of information is lost. For this reason, every precaution was taken to enhance the possibility of completing the experimental work without having to change part of the system due to leaks. The fittings and tubing were not a big worry (relatively speaking) since once these items are made up leak-tight they are only subjected to minor stress changes due to varying pressures and temperatures. However, the valves must be continually opened and closed during the course of the experimental work and are therefore subject to wear.

Two-piece stem High Pressure, Inc. valves with Teflon packing were chosen for this service. The divided stem feature is very important for two reasons. First, this allows the seal between the stem and valve seat to be accomplished without rotation of the stem against the seat. This prevents the stem from scoring due to the grinding motion that would accompany rotation. Secondly, the packing is below the threads used to thrust the stem, thus insuring that no metal particles from the threads could find their way into the system. This is significant due to the ease with which the DPI diaphragm can be punctured by small particles. In a recent study (38), a diaphragm was ruptured when small pieces of Teflon tape which had been used to seal pipe threads in the apparatus had inadvertantly entered the system.

To prepare the valves for installation, they were first disassembled and inspected under magnification to make sure the stems were relatively smooth and free of any pitted spots or other defects. Several valves were inspected but little discernible difference could be found between them. The quality of all valves inspected seemed uniformly high. Thus, three valves were selected in a more or less random fashion. The stems of the selected valves were hand polished with crocus cloth and then coated with molybdenum disulfate lubricant. The lubricant was applied with a soft cotton cloth. Care was taken to prevent any excess lubricant from remaining on the stem. The valves were then reassembled. The packing nut was tightened at room temperature until rotation of the stem required two or three times the torque required to rotate an off-the-shelf valve.

The three valves worked satisfactorily with no leaks for the entire course of the experimental work. Occasionally, a run would be spoiled by leakage past the seal of the expansion or the exhause valve due to improper closure of the valves. However, this was due only to the extreme care used in closing these valves. Every effort was made to try to estimate the right amount of torque to give a leak-tight shut-off without applying excess torque that would permanently damage the valve stem or seat.

Constant Temperature Bath

One of the most important design parameters for the type of experimental work undertaken in this study is the temperature control in the constant temperature bath. Both gas and liquid baths were considered. Both types offer some advantages but also have some shortcomings. The major advantage of a gas bath is the fact that very large temperature ranges are compatible with this type bath. However, heat transfer rates are much slower in a gas bath making temperature gradients in the experimental equipment contained in the bath more likely. Liquid temperature baths have three major shortcomings. First, and perhaps most important, is the problem associated with the small temperature range that can be achieved with a single bath fluid. Most liquids have a practical temperature of about 50^{o} C between their freezing point (or the point where the viscosity becomes excessive) and the point where the vapor pressure becomes a problem. Secondly, many fluids that would be compatible in terms of viscosity and vapor pressure are expensive, extremely flammable, corrosive and often toxic. The third problem is viscous dissipation of energy in a liquid bath.

At times, this energy input can become a significant quantity relative to the total flow of energy through the bath. This requires designing additional flexibility into the control heaters and heat sink as well as requiring stringent control on the stirrer speed to avoid pertubations in the control system.

Despite these shortcomings, a liquid bath was chosen for this work. This writer concluded that the disadvantages of a liquid bath were in the catagory of inconveniences, whereas the heat transfer problem associated with a gas bath could actually limit the precision with which the temperature of the equipment in the bath could be controlled.

The design basis for the temperature bath was set with the following requirements:

Temperature Range of -75 to 100^{o} C

Temperature control within 0.001^{o} C

The control precision specified as the goal for this work represents the ultimate practical limits for control precision. This is due to the present state-of-the-art in temperature measuring systems. A thousandth of a degree centigrade approaches the sensitivity limit for most measuring devices. In other words, control within 0.001^{o} C represents stable temperature control in terms of observable phenomena.

Two bath fluids were selected which would, collectively, satisfy the design basis temperature range. Ethanol was chosen for the lower part of the range (0 to -75^{o} C) and ethylene glycol for the upper end of the range. These fluids were selected primarily for their low toxicity and flammability properties as well as having reasonably low viscosities.

The bath proper was a double-walled stainless steel Dewar which measured 11 5/8 inches I.D. by 30 inches deep. The Dewar was mounted in an aluminum cylinder (18" O.D. x 34" deep) with 4 inches of Styrofoam below the Dewar. Foamed-in-place insulation was used to fill the space between the inside of the aluminum cylinder and the exterior of the Dewar. The top for the bath was mounted in place on the top of an angle iron framework. The Burnett cell and the cryogenic DPI were suspended from the bath top. Thus, the Burnett cell component could be exposed by lowering the Dewar. A small angle iron cage which could be lowered and raised with a hand-operated wench was constructed to facilitate the raising or lowering of the bath.

The top for the bath was constructed from two layers of 3/4 inch plywood and then coated with an epoxy based paint. A piece of Styrofoam cut to the dimensions of the Dewar I.D. was segmented to fit around the various pieces of equipment entering through the bath top and then tacked in place.

Temperature Control

One important parameter in the design of a constant temperature bath is the controlled flow of energy through the bath relative to uncontrolled energy inputs and outputs. The controlled flow should always be large compared to possible disturbances. Ideally, this can best be achieved by cascading, or using layers of control, with each succeeding layer controlled with increasing precision. Given enough control layers, this would eliminate disturbances from the final layer which would, of course, contain the experimental equipment. In practice, this ideal method is not used due to the obvious

disadvantages of cost and complexity. However, the concept can be applied, at least directionally, and the first step is to properly insulate the bath and use a laboratory with some form of room temperature control. The second step (and the one most often overlooked by experimenters) is to carefully control the heat withdrawal so that pertubations from this source are minimized if not eliminated.

The refrigeration for the heat sink was supplied by two different methods, depending on the temperature level. At 0^{o} C and higher, a Blue-M laboratory temperature controller was used to control the temperature in a 12-gallon reservoir containing a mixture of ethylene glycol and water. The temperature in the reservoir was controlled at approximately 5^{o} C below the desired experimental temperature. The temperature of the reservoir was indicated by a standard mercury thermometer and, after lining out, no temperature fluctuations could be detected. However, the control precision was estimated to be within $\pm 0.05^{o}$ C which conforms to the specifications listed by the manufacturer. The fluid from the reservoir was pumped through 3/8 inch insulated copper tubing to the temperature bath. Inside the bath, 150 feet of 1/4 inch tubing was coiled tightly against the interior wall of the Dewar and virtually covered the entire inner wall of the Dewar. The tubing was arranged so that the fluid entered the coil at the bottom of the bath and then flowed upward and out of the coil at the top of the bath. The flow rate of the fluid through the coil was not controlled. The pump used for this application supplied sufficient head to give a good flow rate through the system. To change the amount of heat withdrawal, the temperature of the secondary bath was varied.

For the -50° C isotherm, liquid nitrogen was used for refrigeration. The nitrogen was purchased in 110 liter containers. The containers were provided with a pressure controller that maintained the pressure at a constant value, thus vaporizing sufficient nitrogen to maintain the temperature of the contents. The nitrogen was transferred to the bath through 3/8 inch insulated copper tubing. The container was placed as close as possible to the bath to minimize heat leak into the transfer line. After passing through coils in the bath, the nitrogen exited through uninsulated 1/4 inch copper tubing containing a needle valve and a rotameter. Since the nitrogen was in the two-phase regime during the transfer, controlling the flow rate on the inlet side of the bath would have been difficult, if not impossible. However, very good control was achieved with the control action located downstream from the bath, where the nitrogen was in the gaseous phase.

Since the pressure in the container was used as the driving force for the nitrogen flow, the maximum flow rate attainable through the system was dependent on the pressure control device on the tanks. These devices were found to vary radically from one tank to another, but fortunately, the supplier was kind enough to check through his stock and sort out the tanks with sufficient pressure (above 20 psig) for delivery to the writer's laboratory.

Since the liquid nitrogen was a high cost item for the research budget, the work at -50° C was expedited to cut the cost for this item. Also, every effort was made to find the lowest possible flow rate that would yield the minimum amount of refrigeration for stable temperature control. In this manner, a tank of nitrogen was "stretched" to last,

on the average, about 30 hours. This was sufficient to line the system out and make one complete run.

The control heat for the bath was supplied by a 500 watt Briskheat electrical heater which was regulated with a Hallikainen Thermotrol temperature controller. The controller used a completely enclosed nickel resistance thermometer as the sensing element. The Thermotrol is an off-the-shelf laboratory controller which provides three modes of control (proportional, reset and rate).

The only other equipment item associated with temperature control of the bath deserving mention is the mixer. As discussed earlier, the viscous energy input from the mixer is a significant portion of the total energy input and therefore should be controlled closely. To achieve this, a Servodyne laboratory mixer was purchased which provided a variable, controlled mixer speed. The speed control was accomplished with a feedback electronic controller as opposed to less precise devices which utilize rhestatic control of the voltage. The mixer speed could be varied from 0 to 3,000 rpm.

At higher speeds, the mixer shaft was found to vibrate excessively and a Teflon foot bearing was installed in an attempt to correct the vibration. This made considerable improvement, but several shafts were experimented with before one was found that operated satisfactorily over the entire range of the speed controller.

Temperature Measurement

The International Practical Temperature (IPT) Scale is defined by six reproducible thermodynamic equilibrium points. (The six points are the boiling points of oxygen and water, the melting points of

sulfur, silver and gold, and the triple point of water.) As this implies, some type of interpolation device is necessary to achieve continuous temperature measurement between the defined points on the practical scale. The standard device used for the temperature range of interest in this work is the strain-free, high-purity platinum resistance thermometer. This type resistance thermometer can be certified and guaranteed to reproduce the IPT scale to within 0.01° C by having the National Bureau of Standards (NBS) calibrate the thermometer. Three different platinum resistance thermometers were used during the course of this work. The thermometers had been certified as standards by the NBS. The thermometers were purchased from Leeds and Northrup. The model and serial numbers, in the chronological order of usage, are: 1) Model 8163, Serial No. 1576919, 2) Model 8164, Serial No. 1612800, and 3) Model 8164, Serial No. 1697602.

The installation of the thermometer for this work was slightly different than the method used by most previous investigators. In prior work, the method favored has been to drill a thermowell into the wall of the Burnett cell parallel to (but not in) the top chamber of the cell. For gas baths, this is probably best procedure in lieu of actually tapping into the Burnett chamber, which is not presently feasible in high pressure work since there is not a commercially available standard thermometer suitable for this application. However, in a liquid bath, the assumption that the Burnett cell is in thermal equilibrium with the bath fluid is valid since the fluid offers good heat transfer characteristics. For this reason, the thermometer in this work was simply positioned in the bath fluid near the center of the Burnett cell.

As indicated in the above discussion, the absolute accuracy with which a temperature determination can be made is 0.01° C. However, the stability of a platinum resistance thermometer is much better than 0.01° C, and the ultimate precision of a measurement is limited by the bridge used to measure the thermometer resistance. In this work, a Leeds and Northrup Mueller bridge, Model 8069-B, Serial No. 15550042, was used in conjunction with a Leeds and Northrup Model 2284-D ballistic type galvanometer to measure the resistance of the thermometer. The combined sensitivity of these devices was very high with the last decade on the bridge representing approximately 0.001° C. (This last decade on the bridge corresponded to a deflection of approximately 2 mm on the galvanometer readout scale.) Thus, the precision of the total temperature measuring system was estimated to be $\pm 0.001^{\circ}$ C.

The calibration data compiled by NBS was supplied in both equation and tabular form. The use of the data requires the knowledge of the resistance of the thermometer at the ice point (designated R_o). This value is reported by NBS, but the recommended procedure is to determine this value experimentally utilizing the user's bridge and wiring.

Since the ice point is difficult to reproduce accurately, a triple point cell was used in this work. The cell was guaranteed by the manufacturer (Trans-Sonic, Inc.) to reproduce the triple point within 0.0005° C. Using this relatively easy procedure to check the bridge circuitry and thermometer, calibrations were carried out before the experimental work at each isotherm was started. No significant shift in the reference resistance was ever detected.

Auxilliary Equipment

Barometer

Due to the extreme precision with which the gauge pressure was measured with the dead weight gauge (better than 1 part in 10,000), the barometric pressure determination required to convert to absolute pressure had to be very precise to avoid having the precision of the experimental results limited by a seemingly simple device, namely the barometer. A quartz Bourdon tube gauge, Texas Instruments (TI) Inc., Model 141, was available for use during most of the experimental work. This gauge had been calibrated by the manufacturer and had a reported accuracy of 0.015% of full scale. This translates to about $\pm$0.015 mm Hg. Thus, when the T.I. gauge was available, the barometric determinations were easily compatible with the precision of the gauge pressure measurements. When the T.I. gauge was not available, a standard inverted-tube mercury barometer was used. The barometer was compared with the T.I. gauge. After making all appropriate corrections, the barometer and the T.I. gauge were found to agree within the precision with which the barometer could be read ($\pm$0.1 mm Hg).

Controlled Environment for Instruments

The electronic circuitry of the instrumentation and the ambient DPI were enclosed in temperature controlled air bath. Only the instrument faces (or read-outs) were exposed to the room environment. This was necessary because the room temperature varied $\pm 2^{\circ}$ F daily, and variations of this magnitude would certainly affect the stability of

the instrumentation. This is particularly true with regard to the Thermotrol, as documented by Canfield (16).

Sample Gases

The krypton and helium-krypton mixtures were purchased from Air Products, Incorporated. The krypton and the components for the mixtures were Research Grade materials. The pure helium was donated by the Department of Interior, Bureau of Mines and was certified ultra-pure by the Bureau. Composition analyses for the mixtures are presented in Appendix D.

CHAPTER IV

EXPERIMENTAL PROCEDURE

The experimental procedure followed during the data acquisition phase of this study is presented in this chapter. The experimental procedure was designed to insure that the data were compatible with assumptions made in deriving the equations describing the Burnett method. The obvious assumptions inherent to the Burnett method are that the temperature and pressure of the gas sample are known precisely and that the mass of the sample before an expansion is equal to the mass after an expansion. Less obvious, but of equal importance, is the requirement of pressure equilibrium between the two Burnett chambers while simultaneously insuring that the volume of the chambers after an expansion is equal to the volume before an expansion. This requirement is not easily achieved due to the variation in volume caused by the movement of the stem in expansion valve and by the movement of the diaphragm in the cryogenic differential pressure cell.

Temperature Control and Run Preparation

There were two alternate methods possible for collecting the experimental data. One possibility was to hold composition constant and vary the experimental temperature. The other possibility was to vary composition and take the data along an isotherm. The first method offers the advantage of having to purge the system only once for each composition. The second method requires purging the system

before each composition change, but offers the advantage of working at one temperature until all data on that isotherm are collected. The isothermal method was chosen in this work since establishing temperature control was a difficult task.

Before starting an isotherm, the platinum resistance thermometer (PRT) and bridge calibration were checked with the triple point cell. The PRT was then installed in its supports next to the Burnett cell. The Dewar was then filled to a predetermined level with the proper bath fluid (ethanol for 0^{o} and -50^{o} C and ethylene glycol at $+50^{o}$ C). Next, the Dewar was hoisted into position and the mixer turned on and adjusted to about 1500 rpm. The refrigeration system (liquid N_2 at -50^{o} C or the Blue-M equipment at 0^{o} and $+50^{o}$ C) was then connected to bath cooling coils and the flow of refrigerant initiated. For runs below ambient temperature, the bath was allowed to cool to the desired temperature before the temperature controller was turned on. The Thermotrol was initially operated in the on-off mode. Rough control settings were estimated from a graph supplied by the manufacturer and these values were dialed into the Thermotrol. By monitoring the bath temperature, the values were then adjusted until temperature control was established within 0.1^{o} C of the desired value. The system was then allowed to stabilize for approximately 4 hours before further adjustments were made. After the waiting period had elapsed, the operation of the Thermotrol was observed and an estimate of the stability of the temperature control loop was made. If the total heat flow through the bath was judged to be too high or low, adjustments were made to the amount of heat removed by the heat sink by either changing the temperature of the refrigerant (Blue-M) or varying the

flow rate in the case of liquid nitrogen. This procedure was repeated until the bath characteristics were judged to be compatible with the possible values of gain, reset and rate available in the Thermotrol.

The next step in the procedure was to tune the Thermotrol. A modified Ziegler-Nichols (95) method as recommended by the manufacturer was used to accomplish this task. At 0 and -50° C this tuning method worked quite well and no further efforts were required to tune the controller. At 50 and 100° C, the method proved to be inadequate. A trial and error technique was finally successful at 50° C but temperature control was never achieved with the Thermotrol at 100° C. (This problem will be discussed in more detail in Chapter V.)

After the controller was tuned satisfactorily, the only remaining task in establishing temperature control was to adjust the Thermotrol settings until the bath temperature was brought to within $\pm$ 0.005° C of the desired value. This was accomplished by monitoring the bath temperature with the PRT and then making very small adjustments to the controller. Sufficient time was allowed between adjustments to insure steady state conditions. Althought the controller had two potentiometers, one for large temperature changes and one for fine adjustment, this procedure was usually tedious and time consuming. Moving the fine adjustment by the smallest discernible amount often proved to be too much setpoint change. Fortunately, once the proper setting was found, no further adjustments were normally required during data acquisition along an isotherm.

After establishing temperature control, the system was ready for data acquisition along that particular isotherm. Pure helium was always selected for the first composition to be run at the newly

established temperatue. This procedure was followed as a precaution taken to insure that if a leak had developed during the change to the new temperature, it would be found during a helium run. This, of course, would conserve the expensive krypton and helium-krypton mixtures. Also, the helium runs were always duplicated after finishing data acquisition for all composition. This gave a direct check on the equipment performance during all runs on an isotherm.

DPI Zeroing

The next step in the experimental procedure was to zero the differential pressure indicators. This is purely a base adjustment to the electronic circuitry to insure that the read-out for the instrument was equal to zero when the pressures on the opposite sides of the diaphragm were equal. As this implies, the only prerequisite to successful completion of this task was to ascertain that the pressure was indeed the same both sides of the respective diaphragms of the two instruments. As described in Chapter III, tubing and valves were installed specifically for this purpose. Using this previously described equipment, the pressure could readily be equalized across the diaphragms. However, due to the inherent nature of the instruments, better results were achieved if the diaphragms were first conditioned by overpressuring from the top side before zeroing. Thus, pressure equal to maximum run pressure was applied to the top side of the DPI's with helium gas and then slowly released. Following this procedure, the pressure was equalized across the diaphragm. About two hours were allowed to elapse at this point to insure that all heat transfer effects had lined out. The electronic read-outs were then zeroed. At

this point, the Burnett cell was ready for charging. Purging of the system was not necessary since all gas introduced to the system during the zeroing procedure was helium, and since the first and last run on each isotherm was always a helium run.

Charging, Expansions and Composition Changes

As mentioned previously, the helium supply was adequate and at sufficient pressure to charge the Burnett cell without the aid of a compressor. For all other samples, the air driven diaphragm compressor was used to compress the gas into the Burnett cell. Thus, for a run on a particular sample the sample bomb containing the gas under study was connnected to the suction side of the compressor with a valving system specifically designed for this task. After making the necessary connections, the configuration was such that a small sample of gas could be trapped between two valves and then subsequently injected in the suction of the compressor. Simultaneously, a vacuum was pulled on the exhaust side of the Burnett cell with the valves arranged in such a way as to expose the entire system, including the compressor discharge, to the vacuum. With the compressor running, gas samples were repeatedly trapped and then charged to the compressor. The main objective of this procedure was to purge the suction side of the compressor since the discharge side could have been evacuated with the vacuum pump to a sufficient extent to eliminate the danger of sample contamination.

After purging the system, the Burnett cell was charged to the desired run pressure. During this operation, as well as during the expansions performed later, care was exercised to prevent overpressure

of the DPI's from the side opposite of the side purposely overpressured before the instruments were zeroed. This required considerable patience and perserverance but was necessary due to the well known (7,16) fact that discernible zero shifts occur if overpressure is applied to alternate sides of the instruments.

The design of the equipment more or less dictated the correct procedure to follow in order to avoid an overpressure from the non-conditioned side of the DPI's while charging the Burnett cell. The first step was to apply pressure on the oil (conditioned) side of the ambient DPI. Since the oil was essentially incompressible, only a small pressure (about 200 psi) was required to keep the diaphragm positioned away from the center of the chamber during the entire charging procedure. Next, helium was slowly charged to the intermediate gas system between the two diaphragms. This was continued until the pressure reached about 500 psi. At this point, the sample gas was charged to the upper chamber of the Burnett cell. Simultaneously, additional helium was charged to the intermediate gas system with sufficient rate to keep the pressure approximately 200 psi above the pressure of the sample gas. As the interemediate gas pressure reached a value approximately 50 psi above the desired run pressure, the intermediate gas addition was stopped and the rate of addition to the Burnett cell slowed. (When using the air-driving compressor, the charge rate was controlled by regulating the air supply to the compressor.) This slow addition was continued until the sample pressure

reached the desired run pressure as indicated on the large Heise gauge in the sample line. The Burnett charge valve was then closed and the system allowed to equilibrate for approximately one hour.

After the initial waiting period had elapsed, the system was brought to rough pressure balance. During this phase, the sensitivity of the DPI's was first set on a very low value so that the read-out would be on-scale as soon as the pressure imbalance reached the point where the diaphragm first moved away from the chamber wall where it had been held firmly in place with the purposely applied overpressure. Adjustment of the intermediate gas pressure was accomplished with the Ruska hand-pump until a rough balance between the sample and the intermediate gas was achieved. The sensitivity of the cryogenic DPI was then adjusted to the original position which corresponded to the setting where the instrument had been zeroed. Next, the pressure on the oil side of the ambient DPI was adjusted with a second hand-pump for oil service. As the diaphragm in the ambient DPI responded to the pressure adjustment, the intermediate gas pressure changed slightly. Thus, simultaneous adjustment of the oil and gas pressure was required to balance the DPI's. When the ambient DPI indicated a balance, its sensitivity was adjusted back to the original setting. The final adjustments to the system were then made.

Next, the oil hand-pump was isolated from the system by closing a valve between the pump and the DPI. Closure of the valve caused a small volume change and a corresponding overpressure on both DPI's. To compensate for this change, the oil hand-pump was adjusted simultaneously so that the system was in balance when the valve reached a closed position. After isolating the hand-pump from the DPI, the

valve between the pump and the dead weight tester was opened. The tester was then loaded with sufficient weights to approximate the sample pressure as indicated by the Hiese gauge in the intermediate gas system. The electric drive was then turned on so that the weights were set in motion. Using the hand-pump, the weights were lifted to mid-range.

Next the valve which isolated the tester from the ambient DPI was carefully cracked and then quickly closed. By watching the movement of the ambient DPI read-out, an estimate of the additional mass required to balance the system could be made. If the imbalance was small, the weight change was made with the weights spinning. For large adjustments or adjustments requiring a different combination of weights, the weights were stopped and lowered to the rest bearing before making the change. This procedure was repeated until a balance between the tester and the rest of the system was attained. At this point, the valve between the tester and the ambient DPI could be left open. Next, the weights were adjusted slightly so that the tester was near the top of its range and a slight overpressure showed on the ambient DPI. The tester was designed to allow a very small leakage of oil past the piston. Thus, as the oil flowed out of the system, the piston gradually fell, thereby reducing the oil head. As the oil head decreased the ambient DPI would reach the null point. Since the cryogenic DPI had been kept in balance at all times by adjusting the intermediate gas pressure, when the ambient DPI reached null the entire system was in balance. The position of the weights relative to a preselected data plane (a mark on the oil manometer corresponding to the height of the diaphragm in the ambient DPI) was measured with

a cathetometer. This reading along with the identification of the weights on the tester was all the necessary experimental information required to calculate the sample pressure in the Burnett cell. After recording this data, the remaining experimental data were read and recorded. The required data for one complete measurement are listed below.

1) Identification of weights used on dead-weight tester
2) Position of weights relative to data plane (oil head)
3) Mueller bridge reading (temperature)
4) Barometric pressure
5) Temperature of oil at base of dead-weight tester piston
6) Room temperature
7) Temperature of air bath (controlled environment for electronic circuitry)

Having recorded the above data, the first pressure point of the series of points required for a run had been determined. The dead-weight tester was then isolated from the system, lowered to its rest bearing and then turned off. The sensitivities of the DPI's were then lowered. Next, the gas in the upper chamber of the Burnett cell was expanded to the previously evacuated lower chamber. To avoid wear in the packing of the expansion valve, the valve was never opened more than one full turn. After expanding to the second chamber, the vacuum on the exhaust side of the cell was checked to insure that the exhaust valve was not leaking. The intermediate gas pressure was then reduced by bleeding gas from the system. Using the procedure described

earlier, the sample, intermediate gas, and dead-weight tester were brought into balance. Next, the tester was isolated from the system by closing the valve between the ambient DPI and the oil pump. Then the expansion valve was closed down until only about 1/8 turn remained for complete closure. Simultaneously, the intermediate gas pressure was adjusted to compensate for the pressure increase as the expansion valve was closed. One hour was then allowed to elapse to insure that the system had equilibrated. Then the expansion valve was completely closed. While closing the expansion valve, it was imperative that the intermediate gas pressure be kept in perfect balance with the sample pressure. Otherwise, the diaphragm position will not be correct, thereby changing the effective volume of the Burnett cell. Completing this task, the dead-weight tester was again balanced to the system and the required data for a pressure point were taken and recorded. Following this, the gas in the lower chamber of the Burnett cell was exhausted. In the case of krypton and mixtures, the gas was collected in high-pressure containers for reuse in the event that the original supply was depleted. Fortunately, no experimental problems causing a loss of the original supply occurred and the supply was sufficient to conduct all the experiments in this work. After the pressure in the container and the Burnett chamber equalized, the container was isolated and the remaining gas was exhausted through the vacuum system. For the purpose of leak checking, the vacuum system was allowed to pump on the lower chamber of the Burnett cell until the pressure was reduced to one micron of mercury. This check was very important because the expansion valve was never closed with excessive torque to avoid wear on the valve.

After reducing the pressure in the lower chamber of the Burnett cell down to one micron, the exhaust valve was closed. The gas was then expanded from the upper chamber using the procedrue described above. In this manner, repeated expansions were carried out until the sample pressure was reduced to approximately 100 psia. This completed one iso-composition, isothermal run. A second run at the same composition was then made starting at a pressure midway between the initial pressure and the first expansion of the previous run. This not only increased the number of data points but also gave a data consistency test since the two runs were independent.

CHAPTER V

EXPERIMENTAL PROBLEMS

In this chapter, a discussion is offered of the significant experimental problems that were encountered during the course of this work. These problems are not pointed out to emphasize the difficulty in gathering experimental data with the precision required in PVT studies; this difficulty is a recognized fact among experimentalists in this field. Rather, this chapter, hopefully, will define some problem areas that otherwise might not be anticipated, thereby precluding the possibility that a future worker will be caught unaware. The problems will be discussed in the chronological order of occurrence.

Initial Leak Detection

As stated previously, the Burnett method is dependent on a perfectly leak-tight system. In this work, the intermediate gas system also had to be leak tight since the pressure balancing problem would have otherwise been insurmountable. Having previous experience in this area, this worker had long ago reached the conclusion that leak prevention was much easier than leak detection. Thus, great care was exercised in purchasing only high quality valves, tubing and fittings. The system was then assembled carefully, making each connection according to procedures that had been successful in past work. After the construction phase was completed, the Burnett cell and the intermediate

gas system were pressured up and left about eight hours. After eight hours, both the systems had lost pressure. The leak in the intermediate gas system was quickly traced to the bleed valve in the Hiese gauge. After finding this, the second Hiese gauge (in the charge line to the Burnett cell) was checked and also found to be leaking. Since these instruments were new, they had evidently been shipped from the factory in this condition. After repairing these leaks, attention was focused on the Burnett cell. First, each connection was tested, without result, with soap bubbles. Next, a glass Dewar was located that was sufficiently large to enable complete submersion fo the Burnett cell, cryogenic DPI and associated fittings under water. This leak detection method also failed. The leak was not of sufficient magnitude to cause discernible bubble formation. The gas simply diffused into the water. Next, a helium leak detector (mass spectrometer) was borrowed from the School of Mechanical Engineering, but this method was also unsuccessful. As a last resort, the equipment was disassembled and tested in sections. Although this method was a natural candidate from the beginning, it had been avoided until other methods had been exhausted. The reason for this was that fittings usually have the best chance of being leak-tight the first time they are assembled. Fortuitously, the first section tested was the Burnett cell and all valves and fittings below the cryogenic DPI. This section of the apparatus was found to be leak tight. Thus, the majority of connections did not have to be broken. Having traced the leak to the cryogenic DPI, the instrument was returned to the manufacturer for repair. At this point, the exact cause and location of the leak was still unknown. The manufacturer was able to find and repair the

problem. The source of the leak was found to be around the diaphragm between the upper and lower bodies of the cell. The cause of the leak was traced to the fact that the bolts which run through the cell and supply the necessary force to make the metal-to-metal seal effective had not been retorqued after the instrument had been pressure tested (50,000 psi) at the factory.

Equipment Performance at 100° C

Two unrelated and completely unexpected problems were encountered while attempting to run the experimental apparatus at 100° C. Insufficient stability in the temperature control loop was the first problem encountered. After partially solving this problem, it was discovered that the stability of the cryogenic DPI was completely unsatisfactory. Since the solution to these problems would have major equipment revision, possibly making the data taken subsequently inconsistent with the first three isotherms, the equipment was not modified.

A more detailed discussion of these problems is given below.

Temperature Control

As discussed in Chapter III, the design of the temperature control system allowed for wide variation in parameters such as mixing and the total heat flow through the bath. This flexibility was incorporated in the design to enhance the possibility of having a stable temperature control loop for a wide operating range. As expected, the temperature bath functioned quite well while acquiring data on the first three isotherms (-50, 0 +50° C). The temperature fluctuations were normally within $\pm$0.002° C. At 0° C, the temperature control

was better than anticipated, exhibiting fluctions of less than $\pm 0.0005^{\circ}$ C for time periods as long as 24 hours. In spite of this proven performance and the experience gained on the first three isotherms, acceptable temperature control could not be established at 100° C with the system as originally designed. The control loop displayed fluctuations of $\pm 0.2^{\circ}$ C with long term (24 hours) drifts of $\pm 0.5^{\circ}$ C.

The first efforts to solve this problem were directed toward varying the heat flow through the bath by changing the temperature of the heat sink. After allowing sufficient time for the system to lineout, a new attempt to tune the Thermotrol would be made. For each new condition, the preliminary check always indicated that the response of the system was well within the range that would be compatible with the possible adjustment of gain, reset and derivative in the controller. After exhaustive experimentation with different heat loads, the performance of the bath had been improved only marginally.

Following the attempts to make the existing system work, a complete control package taken from idle research equipment was substituted for the original equipment. The temperature control equipment had been custom designed and built by Leeds and Northrup Co. and has been previously described by Lee (48). The control system was of the resistant bridge type, consisting of a sensing element (PRT), a setpoint unit (Wheatstone bridge), a D.C. null detector, a three mode controller, and an A.C. power supply. This system did not noticeably improve the stability of the temperature bath. However, after modifying the system by substituting the precision Mueller bridge and PRT normally used for measurement of the temperature for the existing setpoint unit,

stable control was achieved. In fact, the stability was superior to even the best control (0^{o} C isotherm) that had been attained with the Thermotrol. Although this solved the control problem, it had introduced another. There was no other equipment available for temperature measuring service that offered the required precision. However, the controller could be operated in both manual and feedback modes. Thus, plans were formulated to switch the Mueller bridge and PRT alternately from control and temperature measuring service and normal run preparations were initiated.

Cryogenic DPI Instability

While attempting to zero the DPI's for the first helium run, a problem was encountered that was never successfully resolved. The electronic zero adjustment did not have sufficient range to bring the read-out on scale. This did not appear to be a serious difficulty initially since the instrument also had a mechanical adjustment that actually moved the coil which surrounds the iron core within the instrument. Thus, the temperature bath was lowered and the mechanical adjustment was made such that the read-out was on scale after the temperature had again been established at 100^{o} C. However, the instrument was very unstable. Typically, the read-out would randomly swing full scale with a short period of oscillation (1 to 2 minutes). After a few hours, the read-out would be pegged completely off scale, requiring adjustment to bring it back in range. Within a day, the zero point shift was so large that mechanical adjustment would be required again. After several cycles of adjusting the instrument, the bath temperature was lowered to 50^{o} C to check the possibility

that the problem might not be directly related to the higher temperature operation. However, the instrument performed quite well at the lower temperature, thus substantiating the suspicion that the instability was caused by the elevated temperature.

In fairness to the manufacturer (Ruska Instruments Corp.) of the cryogenic DPI, the specified (or guaranteed) temperature range for the instrument was only 40 to 160^{o} F. However, other workers had used this instrument at temperatures approaching the N_2 boiling point (78^{o} K) without encountering difficulty with stability. Also, the chief designer of the instrument, Mr. Claude Miks, indicated in a private communication that it was quite probable that the instrument would be stable above the specified range as well as below it. This information seemed sufficient to support the assumption made at the beginning of this work that no problems associated with the effect of temperature on the stability of the cryogenic DPI would arise.

The 100^{o} C isotherm could have been completed by modifying the equipment. Specifically, the cryogenic DPI could have been removed to a separate temperature bath and the data subsequently corrected for the varying temperature of the sample gas. However, since future projects were planned in the low temperature range where the instrument was stable, and since the original design with the instrument at the experimental temperature is superior, the decision was made to forego the 100^{o} C data and leave the equipment intact.

CHAPTER VI

PRESENTATION, ANALYSIS AND APPLICATION OF RESULTS

This chapter describes the data reduction method employed to reduce the experimental measurements to compressibility factors and virial coefficients. These results are then compared with results of previous studies. Finally, the results of this work are combined with other experimental information to form the basis for a brief study of molecular interactions, utilizing the Kihara intermolecular potential function.

Data Reduction

As outlined in Chapter II, the experimental measurements associated with a Burnett apparatus do not yield compressibility factors directly. The data must first be reduced by either graphical, linear or non-linear regression techniques. In the present study, a combination of graphical and non-linear regression analysis was used for reduction of the data. While this combination may seem unlikely, the two methods actually compliment each other quite well. The non-linear regression technique offers both the ultimate in precision and the better possibility of determining optimal values for the Burnett parameters as well as the optimal approximations for the virial coefficients. However, this method, if not used judiciously, can also lead to grossly

inaccurate results. (The reasons for this possibility will be discussed in detail later.) The graphical technique, on the other hand, is essentially fool-proof and is limited only by lack of precision and the inability to estimate values for virial coefficients of higher order than the third virial coefficient.

The details of the reduction scheme used in this study are outlined below.

Graphical Regression

The graphical techniques used to reduce Burnett data were presented in Chapter II. For completeness, some of the important features will be reviewed here. First, recalling Equation (4)

$$\frac{P_{j-1}/T_{j-1}}{P_j/T_j} = N_j \frac{Z_{j-1}}{Z_j}$$

From Equation (4), it is apparent that in the limit of an infinite number of expansions the ratio of the compressibility factors will approach unity. Also, the volume ratio, N_j, will approach N_∞ since the pressure corrections will become nil, i.e.,

$$\lim_{P \to 0} \left[\frac{P_{j-1}/T_{j-1}}{P_j/T_j}\right] = N_\infty \qquad (15)$$

Thus, a plot of the pressure-temperature ratios as a function of pressure can be used to evaluate the cell constant N_∞. Using the Burnett runs on helium, the cell constant was evaluated for each isotherm in the above manner. Special mention should be made that the cell constant would be expected to vary slightly with temperature.

However, since the physical make-up of the Burnett apparatus was not altered during the course of the experimental work, variation along an isotherm should not occur.

The next step in the graphical regression is determination of the initial compressibility, Z_0. This procedure is carried out by employing Equation (9).

$$\frac{P_0/T_0}{Z_0} = \frac{P_k/T_k}{Z_k} N_{00}^k \prod_{j=0}^{k} X_j$$

As k become large, Z_k approaches unity. Thus, if $(P_k/T_k) N_{00}^k \prod_{j=0}^{k} X_j$ is expressed as a function of pressure, the limit of this quantity as the pressure approaches zero is equal to $(P_0/T_0)/Z_0$. That is,

$$\lim_{P \to 0} \left[(P_k/T_k) N_{00}^k \prod_{j=0}^{k} X_j\right] = \frac{P_0/T_0}{Z_0}$$

Combining the results obtained from Equation (10) with the experimental value of P_0/T_0 yields the value of the initial compressibility factor. The remaining compressibility factors can then be calculated from Equation (8).

$$Z_k = (P_k/T_k) N_{00}^k \frac{Z_0}{(P_0/T_0)} \prod_{j=0}^{k} X_j$$

In this manner, the compressibilities for each expansion on the three isotherms were evaluated.

The evaluation of the compressibility factors via the above analysis is the step in the graphical technique which limits the precision of the method. The determination of N_{00} can be made with a precision of approximately 1 part in 15,000 by using expanded scales

and selecting helium (linear compressibility as a function of pressure) as the fluid for the determination. However, the determination of the initial compressibility, Z_0, via Equation (10) is much more restrictive. This is due to the fact the plot of $(P_k/T_k)\ N_{00}^{k}\ \prod_{j=0}^{k} X_j$ versus pressure does not yield a linear relationship for the helium-krypton mixtures or the krypton samples. Thus, subjective extrapolation of this curve is difficult. Accordingly, the resulting compressibility factors are estimated to be precise to no more than 1 part in 1,000. For this reason, the compressibility factors from the graphical regression analysis are not reported. The next step in the graphical analysis is to estimate values for the second and third virial coefficients. Starting with the virial equation of state,

$$Z = 1 + B(T)\rho + C(T)\rho^2 + \text{---}$$

Rearranging Equation (12) and stipulating isothermal conditions gives

$$\frac{Z-1}{\rho} = B + C\rho + \text{---} \qquad (16)$$

Examining Equation (16) reveals that a plot of $(Z-1)/\rho$ as a function of molar density (ρ) will result in an estimate of the second virial coefficient, B, as the intercept of this plot and an estimate of the third virial coefficient, C, as the slope of the line at zero density. In all cases, of course, the molar densities are generated by using the previously derived compressibility factors.

Using the procedures described above, the second and third virial coefficients were determined from the Burnett data generated in this study. These values are shown in Table III along with the values obtained for the cell constant, N_{00}. While the results shown in

TABLE III

RESULTS OF GRAPHICAL DETERMINATION OF THE SECOND AND THIRD VIRIAL COEFFICIENTS FOR THE HELIUM - KRYPTON SYSTEM

Composition	B(cc/mol)	C(cc/mol)^2	N_{00}
		50° C	
He	11.59	0.114×10^3	1.58853
25% Kr	12.04	0.33×10^3	
50% Kr	3.50	0.68×10^3	
75% Kr	-14.55	0.125×10^4	
Kr	-41.70	0.212×10^4	
		0° C	
He	11.83	0.126×10^3	1.58823
25% Kr	10.72	0.36×10^3	
50% Kr	- 1.54	0.72×10^3	
75% Kr	-26.04	0.144×10^4	
Kr	-61.65	0.256×10^4	
		-50° C	
He	12.12	0.124×10^3	1.58806
25% Kr	8.30	0.38×10^3	
50% Kr	-10.60	0.92×10^3	
75% Kr	-45.8	0.201×10^4	
Kr	-93.6	0.34×10^4	

Table III are not intended to be the final results for the parameters presented, the results are reliable estimates and further analysis of the data can only serve to refine these values. In other words, any technique yielding values significantly different from those shown in Table III would not be acceptable. The reasons for this are twofold. First, the plot of $(Z-1)/\rho$ as a function of molar density is a foolproof method for an overall evaluation of the precision of the Burnett data. Random errors in the data would result in a scattering effect. Secondly, large systematic errors and/or improper evaluation of the Burnett constants (N_{00} and Z_0) would result in a drastic curvature for the low pressure points on the plot of $(Z-1)/\rho$ verses ρ. This effect is well documented by Canfield (16). Thus, visual inspection of the plots made during the course of the graphical regression analysis are invaluable in the total assessment of the validity of the results of a Burnett study. For the purpose of illustration, an example plot of $(Z-1)/\rho$ is shown in Figure 3.

Non-Linear Regression

Reduction of Burnett data via non-linear regression is a well recognized complex problem and many studies have been conducted in this area.

One of the most comprehensive and fruitful studies is the recent work of Hall (30). Hall developed and subsequently computerized a method which optimally (in a least-square sense) fits a polynomial approximation to the infinite series virial equation of state. Hall's method was originally programmed in Algol but was later converted to Fortran IV by Provine (67). The Fortran IV version of Hall's

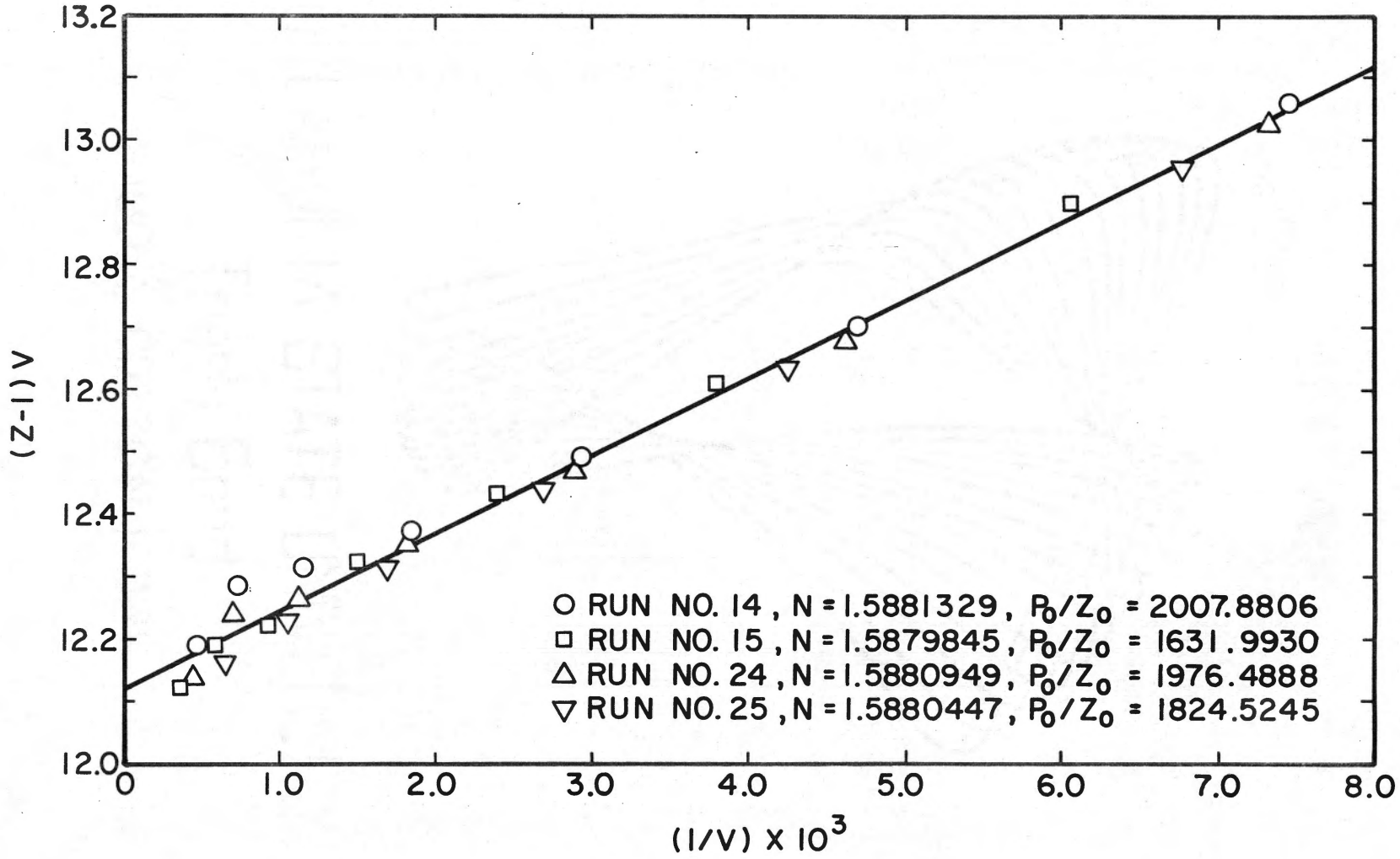

Figure 3. Graphical Determination of the Second Virial Coefficient for Pure Helium at -50° C

method was used in the present study. Since Hall's work is well documented elsewhere (31,32), only a cursory description will be given here.

Recalling Equation (13) from Chapter II,

$$\sum_{k=0}^{\ell} \left[P_k N_{00}^k \left(Z_0/P_0\right) \prod_{j=0}^{k} X_j - \sum_{i=1}^{m+1} B_i \rho_k^{i-1}\right]^2 = \text{Minimum}$$

and remembering that the regression parameters are N_{00}, (Z_0/P_0) and the B_i's, we have the starting point for a non-linear regression analysis. As mentioned in Chapter II, other objective functions are possible but the above function offers the advantage of determining the optimal values of the Burnett constants as well as the virial coefficients. When multiple runs are made at the same composition and temperature, as was the case in this work, Equation (13) is simply duplicated for each run and then summed, i.e.

$$\begin{aligned}\Sigma F^2 = &\sum_{k=0}^{\ell_1} \left[P_{k_1} N_{00_1}^k \left(\frac{Z_0}{P_0}\right)_1 \prod_{j=0}^{k} X_{j_1} - \sum_{i=1}^{m+1} B_i \rho_{k_1}^{i-1}\right]^2 + \\ &\sum_{k=0}^{\ell_2} \left[P_{k_2} N_{00_2}^k \left(\frac{Z_0}{P_0}\right)_2 \prod_{j=0}^{k} X_{j_2} - \sum_{i=1}^{m+1} B_i \rho_{k_2}^{i-1}\right]^2 + \text{---} = \text{Minimum}\end{aligned} \tag{17}$$

where ℓ_1 and ℓ_2 are the number of expansions in each series of pressure measurements.

Equation (17) represents a general objective function which could be used in any non-linear regression method. In the present work, the above function was first used in conjunction with a non-linear regression method proposed by Marquardt (58) which utilizes the Maximum Neighborhood Method. The approximations for the second and third virial

coefficients and the Burnett constants as obtained from the graphical analysis of the data were used as starting guesses in the Marquardt method. After a converged solution was obtained with the two term form of the virial equation of state, the expansion was extended to the fourth virial coefficient with narrow maximum and minimum limits stipulated on the Burnett constants and on the approximations for the second and third virial coefficients. Essentially unbounded limits were used on the initial guess for the approximation for the fourth virial coefficient. After convergence was obtained with the fourth virial coefficient included, the procedure was repeated by adding one additional term to the virial expansion until the expansion had been extended to include the seventh virial coefficient. The results from this analysis were then used as starting guesses for Hall's method.

Hall's method employs Equation (17) for the objective function but limits to two the number of independent runs which can be regressed simultaneously. Hall's method differs from the Marquardt method in two basic ways. First, a quadratic search as outlined by Wilde (92) is used to regress the Burnett constants. The second, and major difference, is that the virial coefficients are not regressed simultaneously with the Burnett constants. Rather, at each iteration, the calculated Burnett constants are used to obtain compressibility factors and densities. Then, these values are used in a technique employing orthonormal functions to extract coefficients which are the least-squares approximation to the true virial coefficients. This iterative scheme is then repeated until successive iterations differ by less than some prescribed tolerance.

Having outlined the procedural aspects of the non-linear regression technique used in this study, the merits and potential problems associated with this method will be discussed. First, as stated earlier, this method offers the distinct advantage of very high precision. The precision is limited only by the basic computer arithematic which in the present work is estimated to be approximately 1 part per million in the calculation of the compressibility factors. Secondly, the method is easily compatible with the use of an extended form of the virial equation of state. Third, and most importantly, non-linear regression offers the advantage of simultaneously determining the optimum (in a least-square sense) values for the Burnett constants and the approximations to the virial coefficients. However, this last advantage can also lead to completely erroneous results if the method is not used judiciously.

As the above discussion implies, the simultaneous regression of the Burnett constants and the polynomial approximations for the virial coefficients can lead to erroneous results. One source of difficulty results from the interdependence of the "experimental" and calculated compressibility factors produced from the non-linear regression technique. Ideally, the "experimental" compressibility factors are calculated from the experimental pressures N_{∞}, and Z_0/P_0 while the calculated values are derived from the polynomial approximation of the virial equation of state. Unfortunately, the "experimental" compressibility factors generated are influenced by the calculated values of the compressibility factors. In other words, any lack of fit between the actual PVT relationship and the particular polynomial approximation used will be reflected to some degree in the experimental compressibility

factors. In fact, the non-linear regression technique will adjust the values of the Burnett constants until the lack of fit is minimized in a least square sense.

Another important characteristic of non-linear treatment of Burnett data is the possibility of a generated functional dependence between the polynomial approximations to the virial coefficients. This characteristic is normally not serious difficulty until terms of higher order than the fourth virial coefficient are added to the polynomial approximation. However, including the approximation for the fifth virial coefficient in the expansion cannot only result in an order of magnitude change in the approximation for the fourth virial coefficient but also a sign reversal.

To illustrate the method by which the non-linear regression analysis was used to refine the results predicted by the graphical analysis, an example will be used. As indicated earlier, the non-linear regression analysis was repeated for a range of m values (the number of coefficients used to approximate the virial equation of state). Table IV shows the results obtained for the nominal 50 mol % helium in krypton on the -50° C isotherm. The regression analysis on this particular sample was chosen for example since the short-comings of the non-linear regression method are clearly demonstrated. This sample also represents the "worst-case" example.

Several observations are apparent from a cursory analysis of the results in Table IV. First, the sum of squares decrease smoothly as additional terms are added to the polynomial approximation. (This is, of course, consistent with expected results.) Secondly, the values for the approximations for the virial coefficients display a functional

TABLE IV

NON-LINEAR REGRESSION EXAMPLE
50 Mol % He in Kr @ -50° C

Parameter	NUMBER OF COEFFICIENTS					
	2	3	4	5	6	7
$B(2)$, cc/mol	-11.56	-11.22	-12.42	-14.42	-19.06	-24.52
$B(3)$, $(cc/mol)^2$	0.995×10^3	0.930×10^3	0.131×10^4	0.222×10^4	0.506×10^4	0.936×10^4
$B(4)$, $(cc/mol)^3$	--	0.451×10^4	0.531×10^5	-0.279×10^6	-0.133×10^7	-0.342×10^7
$B(5)$, $(cc/mol)^4$	--	--	0.309×10^7	0.300×10^8	0.241×10^9	0.851×10^9
$B(6)$, $(cc/mol)^5$	--	--	--	-0.122×10^{10}	-0.225×10^{11}	-0.125×10^{12}
$B(7)$, $(cc/mol)^6$	--	--	--	--	0.850×10^{12}	0.898×10^{13}
$B(8)$, $(cc/mol)^7$	--	--	--	--	--	-0.324×10^{15}
N_{∞_1}	1.58860	1.58843	1.58883	1.58938	1.59036	1.59135
N_{∞_2}	1.5886	1.58849	1.58890	1.58944	1.59042	1.59140
$(P_0/Z_0)_1$, atm	143.057	142.944	143.23	143.64	144.21	145.24
$(P_0/Z_0)_2$, atm	116.354	116.271	116.50	116.81	117.41	118.04
	0.21×10^{-7}	0.18×10^{-7}	0.79×10^{-8}	0.43×10^{-8}	0.13×10^{-8}	0.82×10^{-9}

dependency on the number of terms used in the approximation. Third, the Burnett constants exhibit a smooth functional trend with increasing terms.

Selecting the best fit from the various cases shown in Table IV would prove to be a difficult task without the benefit of the results obtained from the graphical regression technique. However, comparing the values for N_{00}, the second virial coefficient and the third virial coefficient generated from the graphical results with the various cases results in the selection of the expansion using three terms in the polynomial approximation as the obvious choice. The approximation for the second virial coefficient is -10.6 cc/mol and -11.2 cc/mol for the graphical and non-linear regression, respectively. Furthermore, the values generated for the cell constant, N_{00}, by the two methods are in better agreement for the case selected than the other alternates.

Using the methods described above, the Burnett data from this study were reduced and the results of the regression analysis are presented in Tables V through XXIII. Each table contains the experimental and calculated results for two independent Burnett runs. The series of pressure values reported in the first column of the tables is the experimental information from which all other data were calculated.

Below each table, the least-square approximations for the virial coefficients are presented along with the standard deviations for each parameter. Other information reported includes the Burnett parameters N_{00} and P_0/Z_0 for each run and the total sum of squares for both runs.

The information reported in Tables V through XXIII is the final

TABLE V

RESULTS OF REGRESSION ANALYSIS
FOR PURE KRYPTON AT -50° C

Pressure (ATM)	$Z_{Burnett}$	Z_{Calc}	$(Z_B-Z_C) \times 10^5$	Density (mole/cc)
77.2332	0.3651417	0.3651350	0.68	0.0115514
66.5241	0.4996533	0.4996029	5.04	0.00727115
53.8348	0.6423651	0.6424240	-5.89	0.00457692
39.9777	0.7578163	0.7578041	1.22	0.00288102
27.9198	0.8407869	0.8407725	1.44	0.00181351
18.7509	0.8970569	0.8971003	-4.34	0.00114155
12.2910	0.9341362	0.9341743	-3.80	0.000718569
7.9363	0.9582273	0.9581487	7.86	0.000452317
74.7410	0.3887610	0.3887764	-1.55	0.0104995
64.1646	0.5301925	0.5302165	-2.39	0.00660928
50.9568	0.6688852	0.6688991	-1.39	0.00416048
37.2857	0.7775022	0.7774278	7.44	0.00261899
25.7905	0.8543333	0.8543004	3.29	0.00164864
17.2174	0.9060347	0.9060778	-4.31	0.00103781
11.2442	0.9399680	0.9400064	-3.85	0.000653294
7.2434	0.9619051	0.9618907	1.45	0.000411245

$\Sigma(Z_B-Z_C)^2 = 0.271 \times 10^{-7}$ B(2) = -94.0823 $\sigma = 0.24$

$N_1 = 1.58863$ B(3) = 0.342993×10^4 $\sigma = 0.71 \times 10^2$

$N_2 = 1.58857$ B(4) = 0.228443×10^5 $\sigma = 0.74 \times 10^4$

$(P_0/Z_0)_1 = 211.516$ B(5) = -0.230077×10^7 $\sigma = 0.26 \times 10^6$

$(P_0/Z_0)_2 = 192.254$

TABLE VI

RESULTS OF REGRESSION ANALYSIS
FOR 75% Kr IN He AT -50° C

Pressure (ATM)	$Z_{Burnett}$	Z_{Calc}	$(Z_B-Z_C) \times 10^5$	Density (mole/cc)
138.0542	0.7410941	0.7411098	- 1.57	0.0101735
92.3892	0.7875483	0.7876660	-11.80	0.00640674
62.6109	0.8475031	0.8474836	1.95	0.00403461
41.7141	0.8968395	0.8966855	15.40	0.00254077
27.3129	0.9322477	0.9321027	14.50	0.00160003
17.6392	0.9560445	0.9561293	- 8.49	0.00100761
11.2924	0.9719023	0.9719343	- 3.20	0.000634536
7.1856	0.9820486	0.9821527	-10.40	0.000399596
114.9930	0.7567199	0.7566550	6.49	0.00829908
77.9334	0.8146988	0.8146287	7.01	0.00522420
52.4414	0.8708822	0.8709635	- 8.13	0.00328858
34.6405	0.9138608	0.9139819	-12.10	0.00207012
22.5218	0.9438700	0.9439795	010.90	0.00130312
14.4799	0.9640210	0.9639998	2.12	0.000820300
9.2399	0.9772402	0.9770482	19.20	0.000516370

$\Sigma(Z_B-Z_C)^2 = 0.158 \times 10^{-6}$ B(2) = -45.3972 $\sigma = 0.36$

$N_1 = 1.58794$ B(3) = 0.183094×10^4 $\sigma = 0.63 \times 10^2$

$N_2 = 1.58858$ B(4) = 0.127787×10^5 $\sigma = 0.36 \times 10^4$

$(P_0/Z_0)_1 = 186.284$

$(P_0/Z_0)_2 = 151.963$

TABLE VII

RESULTS OF REGRESSION ANALYSIS
FOR 50% Kr IN He AT -50° C

Pressure (ATM)	$Z_{Burnett}$	Z_{Calc}	$(Z_B-Z_C) \times 10^5$	Density (mole/cc)
138.8258	0.9711884	0.9711786	0.97	0.00780656
87.0972	0.9678342	0.9678283	0.59	0.00491469
55.1993	0.9743139	0.9743065	0.74	0.00309405
35.0028	0.9816603	0.9816986	-3.82	0.00194786
22.1759	0.9876126	0.9876432	-3.05	0.00122627
14.0219	0.9919364	0.9918916	4.48	0.000771998
8.8527	0.9947718	0.9947654	0.64	0.000486010
112.4737	0.9673405	0.9673678	-2.73	0.00634986
71.0227	0.9703035	0.9702769	2.66	0.00399744
45.0527	0.9777242	0.9777147	0.95	0.00251650
28.5601	0.9845570	0.9845706	-1.36	0.00158421
18.0738	0.9897281	0.9897359	-0.78	0.000997299
11.4201	0.9933995	0.9933212	7.83	0.000627826
7.2054	0.9956325	0.9957096	-7.71	0.000395233

$\Sigma(Z_B-Z_C)^2 = 0.185 \times 10^{-7}$ $\quad$ $B(2) = -11.2234$ $\quad$ $\sigma = 0.25$

$N_1 = 1.58843$ $\quad$ $B(3) = 0.929538 \times 10^3$ $\quad$ $\sigma = 0.46 \times 10^2$

$N_2 = 1.58849$ $\quad$ $B(4) = 0.451188 \times 10^4$ $\quad$ $\sigma - 0.31 \times 10^4$

$(P_0/Z_0)_1 = 142.944$

$(P_0/Z_0)_2 = 116.271$

TABLE VIII

RESULTS OF REGRESSION ANALYSIS
FOR 25% Kr IN He AT -50° C

Pressure (ATM)	$Z_{Burnett}$	Z_{Calc}	$(Z_B-Z_C) \times 10^5$	Density (mole/cc)
87.7135	1.0439641	1.0441065	-14.20	0.00443159
52.4284	1.0261325	1.0260439	8.85	0.00279033
32.6817	1.0158888	1.0157135	17.50	0.00175692
20.4561	1.0098842	1.0096223	26.20	0.00110623
12.8204	1.0052065	1.0059510	-74.40	0.000696527
8.0632	1.0040764	1.0037043	37.20	0.000438563
111.9965	1.0603927	1.0603161	7.66	0.00576807
68.8350	1.0349973	1.0350544	- 5.72	0.00363214
42.7537	1.0208787	1.0209131	- 3.45	0.00228714
26.7059	1.0126985	1.0127087	- 1.02	0.00144019
16.7350	1.0077929	1.0078201	- 2.72	0.000906875
10.5073	1.0048660	1.0048519	1.41	0.000571051
6.6044	1.0030489	1.0030265	2.23	0.000359586

$\Sigma(Z_B-Z_C)^2 = 0.832 \times 10^{-6}$ B(2) = 8.28105 $\sigma = 0.83$

$N_1 = 1.58820$ B(3) = 0.377220×10^3 $\sigma = 0.82 \times 10^2$

$N_2 = 1.58807$

$(P_0/Z_0)_1 = 81.1460$

$(P_0/Z_0)_2 = 105.618$

TABLE IX

RESULTS OF REGRESSION ANALYSIS
FOR PURE HELIUM AT -50° C
RUNS 14 AND 15

Pressure (ATM)	$Z_{Burnett}$	Z_{Calc}	$(Z_B-Z_C) \times 10^5$	Density (mole/cc)
149.9418	1.0972087	1.0972121	-0.34	0.00746322
91.1660	1.0594700	1.0594864	-1.64	0.00469934
56.1736	1.0367754	1.0367722	0.32	0.00295897
34.8967	1.0229022	1.0228826	1.96	0.00186313
21.7884	1.0143195	1.0143006	1.89	0.00117312
13.6468	1.0089703	1.0089618	0.85	0.000738659
8.5639	1.0055873	1.0056259	-3.86	0.000465098
119.7385	1.0779079	1.0778942	1.37	0.00606652
73.3001	1.0479094	1.0479105	-0.11	0.00382009
45.3555	1.0297160	1.0297172	-0.12	0.00240550
28.2496	1.0185209	1.0185335	-1.26	0.00151473
17.6671	1.0115691	1.0115994	-3.03	0.000953813
11.0778	1.0072861	1.0072759	1.02	0.000600609
6.9570	1.0046015	1.0045704	3.11	0.000378200

$\Sigma(Z_B-Z_C)^2 = 0.494 \times 10^{-8}$ B(2) = 12.0344 σ = 0.042

N_1 = 1.58817 B(3) = 0.132793×10^3 σ = 3.15

N_2 = 1.58807

$(P_0/Z_0)_1$ = 136.658

$(P_0/Z_0)_2$ = 111.083

TABLE X

RESULTS OF REGRESSION ANALYSIS
FOR PURE HELIUM AT -50° C
RUNS 24 AND 25

Pressure (ATM)	$Z_{Burnett}$	Z_{Calc}	$(Z_B-Z_C) \times 10^5$	Density (mole/cc)
147.3625	1.0952428	1.0952390	0.38	0.00734800
89.6541	1.0582520	1.0582596	-0.76	0.00462673
55.2638	1.0360067	1.0360058	0.10	0.00291321
34.3400	1.0224108	1.0224023	0.85	0.00183429
21.4438	1.0139863	1.0139990	-1.28	0.00115495
13.4324	1.0087847	1.0087722	1.25	0.000727206
8.4303	1.0055009	1.0055066	-0.58	0.000457881
135.0573	1.0873928	1.0873964	-0.36	0.00678304
82.3968	1.0535796	1.0535750	0.46	0.00427106
50.8766	1.0331617	1.0331569	0.47	0.00268932
31.6468	1.0206449	1.0206487	-0.38	0.00169335
19.7755	1.0129025	1.0129109	-0.84	0.00106623
12.3927	1.0081003	1.0080934	0.68	0.000671360

$\Sigma(Z_B-Z_C)^2 = 0.686 \times 10^{-9}$ B(2) = 11.9642 σ = 0.022

N_1 = 1.58819 B(3) = 0.135683×10^3 σ 1.54

N_2 = 1.58816

$(P_0/Z_0)_1$ = 134.548

$(P_0/Z_0)_2$ = 124.203

TABLE XI

RESULTS OF REGRESSION ANALYSIS
FOR PURE KRYPTON AT 0° C

Pressure (ATM)	$Z_{Burnett}$	Z_{Calc}	$(Z_B-Z_C) \times 10^5$	Density (mole/cc)
137.1930	0.6449636	0.6449495	1.41	0.00949042
96.8251	0.7229737	0.7229670	0.67	0.00597522
67.8230	0.8043489	0.8043750	-2.60	0.00376202
46.1023	0.8684025	0.8684283	-2.57	0.00236859
30.5445	0.9138292	0.9138300	-0.08	0.00149127
19.8754	0.9444512	0.9444263	2.49	0.000938910
12.7794	0.9645138	0.9644871	2.76	0.000591140
8.1535	0.9774101	0.9774334	-2.33	0.000372184
117.5426	0.6753317	0.6753696	-3.79	0.00776545
83.2700	0.7598436	0.7597904	5.32	0.00488937
57.5851	0.8345640	0.8345592	0.48	0.00307850
38.6747	0.8902044	0.8902049	-0.05	0.00193832
25.4016	0.9286193	0.9286383	-1.90	0.00122043
16.4342	0.9542007	0.9541839	1.68	0.000768419
10.5272	0.9707714	0.9708021	-3.08	0.000483820
6.7015	0.9814937	0.9814771	1.65	0.000304628

$\Sigma(Z_B-Z_C)^2 = 0.961 \times 10^{-8}$ B(2) = -61.5807 $\sigma = 0.019$

$N_1 = 1.58830$ B(3) = 0.254670×10^4 $\sigma = 1.58$

$N_2 = 1.58823$

$(P_0/Z_0)_1 = 212.714$

$(P_0/Z_0)_2 = 174.052$

TABLE XII

RESULTS OF REGRESSION ANALYSIS
FOR 75% Kr IN He AT 0° C

Pressure (ATM)	$Z_{Burnett}$	Z_{Calc}	$(Z_B-Z_C) \times 10^5$	Density (mole/cc)
137.7038	0.8914387	0.8914400	-0.13	0.00689196
88.9618	0.9145264	0.9145184	0.80	0.00434006
57.5630	0.9396938	0.9397107	-1.69	0.002733040
37.0151	0.9595617	0.9595551	0.66	0.00172105
23.6495	0.9735739	0.9735683	0.57	0.00108378
15.0366	0.9829868	0.9829788	0.80	0.000682479
9.5278	0.9891219	0.9891333	-1.14	0.000429770
114.7363	0.8996366	0.8996349	0.17	0.00569013
74.3158	0.9253920	0.9253989	-0.70	0.00358297
47.9733	0.9486901	0.9486890	0.12	0.00225613
30.7608	0.9660572	0.9660174	3.98	0.00142064
19.6066	0.9778888	0.9779501	-6.13	0.000894543
12.4467	0.9858775	0.9858601	1.74	0.000563273
7.8782	0.9910064	0.9909958	1.06	0.000354680

$\Sigma(Z_B-Z_C)^2 = 0.643 \times 10^{-8}$ B(2) = -25.8655 $\sigma = 0.17$

$N_1 = 1.58801$ B(3) = 0.134340×10^4 $\sigma = 0.38 \times 10^2$

$N_2 = 1.58811$ B(4) = 0.180027×10^5 $\sigma = 0.29 \times 10^2$

$(P_0/Z_0)_1 = 154.474$

$(P_0/Z_0)_2 = 127.536$

TABLE XIII

RESULTS OF REGRESSION ANALYSIS
FOR 50% Kr IN He AT 0° C

Pressure (ATM)	$Z_{Burnett}$	Z_{Calc}	$(Z_B-Z_C) \times 10^5$	Density (mole/cc)
136.5166	1.0164368	1.0164329	0.39	0.00599230
84.8647	1.0035520	1.0035332	1.89	0.00377290
53.2248	0.9996540	0.9996669	-1.29	0.00237549
33.4826	0.9987966	0.9988122	-1.56	0.00149565
21.0822	0.9988504	0.9988733	-2.30	0.000941681
13.2777	0.9991568	0.991427	1.41	0.000592895
8.3620	0.9994233	0.9994022	2.11	0.000373295
110.8253	1.0089987	1.0090130	-1.44	0.00490046
69.2354	1.0012371	1.0012364	0.07	0.00308517
43.4952	0.9991007	0.9990978	0.28	0.00194232
27.3750	0.9988088	0.9987855	2.33	0.00122281
17.2378	0.9990137	0.9989840	2.97	0.000769837
10.8544	0.9992136	0.9992620	-4.84	0.000484659

$\Sigma(Z_B-Z_C)^2 = 0.593 \times 10^{-8}$ B(2) = -1.86340 σ = 0.25

N_1 = 1.58827 B(3) = 0.697024×10^3 $\sigma = 0.56 \times 10^2$

N_2 = 1.58840 B(4) = 0.119462×10^5 $\sigma = 0.48 \times 10^4$

$(P_0/Z_0)_1$ = 134.309

$(P_0/Z_0)_2$ = 109.837

TABLE XIV

RESULTS OF REGRESSION ANALYSIS
FOR 25% Kr IN He AT 0° C

Pressure (ATM)	$Z_{Burnett}$	Z_{Calc}	$(Z_B-Z_C) \times 10^5$	Density (mole/cc)
136.3563	1.0716208	1.0716388	- 1.80	0.00567705
83.5019	1.0423076	1.0423163	- 0.88	0.00357428
51.7270	1.0255460	1.0255372	0.89	0.00225035
32.2525	1.0156425	1.0156400	0.25	0.00141681
20.1875	1.0097227	1.0096732	4.95	0.000892010
12.6639	1.0060701	1.0060213	4.88	0.000561601
7.9540	1.0036614	1.0037637	-10.20	0.000353577
110.2614	1.0569973	1.0569647	3.26	0.00465413
67.9123	1.0339987	1.0339926	0.61	0.00293033
42.2059	1.0206299	1.0206597	- 2.98	0.00184499
26.3660	1.0126619	1.0127132	- 5.13	0.00116163
16.5218	1.0078647	1.0078877	- 2.30	0.000731379
10.3727	1.0049985	1.0049199	7.86	0.000460485

$\Sigma(Z_B-Z_C)^2 = 0.271 \times 10^{-7}$ B(2) = 10.5134 $\sigma = 0.16$

$N_1 = 1.58833$ B(3) = 0.370896×10^3 $\sigma = 0.15 \times 10^2$

$N_2 = 1.58827$

$(P_0/Z_0)_1 = 127.243$

$(P_0/Z_0)_2 = 104.316$

TABLE XV

RESULTS OF REGRESSION ANALYSIS
FOR PURE HELIUM AT 0^{o} C
RUNS 1 AND 2

Pressure (ATM)	$Z_{Burnett}$	Z_{Calc}	$(Z_B-Z_C) \times 10^5$	Density (mole/cc)
144.8133	1.0753987	1.0754057	-0.70	0.00600796
88.7235	1.0464564	1.0464495	0.69	0.00378274
54.9207	1.0288333	1.0288378	-0.46	0.00238166
34.2143	1.0179945	1.0179951	-0.06	0.00149951
21.3998	1.0112931	1.0112658	2.72	0.000944106
13.4168	1.0070436	1.0070677	-2.41	0.000594415
137.6066	1.0717133	1.0717042	0.91	0.00572861
84.4131	1.0442004	1.0442108	-1.04	0.00360674
52.2940	1.0274606	1.0274646	-0.40	0.00227078
32.5938	1.0171611	1.0171447	1.64	0.00142967
20.3910	1.0107272	1.0107359	-0.88	0.000900103
12.7869	1.0067089	1.0067362	-2.73	0.000566695
8.0320	1.0043948	1.0042319	16.30	0.000356785

$\Sigma(Z_B-Z_C)^2 = 0.293 \times 10^{-7}$ $\quad B(2) = 11.8176$ $\quad \sigma = 0.09$

$N_1 = 1.58829$ $\quad B(3) = 0.122072 \times 10^3$ $\quad \sigma = 7.35$

$N_2 = 1.58834$

$(P_0/Z_0)_1 = 134.660$

$(P_0/Z_0)_2 = 128.399$

TABLE XVI

RESULTS OF REGRESSION ANALYSIS
FOR PURE HELIUM AT 0° C
RUNS 3 AND 4

Pressure (ATM)	$Z_{Burnett}$	Z_{Calc}	$(Z_B-Z_C) \times 10^5$	Density (mole/cc)
35.5990	1.0187516	1.0187479	0.37	0.00155904
22.2597	1.0117265	1.0117376	-1.11	0.000981624
13.9551	1.0073757	1.0073639	1.17	0.000618061
8.7626	1.0046217	1.0046261	-0.44	0.000389151
137.6192	1.0717091	1.0717051	0.40	0.00572916
84.4264	1.0442322	1.0442466	-1.44	0.00360720
52.3045	1.0275032	1.0275013	0.19	0.00227114
32.6013	1.0171995	1.0171737	2.58	0.00142994
20.3961	1.0107582	1.017566	0.15	0.000900302
12.7906	1.0067438	1.0067502	-0.64	0.000566838
8.0332	1.0042637	1.0042412	2.25	0.000356886

$\Sigma(Z_B-Z_C)^2 = 0.174 \times 10^{-8}$ B(2) = 11.8419 σ = 0.051

N_1 = 1.58823 B(3) = 0.117633×10^3 σ = 5.27

N_2 = 1.58829

$(P_0/Z_0)_1$ = 34.9437

$(P_0/Z_0)_2$ = 128.411

TABLE XVII

RESULTS OF REGRESSION ANALYSIS
FOR PURE HELIUM AT 0° C
RUNS 4 AND 5

Pressure (ATM)	$Z_{Burnett}$	Z_{Calc}	$(Z_B-Z_C) \times 10^5$	Density (mole/cc)
137.6193	1.0717872	1.0717897	-0.25	0.00572874
84.4265	1.0442928	1.0443063	-1.35	0.00360699
52.3045	1.0275477	1.0275416	0.60	0.00227104
32.6013	1.0172284	1.0172002	2.82	0.00142990
20.3961	1.0107719	1.0107738	-0.19	0.000900290
12.7906	1.0067426	1.0067613	-1.87	0.000566838
8.0332	1.0042476	1.0042483	-0.07	0.000356891
109.1898	1.0571549	1.0571441	1.08	0.00460820
67.3361	1.0354015	1.0354017	-0.01	0.00290153
41.8509	1.0220488	1.0220609	-1.21	0.00182693
26.1381	1.0137902	1.0137994	-0.92	0.00115031
16.3740	1.0086466	1.0086526	-0.60	0.000724278
10.2771	1.0054539	1.0054337	2.02	0.000456033

$\Sigma(Z_B-Z_C)^2 = 0.217 \times 10^{-8}$ $B(2) = 11.8618$ $\sigma = 0.050$

$N_1 = 1.58826$ $B(3) = 0.116895 \times 10^3$ $\sigma = 4.74$

$N_2 = 1.58821$

$(P_0/Z_0)_1 = 128.402$

$(P_0/Z_0)_2 = 103.286$

TABLE XVIII

RESULTS OF REGRESSION ANALYSIS
FOR PURE KRYPTON AT 50° C

Pressure (ATM)	$Z_{Burnett}$	Z_{Calc}	$(Z_B-Z_C) \times 10^5$	Density (mole/cc)
107.0326	0.8485439	0.8486291	- 8.52	0.00475693
70.9213	0.8932621	0.8933250	- 6.29	0.00299422
46.4125	0.9287353	0.9283408	39.40	0.00188464
29.9760	0.9529995	0.9531078	-10.80	0.00118622
19.1949	0.9695550	0.9697770	-22.20	0.000746620
12.2202	0.9806959	0.9806968	- 0.09	0.000469925
7.7474	0.9878346	0.9877393	9.52	0.000295771
137.7226	0.8200587	0.8200196	3.92	0.00633353
91.6008	0.8665060	0.8665089	- 0.29	0.00398670
60.4159	0.9079657	0.9079714	- 0.56	0.00250938
39.3208	0.9388511	0.9389036	- 5.25	0.00157947
25.3131	0.9602442	0.9602886	- 4.44	0.000994143
16.1689	0.9745051	0.9745075	- 0.24	0.000625723
10.2743	0.9838411	0.9837577	8.34	0.000393833

$\Sigma(Z_B-Z_C)^2 = 0.250 \times 10^{-6}$ B(2) = -42.0918 $\sigma = 0.26$

$N_1 = 1.58883$ B(3) = 0.215910×10^4 $\sigma = 0.28 \times 10^2$

$N_2 = 1.58882$

$(P_0/Z_0)_1 = 126.137$

$(P_0/Z_0)_2 = 167.942$

TABLE XIX

RESULTS OF REGRESSION ANALYSIS
FOR 75% Kr IN He AT 50° C

Pressure (ATM)	$Z_{Burnett}$	Z_{Calc}	$(Z_B-Z_C) \times 10^5$	Density (mole/cc)
138.7104	0.9596403	0.9596370	0.33	0.00545112
87.8964	0.9656250	0.9656681	-4.31	0.00343268
55.8840	0.9750120	0.9750124	0.04	0.00216154
35.4775	0.9830088	0.9829714	3.74	0.00136107
22.4712	0.9888230	0.9887748	4.82	0.000857026
14.2056	0.9927582	0.9927351	2.31	0.000539637
8.9672	0.9952643	0.9953482	-8.39	0.000339787
113.3415	0.9612459	0.9612445	0.14	0.00444672
72.0080	0.9698410	0.9698026	3.84	0.00280005
45.7632	0.9788683	0.9787785	8.88	0.00176310
29.0099	0.9854869	0.9857852	-29.80	0.00111015
18.3654	0.9908462	0.9907173	12.90	0.000699003
11.6016	0.9940970	0.9940248	7.22	0.000440122
7.3200	0.9961649	0.9961865	-2.15	0.000277118

$\Sigma(Z_B-Z_C)^2 = 0.134 \times 10^{-6}$ B(2) = -14.0742 σ = 1.06

N_1 = 1.58818 B(3) = 0.112336×10^4 $\sigma = 0.28 \times 10^3$

N_2 = 1.58822 B(4) = 0.183760×10^5 $\sigma = 0.27 \times 10^5$

$(P_0/Z_0)_1$ = 144.544

$(P_0/Z_0)_2$ = 117.911

TABLE XX

RESULTS OF REGRESSION ANALYSIS
FOR 50% Kr IN He AT 50° C

Pressure (ATM)	$Z_{Burnett}$	Z_{Calc}	$(Z_B-Z_C) \times 10^5$	Density (mole/cc)
137.5399	1.0354257	1.0354275	-0.17	0.00500951
85.1598	1.0181873	1.0181890	-0.17	0.00315422
53.1829	1.0099205	1.0099134	0.71	0.00198596
33.3427	1.0056551	1.0056549	0.02	0.00125037
20.9440	1.0033398	1.0033336	0.62	0.000787223
13.1683	1.0019841	1.0020104	-2.63	0.000495625
8.2844	1.0012485	1.0012310	1.75	0.000312038
111.1707	1.0261947	1.0261896	0.51	0.00408551
69.1532	1.0138219	1.0138294	-0.75	0.00257239
43.2771	1.0077010	1.0077033	-0.24	0.00161961
27.1598	1.0044636	1.0044648	-0.12	0.00101971
17.0693	1.0026776	1.0026615	1.62	0.000642006
10.7351	1.0016064	1.0016171	-1.07	0.000404200

$\Sigma(Z_B-Z_C)^2 = 0.156 \times 10^{-8}$ $\quad B(2) = 3.75835$ $\quad \sigma = 0.15$

$N_1 = 1.58837$ $\quad B(3) = 0.594501 \times 10^3$ $\quad \sigma = 0.40 \times 10^2$

$N_2 = 1.58836$ $\quad B(4) = 0.133704 \times 10^5$ $\quad \sigma = 0.41 \times 10^4$

$(P_0/Z_0)_1 = 132.834$

$(P_0/Z_0)_2 = 108.333$

TABLE XXI

RESULTS OF REGRESSION ANALYSIS
FOR 25% Kr IN He AT 50° C

Pressure (ATM)	$Z_{Burnett}$	Z_{Calc}	$(Z_B-Z_C) \times 10^5$	Density (mole/cc)
137.9385	1.0669468	1.0669470	-0.02	0.00487560
84.6743	1.0402958	1.0402970	-0.12	0.00306959
52.5044	1.0246330	1.0246352	0.22	0.00193247
32.7497	1.0152200	1.0152179	0.21	0.00121656
20.5001	1.0094718	1.0094648	0.70	0.000765858
12.8597	1.0059102	1.0059126	-0.24	0.000482123
8.0777	1.0036997	1.0037040	-0.43	0.000303505
68.7433	1.0324979	1.0324940	0.39	0.00251089
42.7528	1.0199669	1.0199659	0.11	0.00158076
26.7529	1.0123612	1.0123748	-1.36	0.000995160
16.7406	1.0077202	1.0077133	0.69	0.000626492
10.5085	1.0048278	1.0048252	0.26	0.000394398

$\Sigma(Z_B-Z_C)^2 = 0.341 \times 10^{-9}$ B(2) = 12.1026 $\sigma = 0.025$

$N_1 = 1.58853$ B(3) = 0.333990×10^3 $\sigma = 2.79$

$N_2 = 1.58850$

$(P_0/Z_0)_1 = 129.283$

$P_0/Z_0)_2 = 66.5797$

TABLE XXII

RESULTS OF REGRESSION ANALYSIS
FOR PURE HELIUM AT 50° C
RUNS 26 AND 27

Pressure (ATM)	$Z_{Burnett}$	Z_{Calc}	$(A_B-Z_C) \times 10^5$	Density (mole/cc)
144.3360	1.0627152	1.0627089	0.63	0.00512204
88.8391	1.0388551	1.0388789	-2.38	0.00322504
55.1480	1.0242570	1.0242386	1.84	0.00203051
34.4129	1.0151744	1.0151654	0.90	0.00127840
21.5447	1.0095024	1.0095102	-0.78	0.000804856
13.5166	1.0059696	1.0059724	-0.29	0.000506717
116.1465	1.0506466	1.0506483	-0.17	0.00416903
71.7882	1.0314852	1.0314855	-0.03	0.00262468
44.6765	1.0196812	1.0196626	1.87	0.00165234
27.9217	1.0123039	1.0123152	-1.13	0.00104020
17.4974	1.0077083	1.0077277	-1.94	0.000654825
10.9837	1.0048568	1.0048548	0.20	0.000412222
6.9021	1.0030735	1.0030522	2.12	0.000259498

$\Sigma(Z_B-Z_C)^2 = 0.240 \times 10^{-8}$ B(2) = 11.7364 $\sigma = 0.052$

$N_1 = 1.58840$ B(3) = 0.988972×10^2 $\sigma = 5.69$

$N_2 = 1.58855$

$(P_0/Z_0)_1 = 135.818$

$(P_0/Z_0)_2 = 110.548$

TABLE XXIII

RESULTS OF REGRESSION ANALYSIS
FOR PURE HELIUM AT 50° C
RUNS 28 AND 37

Pressure (ATM)	$Z_{Burnett}$	Z_{Calc}	$(Z_B-Z_C) \times 10^5$	Density (mole/cc)
129.8976	1.0561231	1.0561238	-0.07	0.00463844
80.1271	1.0347799	1.0347844	-0.45	0.00292023
49.8052	1.0216815	1.0216806	0.09	0.00183842
31.1050	1.0135696	1.0135623	0.74	0.00115734
19.4834	1.0085052	1.0085035	0.17	0.000728572
12.2266	1.0053406	1.0053395	0.10	0.000458647
7.6815	1.0033482	1.0033559	-0.78	0.000288724
103.0856	1.0446574	1.0446544	0.30	0.00372143
63.8504	1.0277604	1.0277596	0.08	0.00234292
39.7897	1.0173389	1.0173360	0.29	0.00147500
24.8894	1.0108415	1.0108582	-1.66	0.000928573
15.6063	1.0068169	1.0068136	0.33	0.000584570
9.8000	1.0042891	1.0042806	0.84	0.000368004

$\Sigma(Z_B-Z_C)^2 = 0.517 \times 10^{-9}$ B(2) = 11.5917 σ = 0.029

N_1 = 1.58855 B(3) = 0.109524×10^3 σ = 3.50

N_2 = 1.58850

$(P_0/Z_0)_1$ = 122.995

$(P_0/Z_0)_2$ = 98.6788

results for the experimental phase of this study. The number of significant figures to which the various values are reported was kept very high for mathematical consistency and is not intended to imply actual precision. The uncertainty of the results will be assessed in a later section of this chapter.

Table XXIV presents a summary of the values obtained for the second and the third virial coefficients. For convenience, the values from the graphical analysis are also reported in Table XXIV along with the values obtained for the cell constant, N_{∞}. The cell constant reported for the non-linear regression analysis is the arithmematic average of the values obtained for the multiple runs at each composition.

The second and third virial coefficients are shown graphically in Figures 4 and 5, respectively. This is an important method of presentation since the virial coefficients would be expected to display a fairly smooth relationship with temperature. A cursory inspection of Figures 4 and 5 indicate that this is the case for the virial coefficients generated in this study. Similarly, the compressibility factors are shown graphically in Figures 6,7,8,9 and 10.

Interaction Virial Coefficients

The mixture virial coefficient can be expressed rigorously as a function of composition, the pure virials and the interaction virial, i.e.,

$$B_M = Y_1^2 B_{11} + 2Y_1 Y_2 B_{12} + Y_2^2 B_{22} \qquad (18)$$

Since all quantities except B_{12} are known from experimental information,

TABLE XXIV

SUMMARY OF REGRESSION ANALYSIS

Composition	Second Virial Coefficient (cc/mol)		Third Virial$_2$ Coefficient (cc/mol)^2 x10^{-3}		Cell Constant	
	Final	Graphical	Final	Graphical	Final	Graphical
			-50° C			
He	11.7	11.6	0.10	0.11	1.5885	1.5885
25% Kr	12.1	12.0	0.33	0.33	1.5885	
50% Kr	3.8	3.5	0.60	0.68	1.5884	
75% Kr	-14.1	-14.6	1.12	1.25	1.5882	
Kr	-42.1	-41.7	2.16	2.12	1.5888	
			0° C			
He	11.8	11.8	0.12	0.13	1.5883	1.5882
25% Kr	10.5	10.7	0.37	0.36	1.5883	
50% Kr	- 1.9	- 1.5	0.70	0.72	1.5883	
75% Kr	-25.9	-26.0	1.34	1.44	1.5881	
Kr	-61.6	-61.7	2.55	2.56	1.5883	
			-50° C			
He	12.0	12.1	0.13	0.12	1.5881	1.5881
25% Kr	8.3	8.3	0.38	0.38	1.5881	
50% Kr	-11.2	-10.6	0.93	0.92	1.5885	
75% Kr	-45.4	-45.8	1.83	2.01	1.5883	
Kr	-94.1	-93.6	3.42	3.35	1.5886	

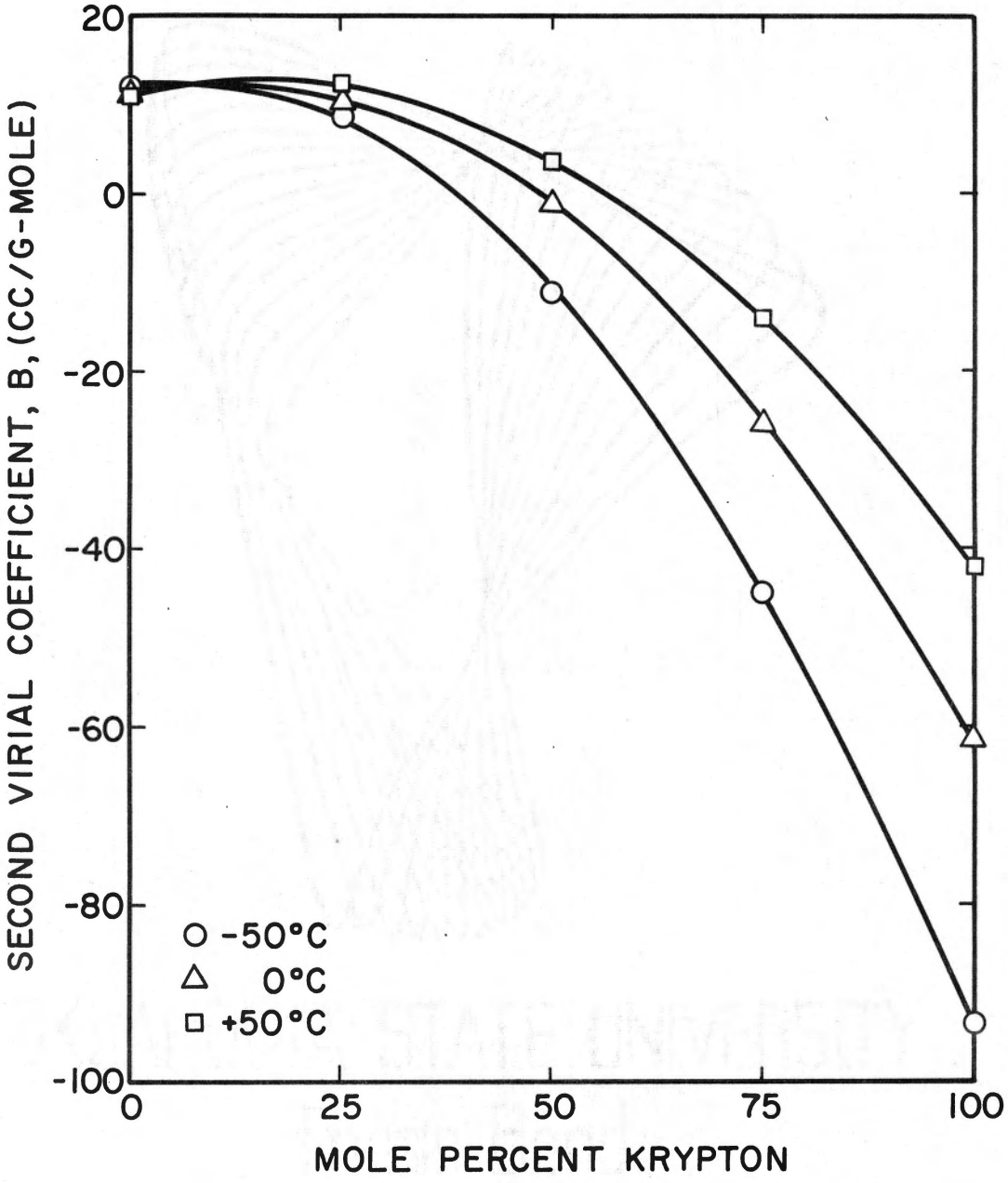

Figure 4. Second Virial Coefficients for the Helium-Krypton System

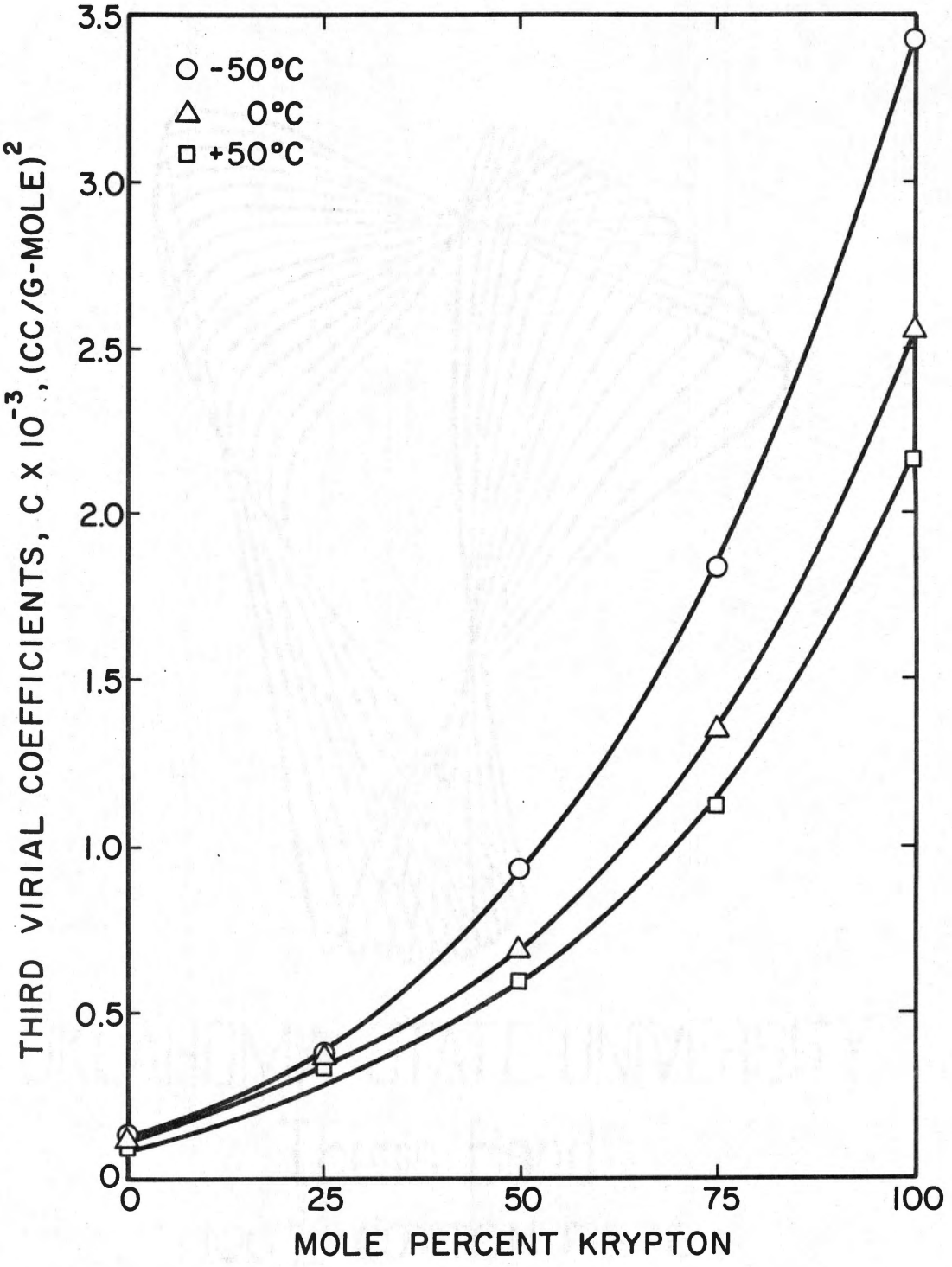

Figure 5. Third Virial Coefficients for the Helium-Krypton System

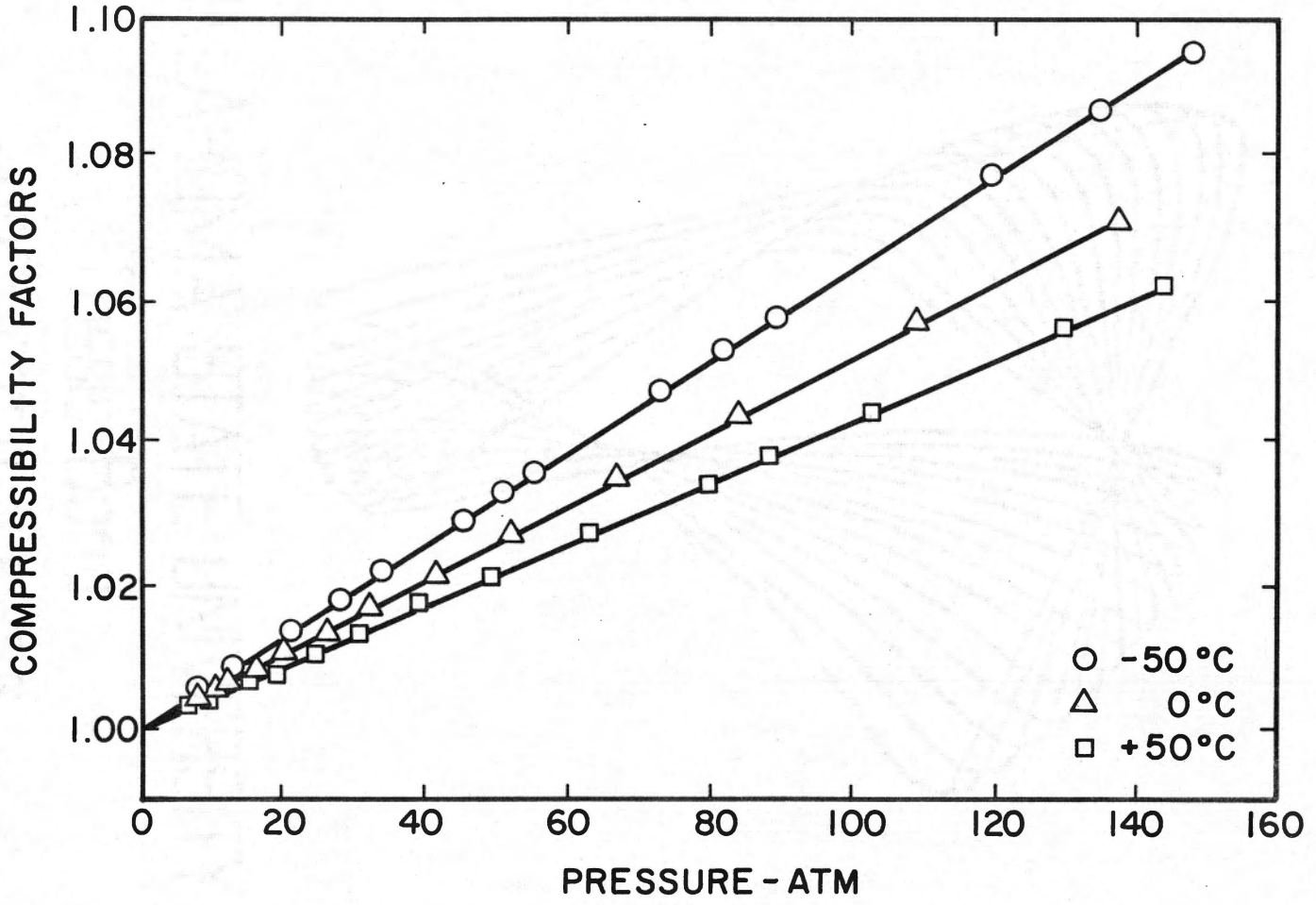

Figure 6. Compressibility Factors for Helium

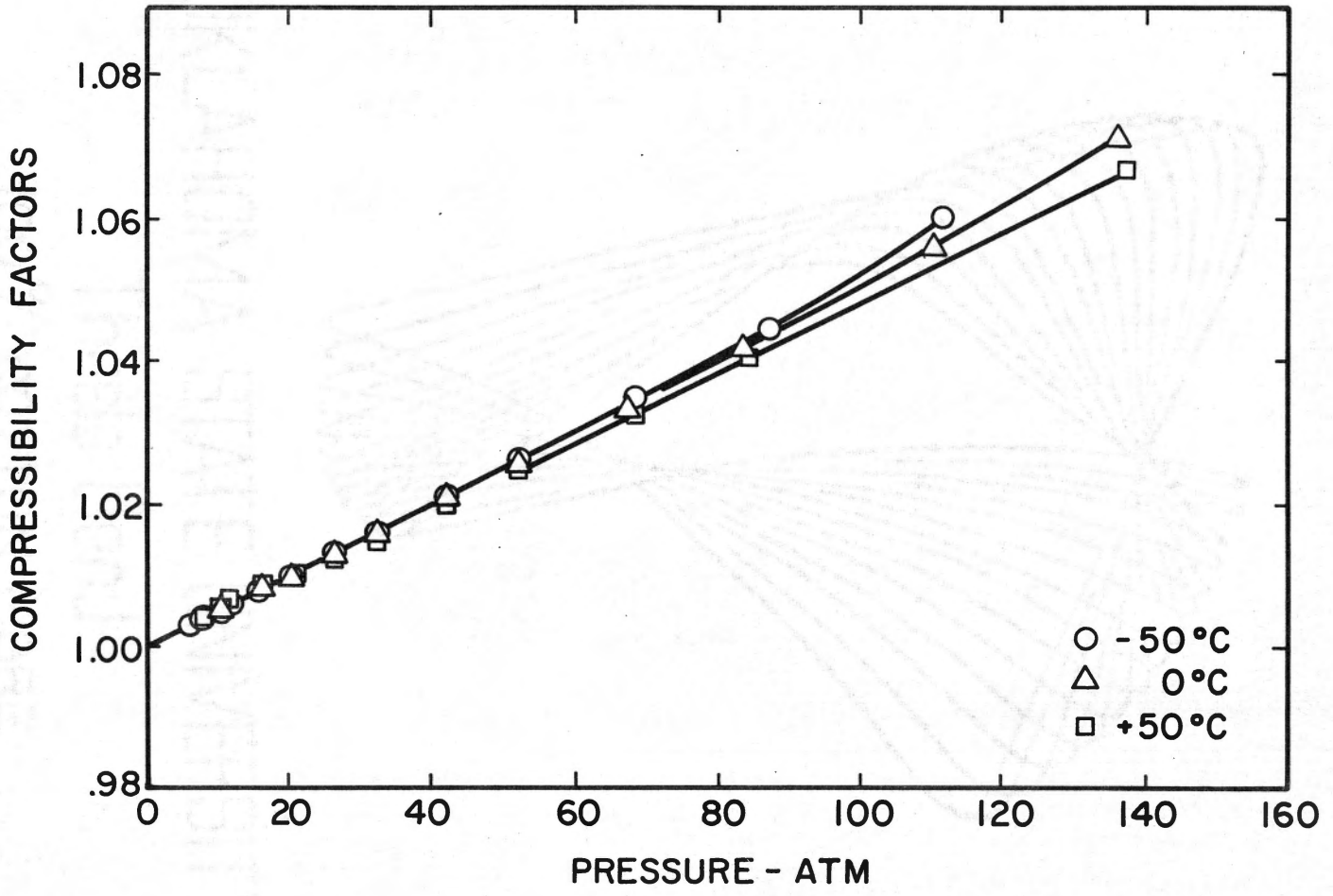

Figure 7. Compressibility Factors for 25 Mol % Kr in He

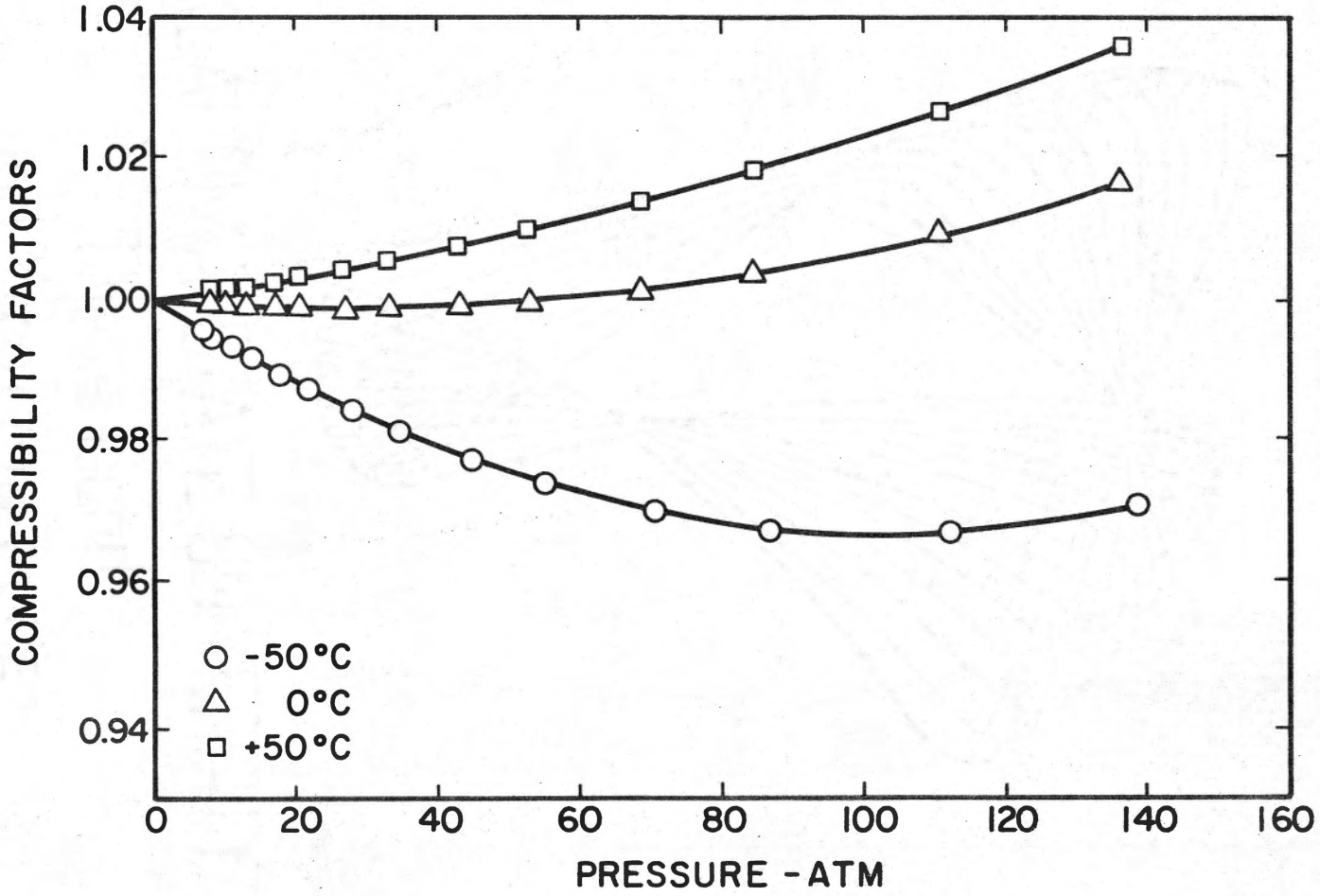

Figure 8. Compressibility Factors for 50 Mol % Kr in He

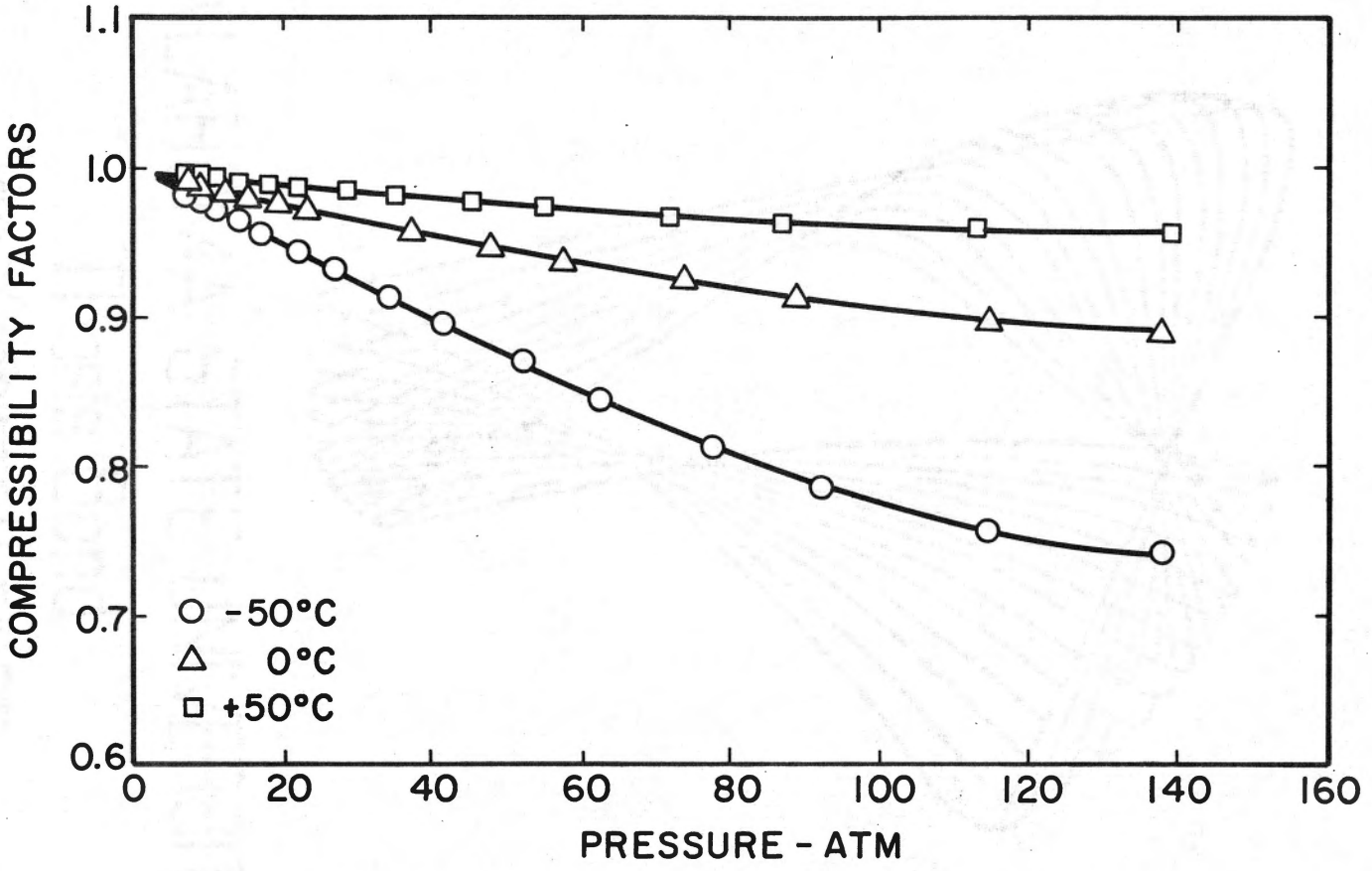

Figure 9. Compressibility Factors for 75 Mol % Kr in He

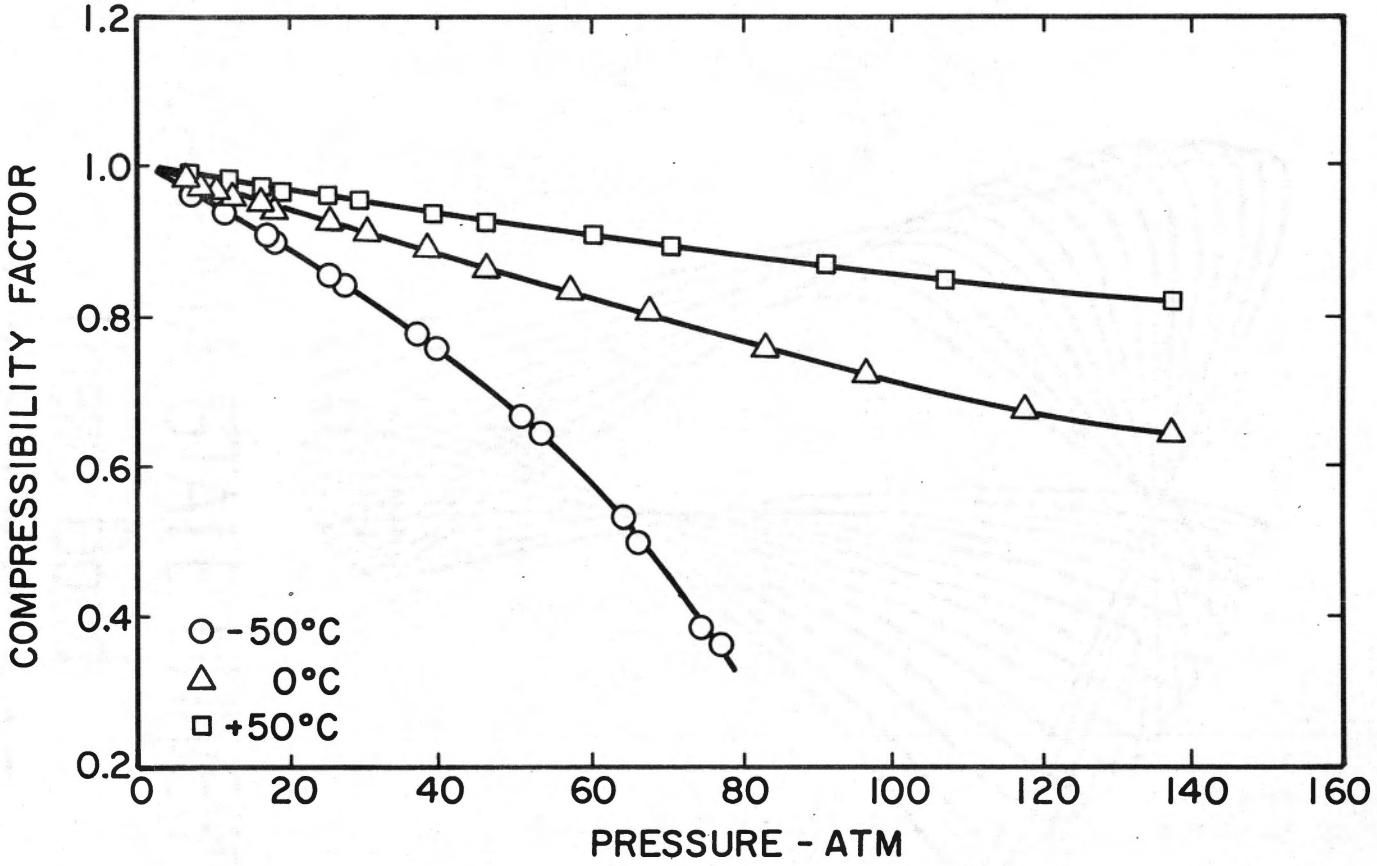

Figure 10. Compressibility Factors for Krypton

Equation (18) can be solved for the interaction virial coefficient. Furthermore, since three mixtures were studied on each isotherm, a least-squares estimate can be determined for the three compositions. Specifically, the best estimate of B_{12} is that value which will minimize the quantity $\sum_{i=1}^{3} [B_m - B_m^*]^2$, where B_m is the calculated mixture virial coefficient and B_m^* is the experimental value. Restating the problem,

$$\text{Min} \sum_{i=1}^{3} [Y_{1i}^2 B_{11} + 2Y_{1i}Y_{2i}B_{12} + Y_{2i}^2 B_{22} - B_{mi}^*]^2 \qquad (19)$$

The mathematical equivalent of (19) is,

$$\partial \Sigma [A^2] / \partial B_{12} = 0 \qquad (20)$$

where A is equal to the bracketed quantity in Equation (19). Performing the operation indicated in Equation (20) yields

$$4\Sigma[A]\Sigma[Y_{1i}Y_{2i}] = 0 \qquad (21)$$

or,

$$\Sigma[A] = 0 \qquad (22)$$

Expanding Equation (22) and solving for B_{12} yields

$$B_{12} = \frac{\sum_{i=1}^{3} [B_{mi}^* - Y_{1i}^2 B_{11} - Y_{2i}^2 B_{22}]}{2 \sum_{i=1}^{3} Y_{1i}Y_{2i}} \qquad (23)$$

The interaction virial coefficients, as calculated by Equation (23), are shown in Table XXV. As indicated in Table XXV, two separate composition determinations were made on the samples and the interaction

TABLE XXV

INTERACTION VIRIAL COEFFICIENTS FOR THE HELIUM-KRYPTON SYSTEM

Temp °C	B_{12} (cc/mol) A.P.[1]	B_{12} (cc/mol) H.R.C.[2]
-50	19.5	20.7
0	21.5	22.3
50	23.1	23.7

[1] Composition analysis by Air Products, Inc. The sum of squares (all temperatures and compositions) for the experimental minus calculated mixture virial equals 1.15.

[2] Composition analysis by the Helium Research Center, sum of squares equals 1.30.

virial coefficient consistent with each of the analyses are shown in the table.

A cursory examination of Equation (23) reveals the critical dependency of the interaction virial coefficients on the accuracy of the composition analysis. The Helium Research Center (U. S. Bureau of Mines) analysis was via mass spectrometry and the Air Products analysis was by gas chromatography. The total sum of squares for the experimental minus calculated mixture virial coefficient was 1.15 and 1.30 for the Air Products and Helium Research Center analyses, respectively. Thus, the values for the interaction virial coefficients as calculated with the Air Products composition analysis were chosen as the final results.

Data Comparisons

Direct comparison of volumetric data generated in different laboratories is normally not possible. Direct comparison would require data taken on identical thermodynamic coordinates and the chances of this occurring are remote. Thus, volumetric data comparisons are normally based on interpolated values and such is the case with the comparisons that will be made between the results of this work and that of previous investigators.

Helium

As mentioned previously, abundant data are reported in the literature for pure helium. Table XXVI contains a sample of these data adjusted to even pressures and temperatures. In all cases, the compressibility factors were generated from reported virial coefficients.

TABLE XXVI

COMPARISON OF SELECTED HELIUM
COMPRESSIBILITY FACTORS

Press. atm	Reference	-50° C	0° C	50° C
25	This Work	1.01636	1.01318	1.01097
	Blancett (7)	1.0166	1.01324	1.01110
	Canfield (16)	1.0169	1.01346	
	White (90)		1.01379	
	Holborn (37)	1.0164	1.01312	
	Schneider (71)		1.01313	
	Bureau of Mines (12)			1.01106
	Michels (59)		1.01318	1.01083
50	This Work	1.03267	1.02630	1.02188
	Blancett (7)	1.0331	1.0264	1.02214
	Canfield (16)	1.0336	1.0268	
	Holborn (37)	1.0329	1.0262	
	Schneider (71)		1.0263	
	Bureau of Mines (12)			1.02205
	Michels (59)		1.02624	1.02161
100	This Work	1.06506	1.05234	1.04351
	Blancett (7)	1.0657	1.0526	1.04402
	Canfield (16)	1.0666	1.0533	
	Holborn (37)	1.0633	1.0525	
	Bureau of Mines (12)			1.04385
	Michels (59)		1.05200	1.04295
150	This Work	1.09708	1.07809	1.06490
	Blancett (7)	1.09800	1.07848	1.06566
	Canfield (16)	1.09914	1.07946	
	Bureau of Mines (12)			1.06541
	Michels (59)		1.07729	1.06404

An examination of the helium data leads to the conclusion that all workers are in very respectable agreement. Only a few points disagree by more than 0.1 percent with the average deviation being about 5 parts in 10,000.

Krypton

Including the present study, a total of nine experimental investigations have been conducted in which volumetric data for krypton were generated. Four previous works fall within the temperature-pressure coordinates covered in this work.

Table XXVII is a tabular comparison of compressibility factors generated in this work and those of Schneider (89). Schneider's work covers a range of 0 to 600° C and 10 to 80 atm. Unfortunately, Schneider did not report compressibility data. Rather, the compressibility data were fitted to a quadratic in pressure (two term Berlin form of the virial equation of state) and only the coefficients were reported. At 0° C, the high pressure data were not satisfactorily represented by even a cubic in pressure. For this reason, Schneider only used the data up to 40 atm. Using the second and third virial coefficients as reported, compressibility factors were calculated corresponding to experimental pressure values of the present study.

Compressibility data are reported by both Beattie (4) and Trappeniers (83). Thus, the virial coefficients generated in this work were used to calculate compressibility factors corresponding to the experimental pressures reported in these two references. Tabular comparisons are shown in Tables XXVIII and XXIX.

As mentioned previously, Bearman's data (77) are isochoric and cover a range of 130 to 240° K for pressures up to 280 atm. (Actually,

TABLE XXVII

COMPARISON OF COMPRESSIBILITY FACTORS FOR KRYPTON

Press. atm	Compressibility Factor		
	This Work	Schneider (89)	ΔZ
----------0° C----------			
10.5272	0.9707714	0.9703774	.000394
16.4342	0.9542007	0.9536007	.000600
25.4016	0.9286193	0.9279184	.000701
38.6747	0.8902044	0.8894346	.000770
----------50° C----------			
10.2743	0.9838411	0.9835995	.000242
16.1689	0.9745051	0.9743484	.000157
25.3131	0.9602442	0.9602258	.000018
39.3208	0.9388511	0.9391302	-.000279
60.4159	0.9079657	0.9085906	-.000625

TABLE XXVIII

COMPARISON OF COMPRESSIBILITY FACTORS FOR KRYPTON

Press. atm	Compressibility Factor		
	This Work	Beattie (4)	ΔZ
----------0° C----------			
21.058	0.94106	0.93950	0.00156
39.663	0.88732	0.88478	0.00254
56.239	0.83853	0.83637	0.00217
71.066	0.79488	0.79265	0.00223
84.416	0.75655	0.75324	0.00331
96.780	0.72308	0.71964	0.00344
108.370	0.69479	0.69070	0.00409
119.620	0.67142	0.66711	0.00431
130.880	0.65297	0.64880	0.00416
142.470	0.63952	0.63563	0.00389
----------50° C----------			
25.432	0.96011	0.95909	0.00102
48.988	0.92451	0.92371	0.00080
70.985	0.89324	0.89232	0.00092
91.762	0.86631	0.86513	0.00118
111.672	0.84369	0.84227	0.00142
131.090	0.82534	0.82394	0.00140
150.370	0.811217	0.81010	0.00117

TABLE XXIX

COMPARISON OF COMPRESSIBILITY FACTORS FOR KRYPTON

Press. atm	Compressibility Factor		
	Trappeniers (83)	This Work	ΔZ
----------0° C----------			
18.566	0.94878	0.94814	-0.00064
27.212	0.92409	0.92344	-0.00065
35.664	0.89962	0.89898	-0.00064
43.827	0.87579	0.87512	-0.00067
53.359	0.84768	0.84704	-0.00064
65.802	0.81078	0.81032	-0.00046
74.855	0.78450	0.78386	-0.00064
83.0791	0.76102	0.76031	-0.00071
93.098	0.73320	0.73276	-0.00046
100.005	0.71531	0.71485	-0.00046
116.759	0.67724	0.67692	-0.00032
126.890	0.65922	0.65890	-0.00032
----------50° C----------			
22.356	0.96538	0.96487	-0.00052
27.700	0.95727	0.95661	-0.00066
38.319	0.94107	0.94042	-0.00065
44.386	0.93212	0.93132	-0.00070
54.342	0.91757	0.91667	-0.00090
67.025	0.89970	0.89869	-0.00101
77.638	0.88541	0.88430	-0.00111
88.182	0.87182	0.87073	-0.00109
97.217	0.86090	0.85977	-0.00113
105.202	0.85189	0.85065	-0.00124
125.019	0.83195	0.83065	-0.00130

the data were obtained along quasi-isochores since the pipet volume varied slightly with temperature and pressure.) In order to compare these data to those of this study, the Bearman data were interpolated back to the -50° C isotherm. The interpolations was achieved by fitting the Redlich-Kwong (68) equation of state to four points on each quasi-isochore around -50° C. The molar volume was then linearly interpolated to -50° C by using the two points adjacent to this temperature. Using the volume and temperature, pressure was calculated and then the desired compressibility factor.

Since the interpolation procedure covered a very small range on the PVT plane, the interpolation technique was sufficiently precise to be well within the experimental precision of the Bearman data.

A total of eight quasi-isochores from which compressibility factors for krypton at -50° C could be calculated were reported by Bearman. The interpolated values cover a range of 65 to 75 atm. and are shown in Table XXX along with values generated from the results of this study.

For the purpose of examining the krypton compressibility data, the compressibility factors from previous works were subtracted from those reported in this work and these differences then plotted as a function of pressure. Figures 11, 12 and 13 correspond to the 50, 0 and -50° C isotherms, respectively.

Examining the 50° C data as shown in Figure 11, several significant observations are immediately apparent. First, the overall agreement is excellent with the data of this work being bracketed by the data of the previous workers. Agreement with the present work is normally within one part per thousand with the data of Beattie and Trappeniers falling almost equi-distant on either side of this work. Equally as

TABLE XXX

COMPARISON OF COMPRESSIBILITY FACTORS FOR PURE KRYPTON AT -50° C

Press. atm	Compressibility Factor		
	Bearman (77)	This Work	ΔZ
65.2034	0.51682	0.51702	0.00020
68.1411	0.47735	0.47733	-0.00002
70.5968	0.44301	0.44255	-0.00046
72.7500	0.41351	0.41298	-0.00053
74.8248	0.38876	0.38793	-0.00083
76.9710	0.36799	0.36730	-0.00069
76.2076	0.37399	0.37399	0.00000
75.3052	0.38281	0.38282	0.00001

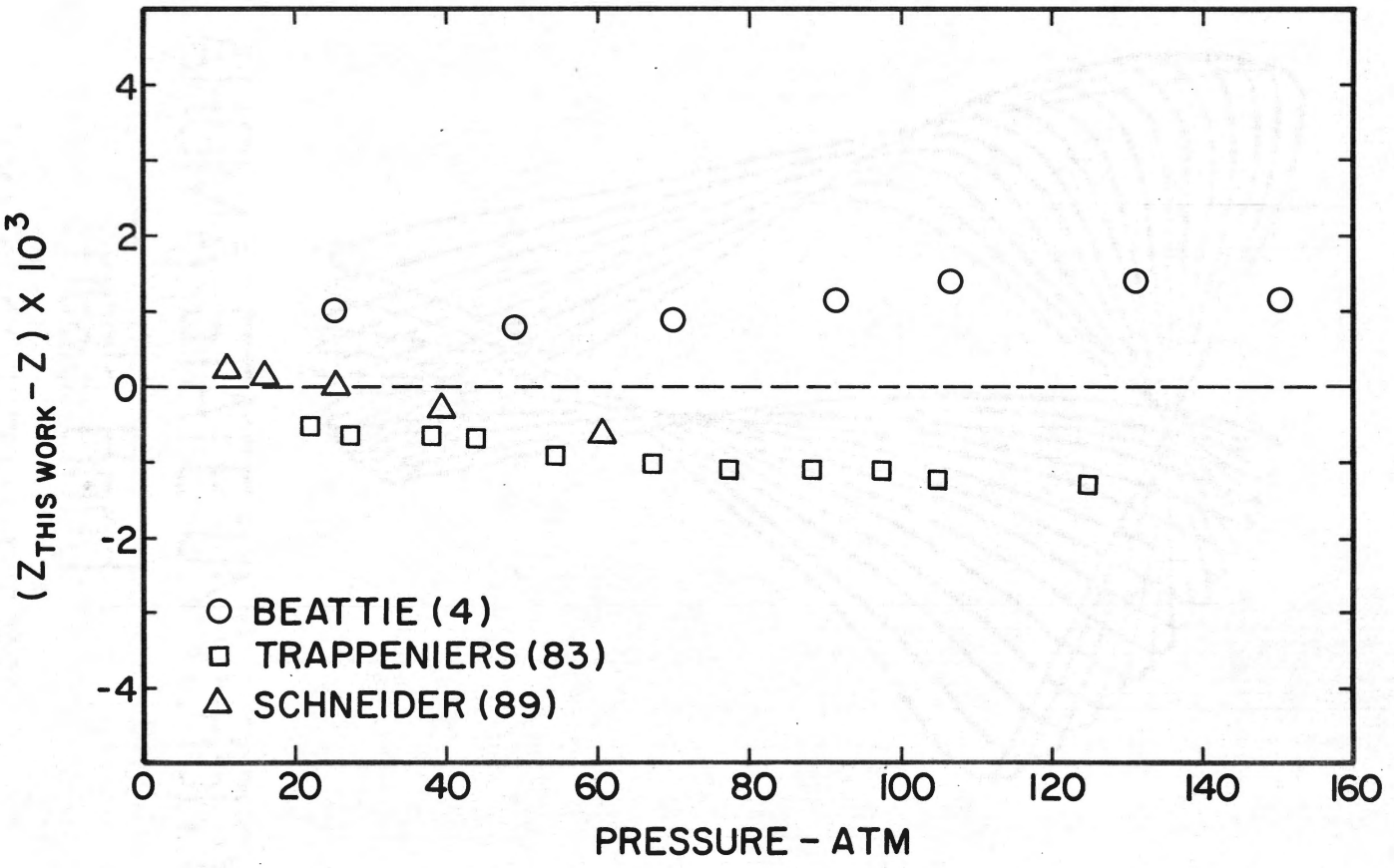

Figure 11. Comparison of Compressibility Factors for Pure Krypton at 50° C

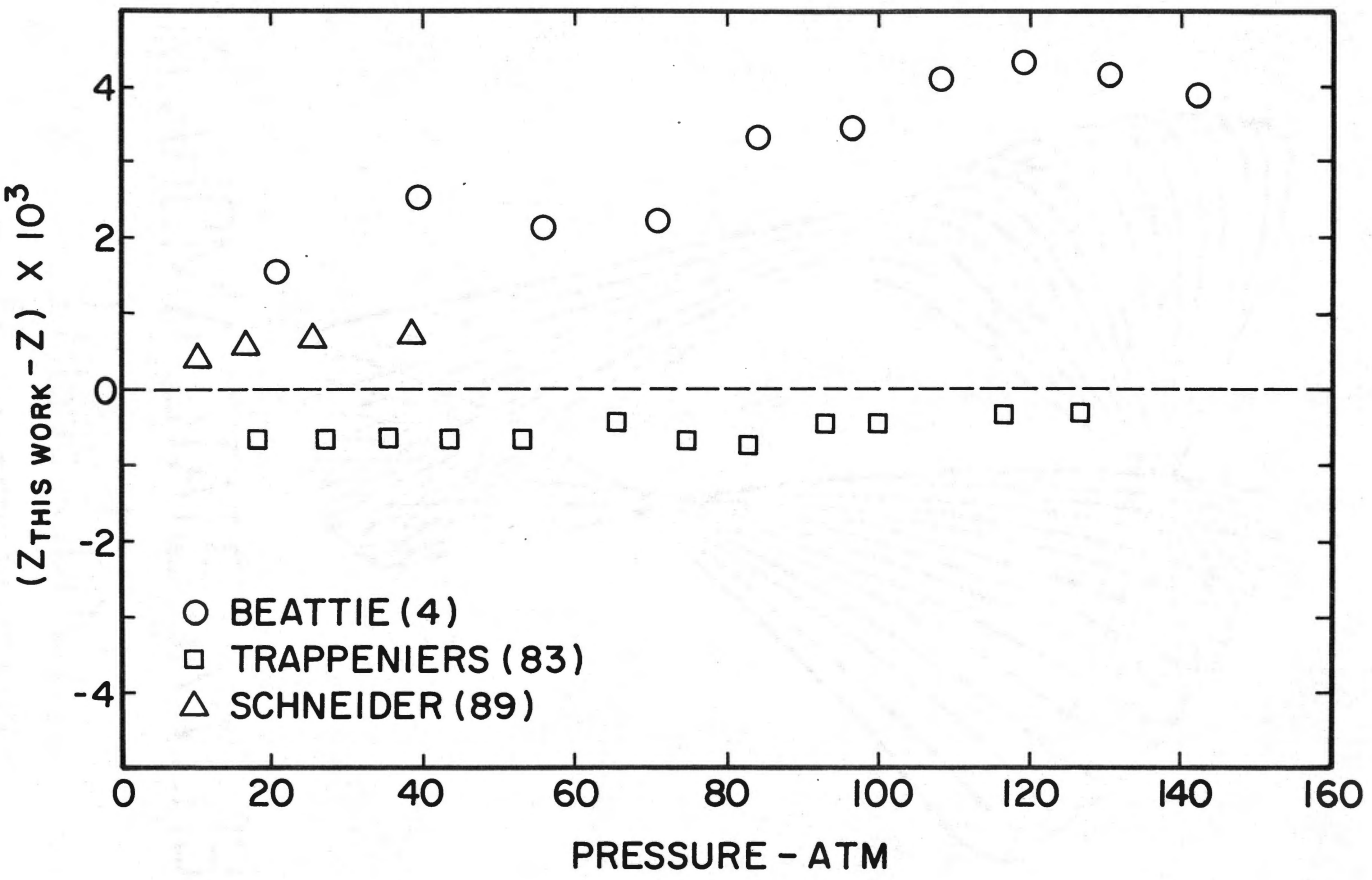

Figure 12. Comparison of Compressibility Factors for Pure Krypton at 0° C

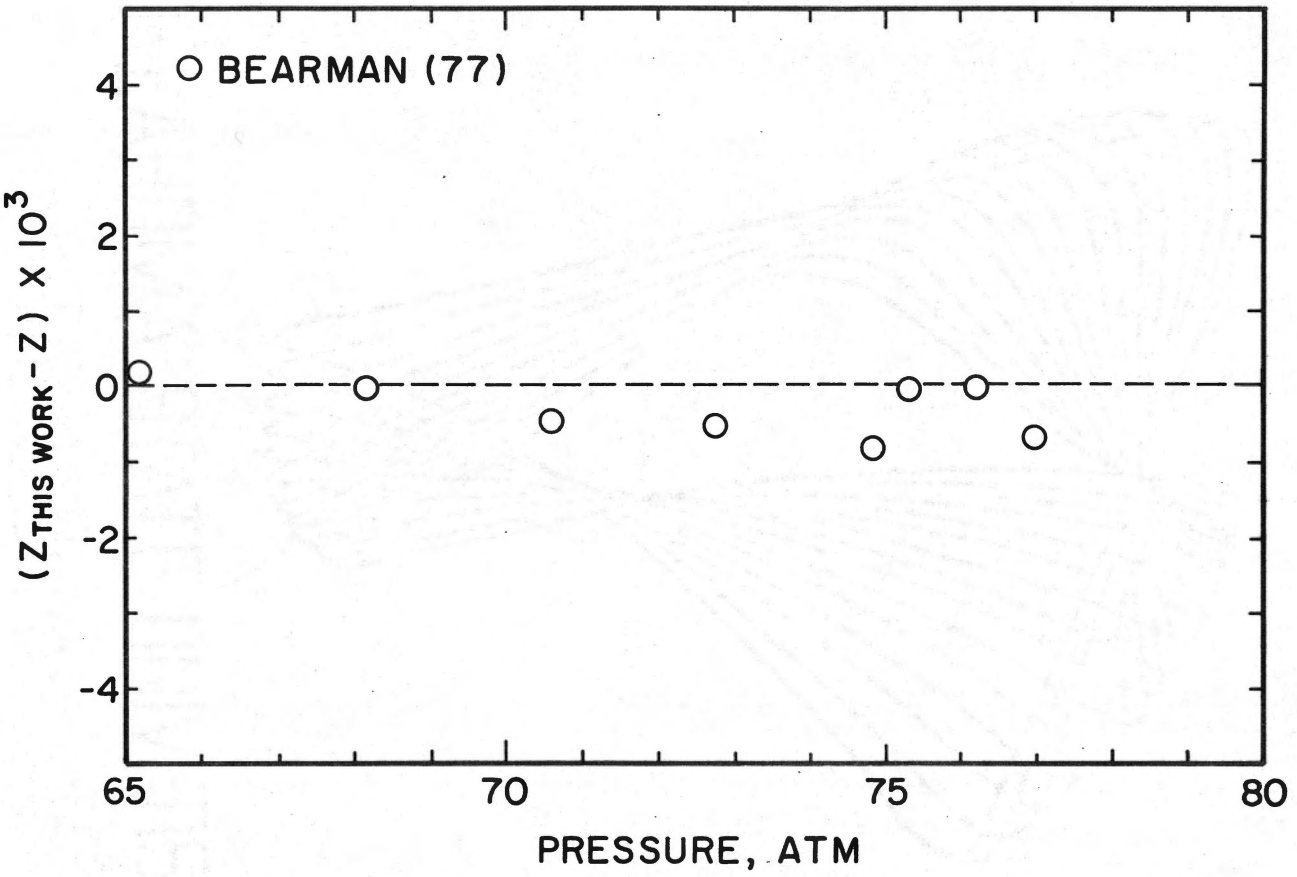

Figure 13. Comparison of Compressibility Factors for Pure Krypton at -50° C

significant as the overall agreement, the data exhibit almost no random scatter and only nominal divergence with increasing pressure. This is a strong implication of very precise data with the majority of error being of a systematic nature.

The overall agreement in the 0^{o} C data is good, but, as shown in Figure 12, Beattie's data do not appear to be of the same quality on this isotherm as that of the 50^{o} C isotherm. Not only do the data diverge from the other data, but the data also display larger scatter. In fact, Beattie's data exhibit more scatter than the average variability between the data of this work and that of Trappeniers. Of course, since these comparisons are relative, the conclusion that one worker's data are inferior to that of other works is open to conjecture. However, the vary excellent agreement between this work and that of Trappeniers adds a measure of credibility to this speculation, since the probability of two workers from different laboratories coincidentally generating compressibility data which agree to better than one part per thousand is extremely remote.

Figure 13 dipicts the comparison of compressibility data from this work and the interpolated values from Bearman's work (77). Bearman's data are the only reported high pressure data from krypton at -50^{o} C. As shown in Figure 7, the results from the present study are in good agreement with those derived from Bearman's data. However, the range for this comparison is quite narrow and this limits the significance of the comparison.

Virial Coefficients

As discussed earlier, the virial equation of state is an infinite power series in reciprocal volume and has theoretical significance

since the coefficients are analytically related to the microscopic energy of interaction between molecules. This theoretical significance provides the prime driving force behind the many studies that have centered on the virial equation of state. In other words, the desired information is the virial coefficients and not simply representation of the data by a power series in reciprocal volume.

The fact that the virial equation of state is not analytically closed is the source of much difficulty in the derivation of virial coefficients from volumetric data. As discussed earlier, statistical methods (linear and non-linear regression techniques) truncate the series to a finite number of terms while the graphical method utilizes subjective extrapolation for the determination of approximations for the virial coefficients. As implied, all reported values for virial coefficients depend both on the accuracy of the volumetric data and the precision of the reduction method used to derive the approximations from the volumetric data.

Helium second and third virial coefficients from the present study and those of previous workers are shown in Table XXXI. Krypton second and third virial coefficients are given in Table XXXII. Since many workers report virial coefficients in units other than the centrimeter-gram-second system, conversion to this system was necessary in some cases. Details of the conversion procedures are given in Appendix E.

The helium virial coefficients as shown in Table XXXI display good overall agreement among the various workers. The helium virial coefficients generated in this study are bracketed by the virials reported by the other workers. The values reported by Keesom (41),

TABLE XXXI

COMPARISON OF SELECTED VIRIAL COEFFICIENTS
FOR PURE HELIUM

Reference	Temp (^{o}K)	Virial Coefficients	
		B(cc/mol)	C(cc/mol)^2
This Work	223.15	12.00	134.2
Blancett (7)	223.15	12.21	116.0
Holborn (37)	223.16	11.93	181.1
Keesom (41)	223.16	11.59	176.0
Canfield (16)	223.13	12.46	108.0
This Work	273.15	11.84	118.9
Blancett (7)	273.15	11.91	114.0
Holborn (37)	273.16	11.85	--
Kesom (41)	273.16	11.48	156.0
Canfield (16)	273.15	12.09	116.0
White (90)	273.16	12.08	--
Wiebe (91)	273.16	11.76	117.0
Michels (59)	273.16	11.87	91.3
Schneider (71)	273.16	11.77	--
Vogl (85)	273.15	11.94	133.5
This Work	323.15	11.66	104.2
Blancett (7)	323.15	11.82	100.0
Holborn (37)	323.16	11.74	--
Keesom (41)	323.16	11.30	136.00
Wiebe (91)	323.16	11.45	110.0
Michels (59)	323.16	11.52	97.9

TABLE XXXII

COMPARISON OF VIRIAL COEFFICIENTS
FOR PURE KRYPTON

Reference	Temp (^{o}K)	Virial Coefficients	
		B(cc/mol)	C(cc/mol)^2
This Work	223.15	-94.08	3430.
Rowlinson (87)	224.19	-95.46	--
This Work	273.15	-61.58	2547.
Beattie (4)	273.16	-62.97	2757.
Schenider (89)	273.16	-62.70	3130.
Trappeniers (83)	273.16	-61.24	2455.
This Work	323.15	-42.09	2159.
Beattie (4)	323.15	-42.78	2260.
Schneider (89)	323.16	-42.78	3000.
Trappeniers (83)	323.16	-41.44	2035.

exhibit a trend toward low values for the second virial and high values for the third virial. While this is a probable consequence of regression techniques, it is noteworthy that the Keesom values are adopted values derived from experimental PVT data reported by other workers. The Keesom values were included in the comparisons mainly as a common reference since these values have been historically included by workers making comparisons of helium virials.

Dropping the Keesom values from consideration, the remaining values for the helium second virial coefficients fall within $\pm$0.3 cc/mol at -50° C and within $\pm$0.2 cc/mol at 0° C and 50° C. Thus, the remaining workers are in excellent agreement with the values reported for this work.

Examining the krypton virial coefficients in Table XXXII two observations are apparent. First, the second virial coefficients at +50 and 0° C are in excellent agreement. All values are within $\pm$1.0 cc/mol with the values from the present study being well bracketed by those of other workers. The most commonly reported precision for second virial coefficients is $\pm$1.0 cc/mol.; thus, these comparisons are within the experimental precision reported by most workers. The value reported by Rowlinson (87) is for 224.2° K versus 223.15° K for the value from this work. Since the slope of the B versus T relationship at -50° C is approximately 1.0 cc/mol/°K, the second virial coefficient reported by Rowlinson would have a nominal value of -96.5 cc/mol at -50° C. Thus, the difference between this work and that of Rowlinson is approximately 2.5 cc/mol. While this agreement can be viewed as acceptable, it is not entirely satisfactory.

The second observation that is apparent on examination of the data in Table XXXII is that the third virial coefficients at +50 and 0° C

do not exhibit the same excellent agreement as displayed by the second virial coefficients. However, recalling that Schneider (89) reported difficulty in fitting the experimental data from hiw work at pressures above 40 atm., it is reasonable to give the value reported by Schneider less weight than the values reported by other workers. Dropping Schneider's third virial coefficient from consideration leaves the remaining workers in excellent agreement. However, a noteworthy trend in the remaining data is apparent. There is a definite relationship between the second and third virial coefficients on both the 0^{o} C and 50^{o} C isotherms. The largest value reported for the second virial coefficient (accounting for the negative sign) corresponds to the smallest value reported for the third virial coefficient. Furthermore, if the data on each isotherm are arranged where the second virial coefficients are in monotonically increasing order, the third virial coefficients would be in monotonically decreasing order. This relationship between the second and third virial coefficients is probably a consequence of regression techniques rather than being related to the experimental data.

Although the maximum deviations for both the helium and krypton virial coefficients are very respectable, the agreement between workers is no less than remarkable in some cases. For example, Beattie (4) and Trappeniers (83) report identical values for the krypton second virial coefficient at $+50^{o}$ C. On the 0^{o} C helium isotherm, the second virial coefficient reported in this work, the work of Holborn (31) and that of Michels (59) agree within ± 0.015 cc/mol.

Analysis and Discussion of Errors

In this section, the calculation of the maximum imprecision due to random errors will be combined with all other factors relating to the accuracy of the results of this study in an effort to arrive at an assessment of the "probable accuracy" of the results. The purpose of the following is to evaluate the accuracy and not just the maximum or probable precision. This is a departure from the type of error analysis normally reported in that most workers attempt only to evaluate the precision of their results. The reason, obviously, relates to the fact that it is usually impossible to quantify the accuracy of even the most basic laboratory measurements. However, in the author's opinion, a qualitative statement by the original investigator of the probably accuracy of the results of a study involving experimental measurements and subsequent data reduction is preferable to leaving this difficult and subjective evaluation solely with the reader.

The only direct measurements required for Burnett data are temperature and pressure. However, the volume (or volume ratio) of the Burnett apparatus, while not measured directly, must be a known function of pressure. Finally, the basic measurements must be combined in a reduction scheme to yield the desired results. The errors associated with each of these factors are discussed below.

Pressure Measurement

The errors associated with the primary measurements are discussed in detail in Appendix F. As shown in Appendix F, the maximum uncertainty due to random errors in pressure is ± 0.0095 psi. (Of this total,

±0.002 psi is the result of the uncertainty associated with the determination of barometric pressure!) The maximum systematic error associated with the measurement of pressure is ±0.26 psi. By far the largest single error in the pressure measurement is due to the uncertainty in the area of the piston in the Ruska dead-weight tester. The area is known to only 1 part in 10,000 which corresponds to possible systematic error of 0.24 psi for a pressure measurement at 2400 psi. This error seemingly overwhelms the other uncertainties involved. However, two important points are apparent on closer examination. First, the error is systematic and therefore has no influence on the precision or consistency of the data. Secondly, the piston area cancels in the calculation of compressibility factors. This is easily shown by recalling Equation (8) from Chapter II.

$$Z_k = (P_k/T_k)N_{00}^k \quad \frac{Z_0}{(P_0/T_0)} \quad \prod_{j=1}^{k} X_j$$

Pressure can be factored as a ratio and then expanded into the more basic components of weight and piston area. Obviously, if this exercise were carried out, the piston area would be shown to cancel. Of course, this exercise results in the conclusion that the compressibility factor, other things equal, is correct, but the pressure coordinate for which it should be reported is only known to 1 part in 10,000. As a practical matter, it is not relevant whether the error is associated with the pressure coordinate or the compressibility factor. However, the distinction was made to emphasize the fact that this source of error definitely should not be included as a random error if statistical weight is to be given each data point on the basis of estimated precision as a function of pressure.

Temperature Measurement

As stated earlier, the combined sensitivity of the platinum resistance thermometer and the associated bridge circuitry is better than $\pm 0.001^{\circ}$K. During the course of the experimental measurement, the bath temperature normally did not vary by more than $\pm 0.002^{\circ}$ K for an entire run. For the various runs along an isotherm, the temperature was always within a range of $\pm 0.001^{\circ}$ K of the desired isotherm. Thus, the estimated uncertainty for any given temperature measurement can be reasonably selected as $\pm 0.002^{\circ}$ K. Since this is the full range of variation from point to point, this estimate should be conservative even in view of the fact that the temperature of the bath fluid and not the actual sample media was being measured.

The variation in temperature from run to run did not constitute an error since the pressure measurements could be corrected back to values corresponding to the temperature of the desired isotherm. The method by which this correction was made in shown below. The development of the correction technique is shown because, to the best of the author's knowledge, this correction was not made by previous workers.

Assume that a particular set of data along a desired isotherm of T_i has been taken where the measured temperature, T_m, is not equal to T_i. For a particular Burnett expansion we can write:

$$P_m = nRZ_1T_m/V \tag{24}$$

But, for the same amount of gas, n, contained in volume V, we can write:

$$P_i = nRZ_2T_i/V \tag{25}$$

Where P_i is the pressure that would have been measured if the bath temperature had been T_i instead of T_m. Combining Equation (24) and (25) gives,

$$P_i = (Z_2/Z_1)(T_i/T_m)P_m \tag{26}$$

For cases where large temperature corrections (say $\pm 0.1^\circ$ K) were necessary, the variation in the compressibility factor with temperature and pressure might need to be accounted for with an iterative scheme. However, for the small corrections necessary in this work, these corrections are not significant and Equation (26) can be reduced to

$$P_i = (T_i/T_m)P_m \tag{27}$$

Using Equation (27) to correct the data back to the desired isotherm, the estimated maximum random uncertainty in temperature measurement remains at the previously stated $\pm 0.002^\circ$ K. However, the maximum systematic error is almost an order of magnitude larger than the random errors. The platinum resistance thermometer, as calibrated by the National Bureau of Standards, is only guaranteed to reproduce the International Practical Temperature Scale to within $\pm 0.01^\circ$ K. Thus, as was the case with pressure measurement, the precision of the temperature measurements was much greater than the absolute accuracy.

Apparatus Volume Ratio

The apparatus volume ratio, N_i, is a function of pressure due to the effect of pressure on the components of the Burnett cells and due to the inherent nature of the differential pressure indicator (DPI) which was an integral part of the upper cell. The null point of the DPI

is a function of pressure. Since all pressure measurement were made at apparent null (zero indication on the electronic read-out), there was actually a slight load on the diaphragm of the DPI. This, of course, would cause a flexure of the diaphragm and a corresponding change in the volume of the upper Burnett chamber. The effect of pressure on the apparatus volume ratio is discussed in detail in Appendix C. The corrections described in Appendix C were based on experimental data taken according to techniques presented in Appendix B.

Two sources of error are possible contributions to the uncertainty in the apparatus volume ratio. First, a knowledge of the diaphragm load at apparent null was necessary in order to calculate the volume change due to the flexure of the diaphragm. Thus, any uncertainty in the load at apparent null would cause a corresponding error in the calculation of the volume change. As shown in Appendix F, the estimated maximum systematic and random uncertainties in the diaphragm load at apparent null were $\pm 5 \times 10^{-5}$ psi and $\pm 3 \times 10^{-4}$ psi, respectively. This corresponds to systematic and random uncertainties of $\pm 0.0034\%$ and $\pm 0.021\%$ in the apparatus volume ratio.

The remaining source of uncertainty is systematic in nature and arises from any error associated with the calculational procedures, as developed in Appendix C, used to predict the volume change in the Burnett cell as a function of pressure. These calculations were estimated to be accurate to within $\pm 5\%$ and this corresponds to a systematic uncertainty in the apparatus volume ratio of $\pm 0.0016\%$. Combining this result with the maximum systematic error due to the uncertainty of the diaphragm load at apparent null yield a total maximum systematic error of $\pm 0.0050\%$ in the apparatus volume ratio.

Composition

Extreme care was exercised during the course of this work to insure that no variation in composition occurred. Thus, it is estimated that no random errors were incurred as a result of this variable. However, the accuracy of the composition analysis for the helium-krypton mixtures was quite low in comparison to the anticipated accuracy of the PVT measurements. The mixture compositions have an estimated uncertainty of $\pm$0.4 mole percent. The uncertainty in the mixture compositions does not affect the precision or consistency of the generated compressibility data. However, the interaction virial coefficients, as presented in Table XXIII, are compsotion dependent quantities and the uncertainty in the composition significantly affects the accuracy of the mixed virial coefficients. For example, the composition related uncertainty in the interaction second virial coefficient is estimated to be approximately $\pm$0.6 cc/mol.

The pure component gases contained impurities of no more than a few parts per million. Thus, the results for the pure components are essentially free of composition related errors.

Combined Errors

The maximum uncertainty in the compressibility data associated with the estimated maximum uncertainty in the primary measurements are shown in Table XXXIII. The necessary partials $(\partial Z/\partial P)_T$ and $(\partial Z/\partial T)_P$ used to relate the uncertainty in pressure and temperature to the compressibility data were evaluated from experimental data at -50° C and maximum run pressure. The error associated with the volume ratio was

evaluated from the basic Burnett relationship. Recalling Equation (4):

$$\frac{P_{j-1}/T_{j-1}}{P_j/T_j} = N_j \frac{Z_{j-1}}{Z_j}$$

Rearranging at constant temperature gives

$$Z_j = Z_{j-1} N_j (P_j/P_{j-1}) \tag{28}$$

Then, to a close approximation, the error in Z_j (ΔZ_j) due to the uncertainty in the volume ratio is

$$\Delta Z_j \simeq Z_{j-1}(P_j/P_{j-1})\Delta N_j + N_{j-1}(P_j/P_{j-1})\Delta Z_{j-1} \tag{29}$$

where the second term in Equation (29) is due to the error in Z_{j-1}. Thus, the error in the final compressibility factor for a complete set of expansions is a function of the error in each of the foregoing compressibilities. Fortunately, there are two compensating factors which keep this from being an almost intolerable accumulation of errors. First, the error in the volume ratio is an inverse function of pressure and ΔN_j decreases with each succeeding expansion. Secondly, and more importantly, the compressibility data are fitted to a model such that

$$\lim_{P \to 0} Z_k = 1.0 \tag{30}$$

Furthermore, the cell constant, N_{00}, and the run constant, (P_0/Z_0), are regressed simultaneously with the virial coefficients. Thus, in the course of the regression, the values for the cell constant and the run constant must be compatible with Equation (30). In other words,

TABLE XXXIII

MAXIMUM SYSTEMATIC AND RANDOM UNCERTAINTY
COMPRESSIBILITY DATA

Quantity	Primary Error		Error in Compressibility	
	Systematic	Random	Systematic	Random
----------KRYPTON----------				
Pressure	$\pm$0.125 psi	$\pm$0.004 psi	$\pm 8.1 \times 10^{-4}$	$\pm 3.0 \times 10^{-5}$
Temperature	$\pm 0.01^{\circ}$ K	$\pm 0.002^{\circ}$ K	$\pm 8.2 \times 10^{-4}$	$\pm 1.6 \times 10^{-5}$
Volume Ratio	$\pm$0.005%	$\pm$0.021%	$\pm 2.5 \times 10^{-5}$	$\pm 1.0 \times 10^{-4}$
Total			$\pm 1.7 \times 10^{-3}$	$\pm 1.5 \times 10^{-4}$
----------HELIUM----------				
Pressure	$\pm$0.24 psi	$\pm$0.0061 psi	$\pm 1.0 \times 10^{-5}$	$\pm 2.7 \times 10^{-7}$
Temperature	$\pm 0.01^{\circ}$ K	$\pm 0.002^{\circ}$ K	$\pm 3.8 \times 10^{-5}$	$\pm 7.6 \times 10^{-7}$
Volume Ratio	$\pm$0.0050%	$\pm$0.021%	$\pm 7.9 \times 10^{-5}$	$\pm 3.3 \times 10^{-4}$
Total			$\pm 1.3 \times 10^{-4}$	$\pm 3.3 \times 10^{-4}$

any factorable error in N_j will simple be reflected in N_∞ since

$$N_j^k = N_\infty^k \prod_{j=0}^{k} X_j \tag{31}$$

The remaining error will be largely concentrated in the high pressure compressibility factors as a result of the effect of Equation (30) on the run constant. Two important conclusions can be drawn from the foregoing discussion. First, the actual error in the compressibility data due to systematic uncertainty in volume ratio is much less than the apparent error. Secondly, random errors in the volume ratio would not be compensated for and, therefore, would reduce the precision of the compressibility data to a greater extent than systematic errors.

As the above analysis implies, the error in the compressibility data due to uncertainty in the volume ratio is not directly calculable. For the purpose of estimating the maximum error, the following expression was used:

$$\Delta Z_{max} = (Z_0/P_0)P_1\Delta N_1 \tag{32}$$

Estimated Precision and Accuracy

The results shown in Table XXIII show the estimated maximum errors in the compressibility data generated in this study. Although this information is a necessary starting point for estimating the probable precision and accuracy of the results, other factors are equally important. The additional factors which should be considered are:

1. Data Comparisons
2. Consistency of experimental and calculated compressibility factors
3. The variation of the isothermal value of the cell constant, N_∞.

As indicated earlier, the data from this work agree well with those of previous studies with this work being bracketed by other works. For example, the Bearman data for krypton at -50^{o} C compare with the present data with an average variation of less than 4 parts in 10,000 in the compressibility factors.

A cursory analysis of the data in Tables V through XXIII indicates a consistency of approximately 1×10^{-5} between the experimental and calculated helium compressibility factors. Similarly, the krypton compressibilities exhibit a consistency of approximately 1×10^{-4}.

The cell constant, N_{∞}, is a function of the physical geometry and/or design of the Burnett cells and the other integral parts such as tubing, valves and the lower chamber of the cryogenic DPI instrument. Thus, it would be expected that the cell constant would be a weak function of temperature due to varying expansion factors of the components. However, for a given isotherm, N_{∞} should be a constant. Therefore, any observed variation in the isothermal value of the cell constant can be qualitatively related to the uncertainty in the final results of the data reduction.

Two factors could cause variation in the regressed results for the isothermal values of the cell constant. First, as discussed earlier, any lack of fit between the experimental data and the truncated form of the virial equation of state would affect the regressed value of N_{∞}. Secondley, null shift in the cryogenic DPI could cause variation in the isothermal value of N_{∞}. While the first factor would clearly give rise to error in the results, the second factor would not necessarily cause uncertainty in the results. For example, if the null shift were to occur during the initial charge of sample gas into the Burnett

cell, the fact that N_{00} is regressed during the data reduction could allow total compensation for the null shift. In other words, the regressed value would be equal to the actual value of the cell constant for that run.

In the present work, the maximum variation in the value for the cell constant along an isotherm is approximately 2 parts in 10,000. This compares quite well with the variation typically reported by workers employing the Burnett method. For example, the work reported by Provine (67) displays a variation of 4.4 parts in 10,000 while Lee (48) reports variations as large as 30 parts in 10,000.

Subjective estimates for both the precision and accuracy of the results of this study are shown in Table XXXIV. The uncertainty reported for the compressibility factors are based on all the factors discussed above. The estimated uncertainty in the helium and krypton virial coefficients is based largely on the results of the data comparisons. The estimated uncertainty in the interaction virial coefficients, B_{12}, was calculated by taking 50% of the value obtained from application of a maximum propagation of error analysis using

$$\epsilon_{B_{12}} = \left|\frac{\partial B_{12}}{\partial B_{11}}\right| \Delta B_{11} + \left|\frac{\partial B_{12}}{\partial B_{22}}\right| \Delta B_{22}$$

$$+ \left|\frac{\partial B_{12}}{\partial B_{m}}\right| \Delta B_{m} + \left|\frac{\partial B_{12}}{\partial Y}\right| \Delta Y \qquad (33)$$

where $\epsilon_{B_{12}}$ = error in B_{12}, cc/mol. and all other symbols are as previously defined.

TABLE XXXIV

ESTIMATED PRECISION AND ACCURACY
OF THE REPORTED RESULTS

Results	Estimated Uncertainty	
	Random	Systematic + Random
HELIUM		
Compressibility Factor	$\pm 3 \times 10^{-4}$	$\pm 5 \times 10^{-4}$
Second Virial Coefficient	±0.1 cc/mol	±0.2 cc/mol
Third Virial Coefficient	$\pm 5.0 (cc/mol)^2$	$\pm 15.0 (cc/mol)^2$
KRYPTON		
Compressibility Factor	$\pm 3 \times 10^{-4}$	$\pm 5 \times 10^{-4}$
Second Virial Coefficient	±0.25 cc/mol	±0.8 cc/mol
Third Virial Coefficient	$\pm 100 (cc/mol)^2$	$\pm 400 (cc/mol)^2$
Interaction Second Virial Coefficient		±1.6 cc/mol

Molecular Interactions

In this section, a brief review of intermolecular potential functions will be given. The results of this study will then be combined with selected data from previous works. The combined data will then form the basis for a study of the applicability of the Kihara (43) intermolecular potential function for prediction of pure second virial coefficients for the helium-krypton system. Next, the adequacy of several commonly used mixing rules for potential parameters will be tested. While the selection of the Kihara model is somewhat subjective, recent studies (27,72) point to this model as being at least as good, and in many cases superior to other models.

Intermolecular Potential Functions

Numerous potential functions have been proposed and studied. To date, the functional form of the various potential proposed have been based largely on empiricism and qualitative theoretical considerations. In all cases, the primary goal of proposed potential functions is to adequately describe the functional relationship between the microscopic pairwise potential energy of interaction, $U(r)$, and the distance of separation, r, between two molecules.

For the purpose of illustration, and to define useful nomenclature, the development of potential functions corresponding to a few of the more elementary conceptual theories on the behavior of gases will be shown below.

If a gas is assumed to be comprised of point-like spheres such that the only interaction possible arises from perfectly elastic collisions,

then the potential energy of interaction is zero for all distances of separation. That is,

$$U(r) = 0, \text{ for all } r \tag{34}$$

From statistical mechanics (35) the second virial coefficient, B, is given by

$$B = -2\Pi N_0 \int_0^{\infty} [\exp(-U(r)/kT)-1]r^2 dr \tag{35}$$

where:

N_0 = Avogadro's number

k = Boltzmann's constant

T = Temperature, ^oK

Substituting U(r) = 0 into Equation (35) gives B(T) = 0. Similarly, the remaining virial coefficients could be shown to be zero. Obviously, the model described above is for an ideal gas with the volumetric behavior being given by the ideal gas law, PV = nRT.

The ideal gas law, of course, does not normally adequately predict the behavior of real gases. As implied, the concept used to qualitatively describe the volumetric behavior of an ideal gas is much too simple for an adequate description of a real gas. Perhaps the most elementary improvement that can be made to the ideal gas theory is the model of rigid spheres. For this case, the particles are assumed to be perfectly rigid having a collision diameter σ. This model gives a simplified representation of very strong repulsive forces at small distances of separation. The rigid spheres potential is shown schematically in Figure 14.

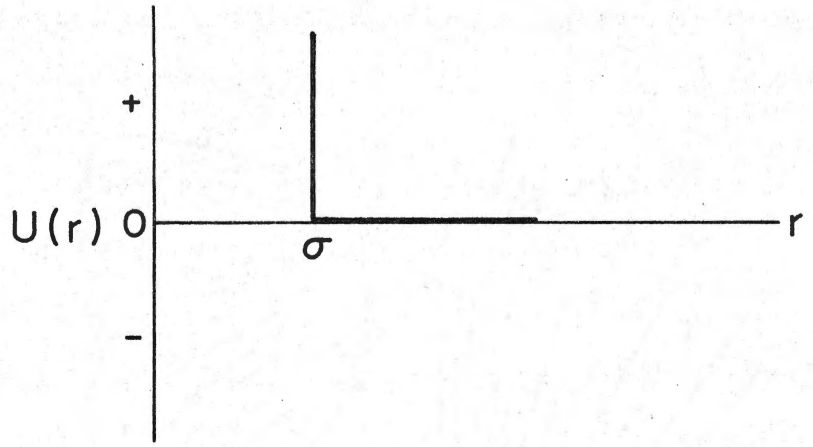

Figure 14. The Rigid Spheres Potential

The quantitative representation of this model is

$$U(r) = \infty, \; r < \sigma$$
$$U(r) = 0, \; r > \sigma \tag{36}$$

Substituting Equation (36) into Equation (35) and carrying out the indicated integration gives $B(T) = \frac{2}{3} \pi N_0 \sigma^3$. Thus, the second virial coefficient for this case is shown to be a positive constant usually denoted by $b_0 (= \frac{2}{3} \pi N_0 \sigma^3)$. Higher order virial coefficients are also positive so that the compressibility factor for the rigid spheres model is always greater than unity. As implied, this model is not very realistic and is only useful at high temperature when better information is not available.

A realistic model for the potential energy of molecular interaction must account for both repulsive forces at small distances of separation and attractive forces at larger distances of separation.

Forces of attraction are known to exist from experimental observations. For example, in the present work, the compressibility factor for krypton at -50^{o} C and 77 atm. was much less than unity (0.365). Furthermore, from perturbation therory (82), the functional dependence of the attractive part of the pair potential function is known to be given by even powers of distance with the first term of the expression being $-br^{-6}$ (b = a constant).

Figure 15 depicts schematically a representation of a potential function consistent with the supposition of the existence of both attractive and replusive forces.

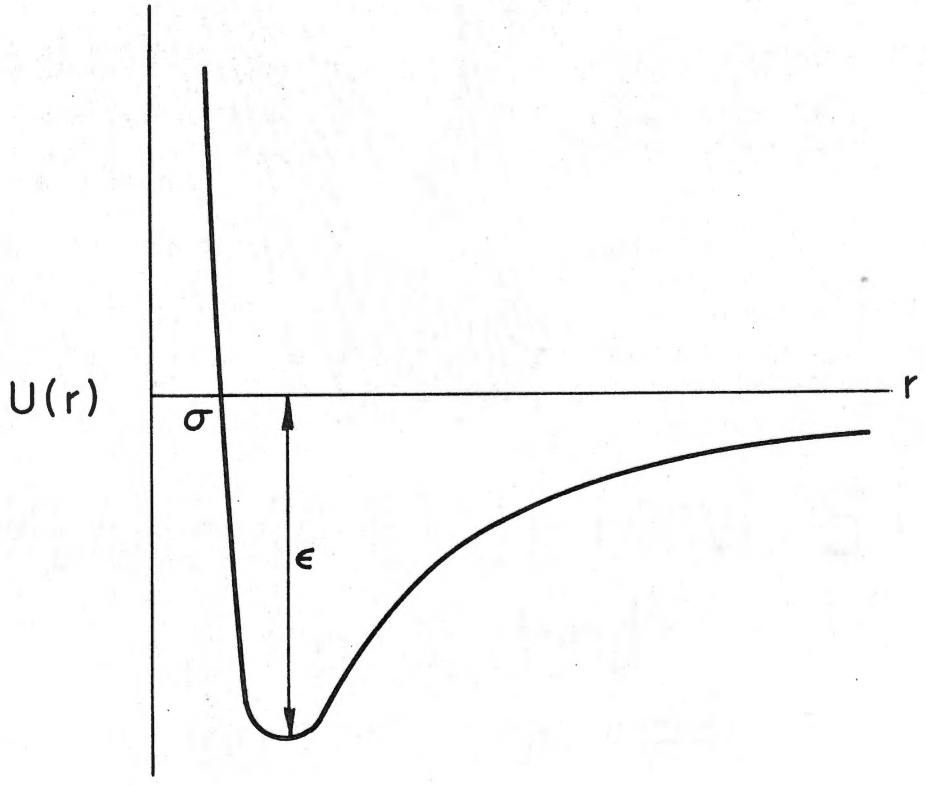

Figure 15. A Conceptually Realistic Potential

An approximate analytical equivalent to the schematic representation shown in Figure 15 is

$$U(r) = a_1 r^{-c} - a_2 r^{-d} \tag{37}$$

where $c > d > 1$ and a_1 and a_2 are constants. The first term of Equation (37) accounts for repulsion while the second term accounts for attraction. Using the criteria that $(\partial U/\partial r) = 0$ for $U(r) = -\varepsilon$ and $U(r) = 0$ at $r = \sigma$, the constants a_1 and a_2 can be expressed in terms of ε and σ. The resulting expression is

$$U(r) = \left(\frac{\varepsilon}{c-d}\right)\left(\frac{c^c}{d^d}\right)^{\frac{1}{(c-d)}}\left[\left(\frac{\sigma}{r}\right)^c - \left(\frac{\sigma}{r}\right)^d\right] \tag{38}$$

Using $d = 6$ from theory and selecting $c = 12$ reduces Equation (38) to the popular Lennard-Jones (49) potential.

$$U(r) = 4\varepsilon\left[\left(\frac{\sigma}{r}\right)^{12} - \left(\frac{\sigma}{r}\right)^{6}\right] \tag{39}$$

For the purpose of extending the above review, Table XXXV shows several of the various pair potential functions that have been proposed and studied. Table XXXVI shows selected relationships for predictions of unlike-molecular potential parameters from pure component data. In Table XXXVII an attempt has been made to summarize some of the most widely accepted factors relevant to selection of pair potentials.

Pure Component Virials

As pointed out in Table XXXVII, virial coefficeint data must extend over a wide temperature range in order to adequately test the applicability of a potential function. Figure 16 shows all available

TABLE XXXV

SELECTED MODELS FOR PAIRWISE MOLECULAR INTERACTIONS

Intermolecular Potential Function	Name and Reference
$U(r) = 4\varepsilon[\sigma/r)^{12} - (\sigma/r)^{6}]$	Lennard - Jones 12:6 (49)
$U(r) = (\frac{n}{n-6})\ (\frac{n}{6})^{6/(n-6)}\ \varepsilon[(\frac{\sigma}{r})^{n} - (\frac{\sigma}{r})^{6}] = ar^{-n} - br^{-6}$	Lennard - Jones n:6 (82)
$U(r) = 4\varepsilon\ [(\frac{\sigma-2a}{r-2a})^{12} - (\frac{\sigma-2a}{r-2a})^{6}]$; for $r > 2a$	Kihara (43)
$U(r) =$ infinity; for $r \leq 2a$	
$U(r) = \frac{\varepsilon}{(1-(6/\gamma)}\ [\frac{6}{\gamma}\ \varepsilon^{\gamma[1-r/r_m]} - (\frac{r}{r_m})^{-6}]$; $r > m$, = infinity; for $r < m$	exp: 6 potential (82)
$U(r) =$ infinity ; for $r \geq \sigma$, $= -br^{-6}$; for $r > \sigma$	Sutherland (82)

TABLE XXXV (Continued)

Intermolecular Potential Function	Name and Reference
$U(r) = \text{infinity};\ \text{for } r \leq \sigma, = -\varepsilon\ ;\ \text{for } \sigma < r < R\sigma, = 0\ ;\ \text{for } r \geq R\sigma$	Squarewell (82)

Nomenclature:

$U(r)$ = the potential energy of a pair of molecules separated by a distance r

$-\varepsilon$ = potential energy minimum

σ = molecular distance for which $U(r) = 0$.

$2a$ = hard core molecular diameter

γ = parameter to correct deviation of exp:6 potential from the corresponding state

r_m = the molecular distance for which the exp:6 potential becomes equal to $-\varepsilon$

m = the molecular distance for which the exp:6 potential goes through a maximum

R = ratio of the well width to σ for the square well potential.

TABLE XXXVI

SELECTED RELATIONSHIPS FOR PREDICTION OF UNLIKE-MOLECULAR INTERACTIONS

Rule No.	Rule	Reference
I	$\varepsilon_{ij} = (\varepsilon_{ii}\varepsilon_{jj})^{1/2}$	35
II	$\varepsilon_{ij} = 2\varepsilon_{ii}\varepsilon_{jj}/(\varepsilon_{ii} + \varepsilon_{jj})$	29
III	$\varepsilon_{ij} = \frac{1}{\sigma_{ij}^3}(\varepsilon_{ii}\sigma_{ii}^3\varepsilon_{jj}\sigma_{jj}^3)^{1/2}$	52
IV	$\varepsilon_{ij} = \frac{2(I_iI_j)^{1/2}(\varepsilon_{ii}\varepsilon_{jj})^{1/2}(\sigma_{ii}\sigma_{jj})^3}{\sigma_{ij}^6(I_i + I_j)}$	52

I = ionization potential

In all cases,

$$\sigma_{ij} = (\sigma_{ii} + \sigma_{jj})/2$$ 35

and for the Kihara, define $\gamma = 2a/\sigma$

then

$$\gamma_{ij} = (\gamma_{ii} + \gamma_{jj})/2$$ 52

TABLE XXXVII

SUMMARY OF FACTORS RELEVANT TO THE SELECTION OF INTERMOLECULAR POTENTIALS FOR SPHERICALLY SYMMETRICAL MOLECULES

No.	Factors	References
I	The correct functional form of the potential function is known on a theoretical basis only for large distances of separation. For this case, perturbation theory gives the functional dependence as even powers of distance The first two terms, $-br^{-6}$ and $-cr^{-8}$, express the induced dipole-dipole and the dipole-quadupole interaction, respectively. The coefficient b can be accurately determined from spectroscopic data.	Toxvaerd (82) Buckingham (13) Dalgarno (23)
II	From an analytical viewpoint, the functional form of the intermolecular potential cannot be uniquely determined from second virial versus temperature relationships unless the potential is monotonic (i.e., everywhere repulsive or everywhere attractive).	Keller (42)
III	Over a limited temperature range, many different potentials will reproduce macroscopic properties within the precision of the data.	Toxvaerd (82)
IV	For any particular potential function different macroscopic properties generate characteristic force constants.	Toxvaerd (82)
V	Second virial coefficients cannot be used to discriminate between the various potential when the virial coefficient data fall inside the range $2<T^*(= kT/\varepsilon)<10$. Reproduction of the data is insensitive to the functional form of the potential in this range.	Hanley (33)

TABLE XXXVII (Continued)

No.	Factors	References
VI	Since the inert gases generally obey the law of corresponding states, the potential function for the rare gases can be expected to be adequately represented by a two parameter model of the form $U(r) = AU^*(r/r^*)$.	Toxvaerd (82)
VII	The Kihara potential contains a third parameter in addition to the two corresponding states parameters σ and ε. Nevertheless, the Kihara is compatible with the theory of corresponding states since the third parameter can be expressed as a function of σ and ε.	Myers (64)

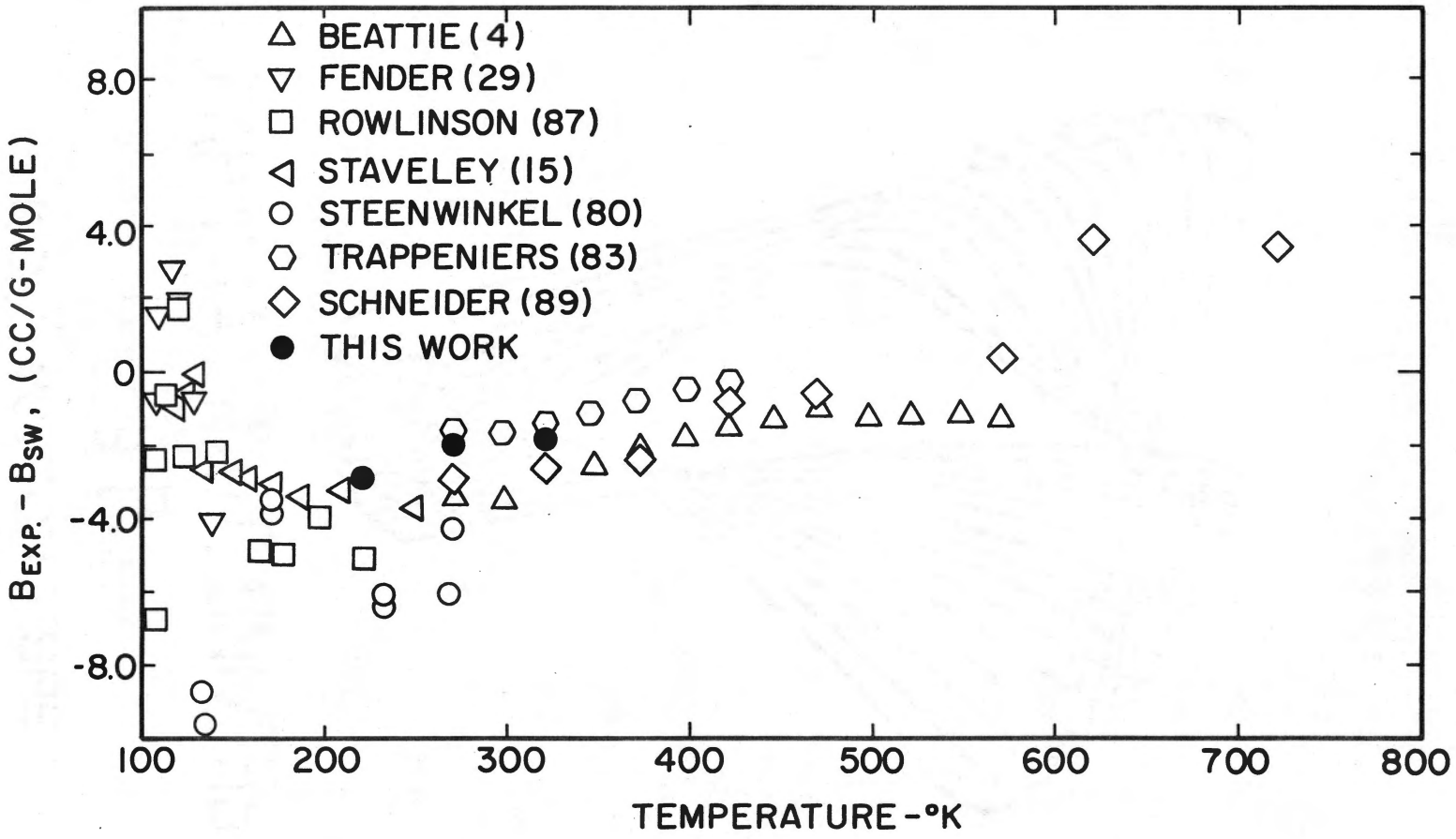

Figure 16. Selected Second Virial Coefficients for Krypton

krypton virial coefficient plotted as a function of temperature in terms of their deviation from values predicted by the square well potential. Use of a deviation plot is simply an effective technique for reducing the scale to emphasize deviations among data sources and no particular significance should otherwise be assumed. (The square well potential is known (72) to reasonably represent second virial coefficient data at nominal and low reduced temperatures, but must fail at high temperatures since it ignores long-range attractive forces.) Using Figure 16, the low temperature data reported by Stavely (15) and the high temperature data of Trappeniers (83) were judged to best suit the objective of adequately extending the temperature range and simultaneously exhibiting consistency with the data of this study. The combined data cover a temperature range of 124 to 423° K.

Selected helium data are depicted in Figure 17. From these data, the second virial coefficients reported by White (90) and those reported by Michels (59) were chosen for combination with the data of this work. The combined data for the helium system extend from 100 to 423° K.

Tables XXXVIII and XXXIX show the results of the application of the Kihara potential to the krypton and helium data, respectively. The results were evaluated from the tabulations reported by Connolly (18) with quantum corrections by Wier (86). The regressions of the Kihara parameters were done via machine calculations as programmed and reported by H.-M. Lin (50).

The results shown in Tables XXXVIII and XXXIX clearly demonstrate the ability of the Kihara potential to describe the pure-component second virial coefficients of the helium-krypton system. Only a few

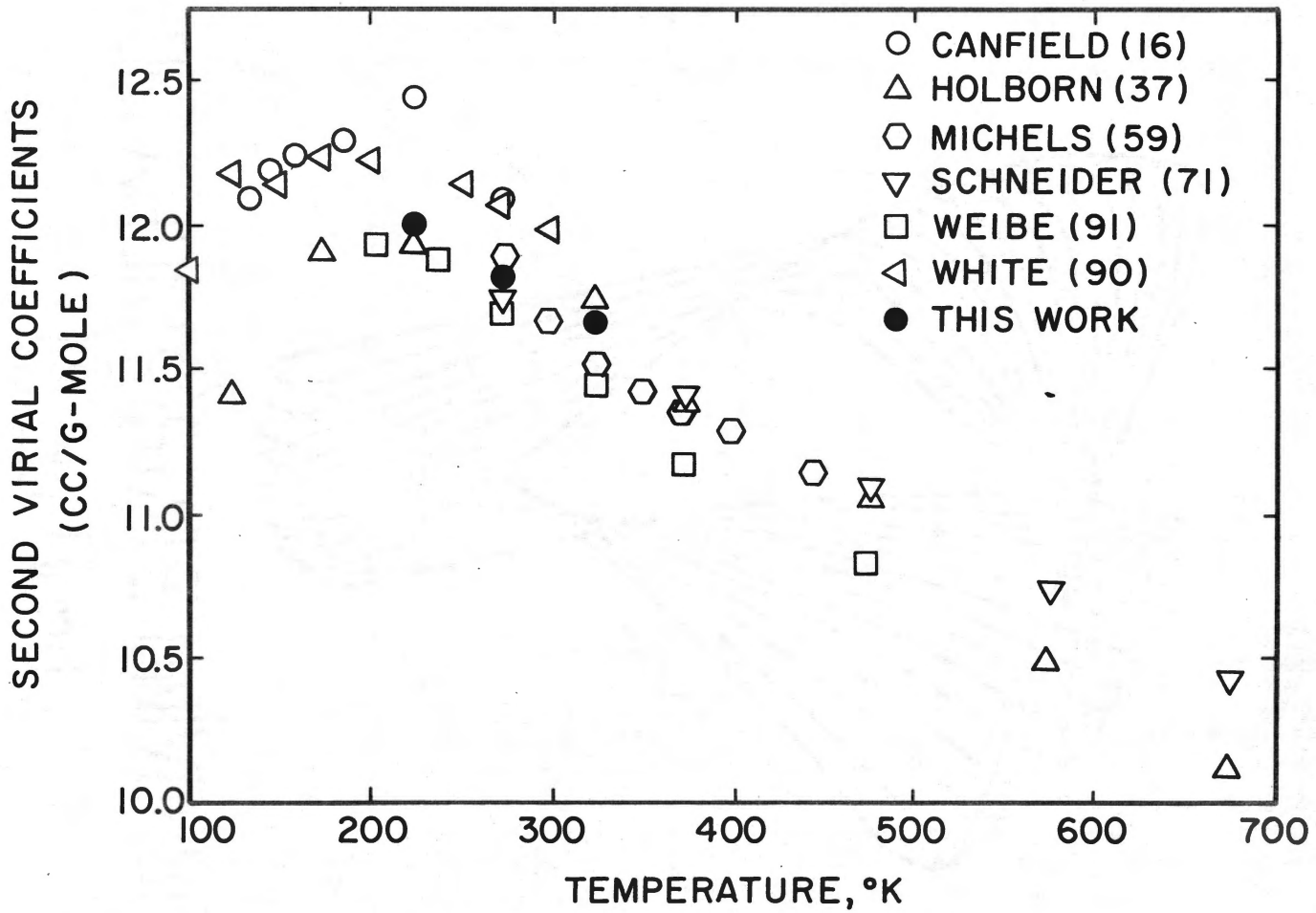

Figure 17. Second Virial Coefficients for Pure Helium as a Function of Temperature

TABLE XXXVIII

RESULTS OF REGRESSION ANALYSIS FOR THE DETERMINATION OF THE KIHARA POTENTIAL FUNCTION PARAMETERS FOR PURE KRYPTON

Reference	Temperature °K	Second Virial, cc/mol		Deviations cc/mol
		Exp	Calc	
Stavely (15)	124.01	-287.50	-287.68	-0.18
Stavely (15)	129.15	-265.40	-266.05	-0.65
Stavely (15)	134.69	-247.00	-245.56	1.44
Stavely (15)	142.45	-220.30	-220.87	-0.57
Stavely (15)	150.98	-198.10	-198.01	0.09
Stavely (15)	161.12	-175.20	-175.33	-0.13
Stavely (15)	172.29	-154.50	-154.66	-0.16
Stavely (15)	186.86	-132.72	-132.75	-0.03
Stavely (15)	209.16	-106.90	-107.00	-0.10
This Work	223.15	- 94.08	- 94.25	-0.17
Stavely (15)	251.94	- 74.80	- 73.63	1.17
This Work	273.15	- 61.58	- 61.88	-0.30
Trappeniers (83)	273.15	- 61.24	- 61.88	-0.64
Trappeniers (83)	298.15	- 50.38	- 50.66	-0.28
This Work	323.15	- 42.09	- 41.54	0.55
Trappeniers (83)	323.15	- 41.44	- 41.54	-0.10
Trappeniers (83)	348.15	- 33.95	- 33.98	-0.03
Trappeniers (83)	373.15	- 27.60	- 27.62	-0.02
Trappeniers (83)	398.15	- 22.22	- 22.20	0.02
Trappeniers (83)	423.15	- 17.53	- 17.53	0.00

ε/k = 217.66

σ = 3.5379

γ = 0.14604

TABLE XXXIX

RESULTS OF REGRESSION ANALYSIS FOR THE DETERMINATION OF THE KIHARA POTENTIAL FUNCTION PARAMETERS FOR PURE HELIUM

Reference	Temperature ^{o}K	Second Virial, cc/mol		Deviations cc/mol
		Exp	Calc	
White (90)	100.02	11.85	11.91	0.06
White (90)	150.04	12.15	12.20	0.06
White (90)	200.11	12.23	12.07	-0.16
This Work	223.15	12.00	12.01	0.01
White (90)	249.99	12.15	11.89	-0.26
This Work	273.15	11.84	11.82	-0.02
White (90)	273.15	11.86	11.82	-0.04
This Work	323.15	11.67	11.62	-0.05
Michels (59)	323.15	11.57	11.62	0.05
Michels (59)	373.15	11.34	11.44	0.10
Michels (59)	423.15	11.05	11.31	0.26

$\varepsilon/k = 8.6703$

$\sigma = 2.5826$

$\gamma = 0.0000$

points display a deviation greather than 1 cc/mol with the average deviation being 0.1 and 0.3 cc/mol for helium and krypton, respectively. The agreement is judged to fall within the precision of the combined data. This leads to the conclusion that the Kihara potential must be viewed as acceptable for representation of the helium-krypton second virial coefficient data. This result is consistent with previous studies, including the work recently reported by Lin and Robinson (52). Lin and Robinson combined pure component rare gas virial coefficient data from approximately 100 literature sources and then applied the Lennard-Jones 6-12, the Kihara and the Dymond-Alder (26) potential to these data. Their work showed that both the D-A potential and the Kihara adequately described the second virials of each of the rare gases. Furthermore, both potentials were shown to be superior to the Lennard-Jones 6-12 potential. However, no significant difference could be shown between the representations displayed by the Kihara and D-A potentials.

Interaction Virial Coefficients

As mentioned in Chapter II, the recent work of Brewer (10) is the only other source of experimental interaction virial coefficient data. Brewer measured only the excess virial, $E = B_{ij} - (B_{ii} + B_{jj})/2$ and these values must be combined with pure component virials in order to evaluate the interaction virial. Since the purpose of this section is to test mixing rules for the Kihara potential, it is essential that the pure component values be in agreement with the Kihara potential. The consistency was achieved by using the pure component potential parameters from Tables XXXVIII and XXXIX to generate pure component virials

at the temperature points corresponding to Brewer's excess virial data. The results are shown in Table XL. For comparison purposes, the interaction virial coefficients from this work are included in Table XL. The values as obtained using the composition analysis of Air Products, Inc., were selected on the basis of exhibiting the smaller sum of squares. The comparison between Brewer's interaction virials and those of this study are in substantial agreement at -50° C where the deviation is less than 0.5 cc/mol. However, the agreement at 50 and 0° C is not entirely satisfactory. The estimated uncertainty in the excess virials is $\pm$0.1 cc/mol and combining this with the estimated uncertainty in the pure component virials yields an estimated uncertainty in the Brewer interaction virials of $\pm$0.7 cc/mol. The estimated uncertainty in the interaction virials from the present study was $\pm$1.6 cc/mol which would imply a maximum band of $\pm$2.3 cc/mol on the comparison of the two works. The deviation of 1.5 cc/mol at 50° C falls within this band, but the difference of 2.6 cc/mol at 0° C exceeds the maximum estimate. Figure 18 shows a plot of the interaction second virial coefficients as a function of temperature from this work and from the work of Brewer. As shown in Figure 18, the data from this work diverge from the data of Brewer as temperature increases. However, the present data appear to display a smooth dependency on temperature whereas the Brewer data exhibit considerable scatter. This is particularly true for Brewer's interaction virial coefficient reported for 0° C where the temperature smoothed plot would yield a value of approximately 20.3 cc/mol. This value is judged to be preferable to the reported value of 18.9 cc/mol. Accepting the temperature smoothed value brings the Brewer data to within 1.2 cc/mol of the present work at 0°C.

TABLE XL

HELIUM-KRYPTON INTERACTION SECOND VIRIAL COEFFICIENTS

Temp °K	Smoothed Kihara Virials (cc/mol)		E (cc/mol)	Interaction Second Virial (cc/mol)	
	He	Kr		Brewer (10)	This Work
323.15	11.626	-41.538	36.52	21.56	23.1
298.15	11.740	-50.661	40.50	21.04	
273.15	11.822	-61.882	43.92	18.89	21.5
223.15	12.010	-94.249	60.21	19.09	19.5
198.15	12.068	-118.739	71.25	17.91	
173.15	12.100	-153.736	86.82	16.01	
148.15	12.207	-205.159	111.75	15.27	

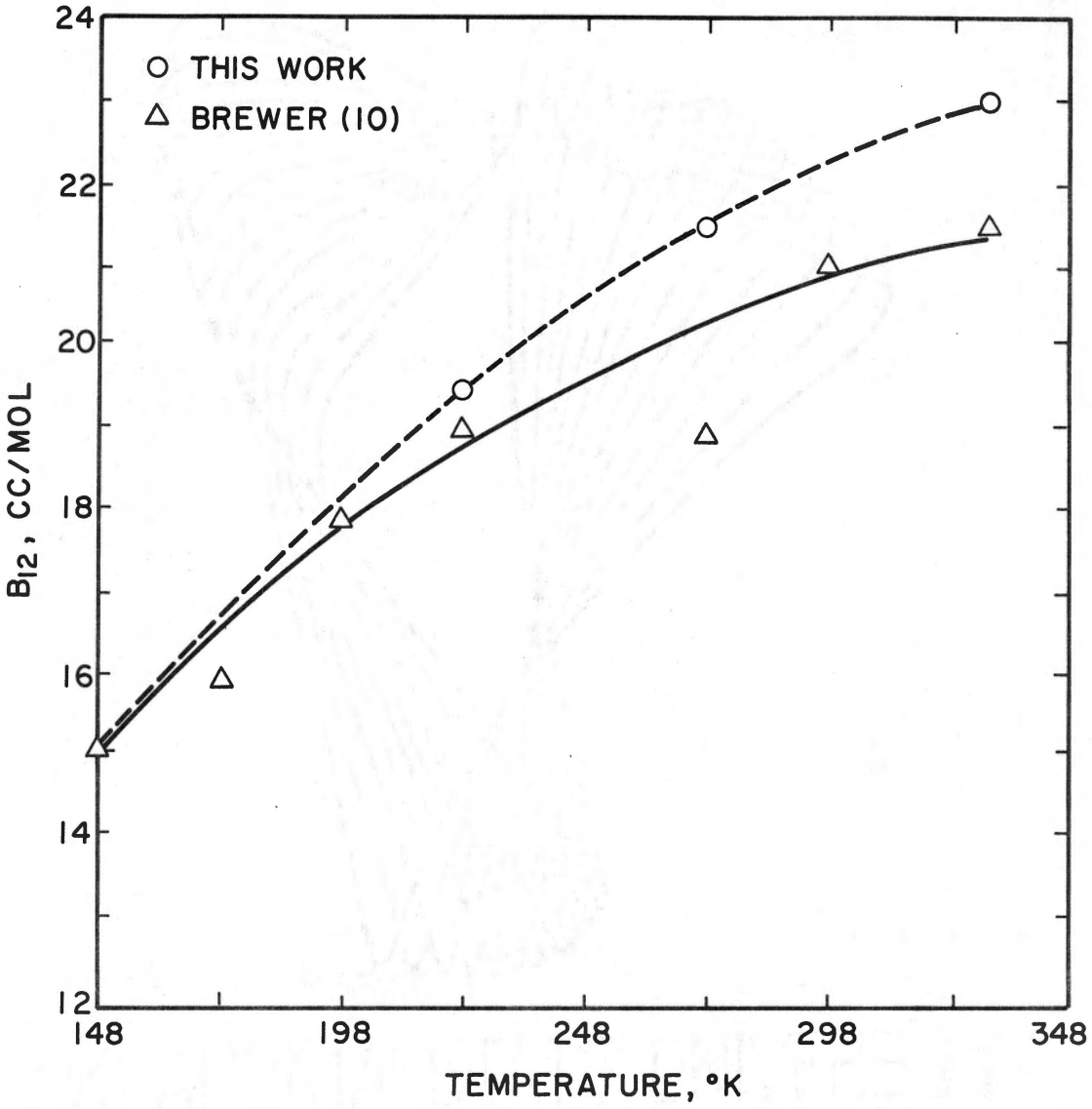

Figure 18. Comparison of the Interaction Second Virial Coefficients for the Helium-Krypton System

Using interaction potential parameters generated via the mixing rules shown in Table XXXVI, interaction virials were generated for comparison with Brewer's values. This comparison is shown in Table XLI. Examination of the results reveals that the harmonic mean, Rule II, $[\varepsilon_{jj} = 2\varepsilon_{ii}\varepsilon_{jj}/(\varepsilon_{ii} + \varepsilon_{jj})]$ is clearly superior to the other combination rules tested. HOwever, none of the mixing rules produce satisfactory results. At the lower end of the temperature range the disagreement is approximately 3 cc/mol for Rule II and from 8 to 10 cc/mol for the remaining mixing rules.

While the failure of the mixing rules to adequately predict B_{ij} values is disappointing, it is not surprising in view of the severe test imposed by the helium-krypton system. The helium and krypton molecules differ markedly in size and ionization potential as demonstrated by the fact that the well depths, ε, for the two species vary by a factor of approximately 25.

The results of the present test of mixing rules are consistent with the results of the work of Lin and Robinson (51), which was done subsequent to the present study. Their work was based on the excess virials reported by Brewer (10) for ten rare gas pairs, including the helium-krypton system. Although their work involved testing of mixing rules for the Dymond-Alder potential, the potential chosen does not seriously affect the conclusions reached, i.e., that Rule II was superior to the other rules tested and that the helium-krypton interaction virial coefficients are not satisfactorily predicted by any of the mixing rules.

TABLE XLI

COMPARISON OF SELECTED MIXING RULES
FOR PREDICTION OF He-Kr MIXED
SECOND VIRIAL COEFFICIENTS

Temp °K	Mixed Second Virials cc/mol				
	Brewer (10)	Rule I	Rule II	Rule III	Rule IV
325.15	21.56	16.66	20.54	16.98	17.56
298.15	21.04	15.94	20.50	16.30	16.96
273.15	20.3	15.06	20.43	15.46	16.22
223.15	19.09	12.54	20.06	13.08	14.09
198.15	17.91	10.70	19.70	11.33	12.51
173.15	16.01	8.23	19.15	8.97	10.39
148.15	15.27	4.77	18.35	5.68	7.43

CHAPTER VII

CONCLUSIONS AND RECOMMENDATIONS

A Burnett apparatus was constructed, tested and then used to collect experimental PVT data for the helium-krypton system. Data were taken along the -50, 0 and 50° c isotherms for a pressure range of 8 to 150 atm. The experimental results were reduced via non-linear regression analysis using the density expansion of the virial equation of state as the analytical model. The Burnett parameters, compressibility factors, and virial coefficients were regressed simultaneously. The volumetric properties thus generated were first compared to values reported by previous workers and then combined with selected data to form a basis for a study of the applicability fo the Kihara intermolecular potential function for representation of both the pure and mixed volumetric properties of the helium-krypton system. Specific conclusions and recommendations relevant to the various phases of this work are summarized below.

Experimental Apparatus

The results of this study confirm the value of the Burnett apparatus for obtaining very precise PVT data. The most important advantage offered by the method is that direct volume and/or mass determinations are not required. However, the method has the distinct disadvantage of requiring rather complicated reduction techniques to produce the desired volumetric properties of the system being studied.

The following recommendations and conclusions relative to the Burnett method and to the particular version of Burnett apparatus constructed in this work are offered:

(1) The apparatus and procedures employed successfully produced very precise data on the -50, 0 and +50° C isotherms.

(2) Due to the instability of the cryogenic DPI, operation of the apparatus at 100° C was unsuccessful.

(3) Efforts should be expended to encourage the manufacturer (Ruska) of the DPI cell to improve the temperature range of the instrument.

(4) The basic design of the apparatus used in this work could be significantly improved by employing a gas-lubricated piston gauge. This would eliminate the need for the intermediate gas DPI and reduce the magnitude of the head corrections.

(5) Barometric pressure measurements contributed significantly to random uncertainty in the experimental data. This resulted from the use of an inverted-tube mercury barometer during a portion of the data aquisition phase of this work. The quartz Bourdon tube gauge used during most of this work was approximately an order of magnitude more precise than the mercury barometer. The accuracy of the quartz gauge was not restrictive and the use of such a device is definitely recommended. However, if a gas-lubricated piston gauge were used, a better solution would be available. Gas lubricated piston gauges are available (Ruska Instruments Corporation) with a vacuum bell enclosure for the weights and this would completely eliminate the need for barometric pressure determinations.

(6) The size of the Burnett chambers should be maximized consistent with contraints such as availability of funds for purchase of sample gases, bath size and the time required for acquiring thermal equilibrium. Maximizing the sample volume minimizes the error associated with null-point shift in the cryogenic DPI cell.

(7) For successful experimental measurements, all instrumentation and the intermediate gas system must be enclosed in a temperature controlled environment.

(8) The two-piece stem High Pressure, Inc. valves with Teflon packing used in this work are highly recommended. The valves gave leak-tight performance during the entire course of the experimental work without replacement.

Reduction and Analysis of Results

The Burnett data generated in this work were reduced by employing non-linear regression analysis as proposed and reported by Hall (30). The methods used are undoubtably equal or superior to methods used in the past. However, further work in this area is indicated in view of the observation that the second virial coefficients from this work and from previous works exhibit a slight functional dependence on the third virials. Another problem that should be addressed is the difficulty in determining whether the convergence is at an absolute minimum or at a relative minimum. This problem is usually handled by employing a secondary regression technique to evaluate precise starting values for the non-linear regression. For example, in this work, graphical regression methods were used to evaluate the starting values for the

parameters. This procedure was tedious and time consuming. Accordingly, attempts were made to improve the technique and a solution to the problem was developed. Unfortunately, the data reduction phase of the present work was in the completion stages before the method was developed. However, the method was tested and based on the excellent results achieved it is recommended for use in future works. Briefly, the method consists of using the Redlich-Kwong (68) equation of state as the analytical model in the non-linear regression analysis. The Redlich-Kwong equation is a two parameter equation of state and the starting values for regression can be evaluated from the critical properties of the system. After the two Redlich-Kwong parameters are determined from the regression analysis, the virial coefficients can be estimated from the parameters by expanding the Redlich-Kwong equation to the virial form. The details of this method are shown in Appendix G.

In Chapter VI, the results of this study were presented and then examined via data comparisons and error analysis. From this examination, the following conclusions are offered:

(1) The compressibility factors generated in this study are in excellent agreement with the values reported by previous workers with one noteable exception. The values reported by Beattie (4) for pure krypton at 0^{o} C diverge significantly from all other workers. With this exception, the compressibility factors from this work are bracketed by the values reported by previous workers with the average agreement being better than one part per thousand.

(2) The helium second virials coefficients from this work display excellent agreement with the values reported by previous workers. The only exception is the adopted values reported by Keesom (41) and this is not considered significant since these values were not determined directly from experimental measurements. All other values fall within $\pm$0.3 cc/mol at -50° C and within $\pm$0.2 cc/mol at 0° C and +50° C. As was the case for the krypton second virials coefficients, the helium second virials from this work were bracketed by the values reported by previous workers.

(3) The second virial coefficients for pure krypton are in excellent agreement with other works at 0° C and +50° C. The values from this study are bracketed by those reported by previous workers with all values falling within a band of $\pm$1.0 cc/mol. Rowlinson (87) reports the only value, other than this work, at -50° C and a comparison between the two values shows a discrepancy of approximately 2.5 cc/mol. While this agreement can be viewed as acceptable, it is not completely satisfactory since the apparent accuracy of both this work and that of Rowlingson was higher than this comparison indicates.

(4) The inaccuracy in the results of this study is estimated to be $\pm 5 \times 10^{-4}$ for both the helium and krypton compressibility factors and $\pm$0.2 cc/mol and $\pm$0.8 cc/mol for the helium and krypton second virials coefficients, respectively.

(5) The estimated inaccuracy in the interaction virial coefficient for helium-krypton system is 1.6 cc/mol. Comparison of the

values from this work with those generated from Brewer's (10) excess virials shows satisfactory agreement at -50° C and ±50° C. The discrepancy of 2.6 cc/mol at 0° C is not entirely satisfactory. However, a plot of Brewer's interaction second virial coefficients as a function of temperature strongly suggests that the value reported by Brewer at 0° C should be approximately 20.3 cc/mol which would be in good agreement with the value of 21.5 cc/mol reported in the present work.

Molecular Interactions

The results of this study were combined with selected virial coefficient data reported by previous workers in order to provide a data base with sufficient temperature range to adequately test the applicability of the Kihara intermolecular potential function for representation of the helium-krypton virial coefficient data. The results of this test clearly demonstrated the ability of the Kihara potential to describe the pure-component second virial coefficients of the helium-krypton system. An excellent fit of the data was achieved with the Kihara potential. Only a few points displayed a deviation in excess of 1 cc/mol with the average deviation being 0.1 and 0.2 cc/mol for helium and krypton, respectively. Accordingly, the Kihara potential is recommended for representation of the helium-krypton pure component virial coefficients in the range studied.

Using Brewer's (10) excess virials coupled with smoothed pure virials generated with the Kihara potential, mixed second virials were generated to form the basis for testing selected mixing rules.

Based on the results of these tests, Rule II [$\varepsilon_{ij} = 2\varepsilon_{ii}\varepsilon_{jj} / (\varepsilon_{ii} + \varepsilon_{jj})$] was shown to be superior to the other rules tested. However, none of the combination rules were judged to produce satisfactory results. Accordingly, further work in this area is recommended. Specifically, emphasis should be given to future work directed toward development of satisfactory theoretical descriptions for unlike-molecular interactions.

SELECTED BIBLIOGRAPHY

1. Amagat, E. H., Anales de Chimie (5) 22, 353 (1881).

2. Barieau, R. E., Bureau of Mines, Information Circular 8388, United States Department of the Interior (1968).

3. Beattie, J. A., Proc. Am. Acad. Arts Sci. 69, 389 (1934).

4. Beattie, J. A., J. S. Brierley and R. J. Barriault, J. Chem. Phys. 20, 1613 (1952).

5. Ibid, 20, 1615 (1952).

6. Beenakker, J. J. M., F. H. Varekamp and A. Van Itterbecck, Commun. Kamerlingh Onnes Laboratorium, Leiden No. 313a.

7. Blancett, A. L, Ph.D. Thesis, University of Oklahoma, Norman, Oklahoma (1966).

8. Bloomer, O. T., Inst. Gas Tech. Res. Bul. 13, (1952).

9. Boyd, M. E., S. Y. Larsen and J. E. Kilpatrick, J. Chem. Phys. 50, 4034 (1969).

10. Brewer, J., "Determination of Mixed Virial Coefficients," Report No. MRL-2915-C, Air Force Office of Scientific Research, No. 67-2795 (1967).

11. Brewer, J. and G. W. Vaughn, J. Chem. Phys. 50, No. 7, 2960 (1969).

12. Briggs, T. C., Report of Investigations 7352, U. S. Bureau of Mines (1970).

13. Buckingham, A. D., Discussions Faraday Soc. 40, 232 (1965).

14. Burnett, E. S., J. Appl. Mech., Trans. ASME 58, A 136 (1936).

15. Byrne, M. A., M. R. Jones and L. A. K. Stavely, Trans. Farad. Soc. 64, 1741 (1968).

16. Canfield, F. B., Ph.D. Thesis, Rice University, Houston, Texas (1962).

17. Cattel, R. A., et al, U. S. Dept. Interior, Bur. Mines, R.I., 3501 (1940).

18. Connolly, J. R. and G. A. Kandalic, Doc. No. 6307, Documentation Institute, Library of Congress, Washington, D. C.

19. Constabaris, J. H., et al, J. Phys. Chem. 63, 1350 (1959).

20. Cook, D., Can. J. Chem. 35, 268 (1957).

21. Cook, G. A., "Argon Helium, and the Rare Gases," Interscience Publishers, New York, (1961).

22. Crain, R. W., Ph.D. Thesis, University of Michigan, Ann Arbor, Michigan (1965).

23. Delgarno, A. and W. D. Davidson, "Advances in Atomic and Molecular Physics," Academic, N. Y., London (1966).

24. DiPippo, R. and J. Kestin, J. Chem. Phys. 49, 2192 (1968).

25. Dymond, J. H., J. Chem. Phys. 49, 3673 (1968).

26. Dymond, J. H. and B. J. Alder, J. Chem. Phys. 51, 309 (1969).

27. Dymond, J. H., M. Rigby and E. B. Smith, Phys. of Fluids 9, 1222 (1966).

28. Dymond, J. H. and E. B. Smith, Oxford Science Research Papers 2, Clavendon Press, Oxford (1969).

29. Fender, B. E. F. and G. H. Halsey, Jr., J. Chem. Phys. 36, 1881 (1962).

30. Hall, K. R., Ph.D. Thesis, University of Oklahoma, Norman, Oklahoma.

31. Hall, K. R. and F. B. Canfield, Physica 33, 481 (1967).

32. Ibid., 47, 99 (1970).

33. Hanley, J. J. M. and M. Klein, Natl. Bur. Stud. (U.S.), Tech. Note 360 (1967).

34. Heichelheim, H. R., et al, J. Chem. Eng. Data 7, 507 (1962).

35. Hirschfelder, J. O., C. F. Curtiss and R. B. Bird, "Molecular Theory of Gases and Liquids," John Wiley and Sons, New York, (1954).

36. Hirth, L. F. and K. A. Kobe, J. Chem. Eng. Data 6, 233 (1961).

37. Holborn, L. and J. Otto, Z. Phys. 33, 1 (1925).

38. Hoover, A. E., Ph.D. Thesis, Rice University, Houston, Texas (1966).

39. Kalfoglou, N. K. and J. G. Miller, Phys. Chem. 71, 1256 (1967).

40. Kang, T. L., et al, J. Chem. Eng. Data 6, 220 (1961).

41. Keeson, W. H., "Helium," p. 49, Elsevier, Amsterdam (1942).

42. Keller, J. B. and B. Zumino, J. Chem. Phys. 30, 1351 (1959).

43. Kihara, T., Rev. Mod. Phys. 25, 831 (1953).

44. Kingston, A. E., J. Chem. Phys. 42, 719 (1965).

45. Knobler, C. M., J. J. M. Beenakker and H. F. P. Knaap, Physica 25, 909 (1959).

46. Kramer, G. M. and J. G. Miller, J. Phys. Chem. 61, 785 (1957).

47. Kuenen, J. P. and W. W. Randall, Proc. Rov. Soc. (London) 59, 60 (1895).

48. Lee, R. C., Ph.D. Thesis, Oklahoma State University, Stillwater, Oklahoma (1969).

49. Lennard-Jones, J. E., Proc. Roy. Soc. (London) 106A 463z (1924).

50. Lin, H.-M., Ph.D. Thesis, Oklahoma State University, Stillwater, Oklahoma (In Preparation).

51. Lin, H.-M. and R. L. Robinson, Jr., J. Chem. Phys. 52, 3727 (1970).

52. Ibid., 54, 52 (1971).

53. Liong, S. T., G. Sukehiro and W. E. Stewart, I. E. C. Fund 5, 363 (1966).

54. Love, A. E. H., "A Treatise on the Theory of Elasticity," Cambridge University Press, 4th ed., 145 (1934).

55. MacCormack, K. E. and W. G. Schneider, J. Chem. Phys. 18, 1269 (1950).

56. Ibid., 19, 845 (1951).

57. Margenau, H., Rev. Mod. Phys. U., 1 (1939).

58. Marquardt, D. W., J. Soc. Ind. Appl. Math. 11, 431 (1963).

59. Michels, A. and H. Wouters, Physica VIII, 923 (1941).

60. Michels, A., H. Wouters and J. DeBoer, Physica 1, 587 (1934).

61. Miller, J. E., L. W. Brandt and L. Stroud, Report of Investigations 5845, U. S. Bureau of Mines (1961).

62. Mueller, W. H., T. W. Leland Jr. and R. Kobayashi, AIChE J. 7, 267 (1961).

63. Munn, R. J. and F. J. Smith, J. Chem. Phys. 43, 3998 (1965).

64. Myers, A. L. and J. M. Prausnitz, Physica 28, 303 (1963).

65. Nicholson, G. A. and W. G. Schneider, Can. J. Chem. 33, 589 (1955).

66. Pfefferle, W. C., Jr., J. A. Goff and J. G. Miller, J. Chem. Phys. 23, 509 (1955).

67. Provine, J. A., Jr., Ph.D. Thesis, University of Oklahoma, Norman, Oklahoma (1969).

68. Redlich, O. and J. N. S. Kwong, Chem. Rev. 44, 233 (1949).

69. Sams, J. R., Jr., et al, J. Phys. Chem. 64, 1689 (1960).

70. Schneider, W. G., Can. J. Res. 27B, 339 (1949).

71. Schneider, W. G. and J. A. H. Duffie, J. Chem. Phys. 17, 751 (1949).

72. Sherwood, A. E. and J. M. Prausnitz, J. Chem. Phys. 41, 429 (1964).

73. Silverberg, I. H., K. A. Kobe and J. J. McKetta, J. Chem. Eng. Data 4, 314 (1959).

74. Ibid., 4, 323 (1959).

75. Stevens, A. B. and H. Vance, The Oil Weekly 106, 21 (1942).

76. Stuckey, A. N., Jr., Ph.D. Thesis, Oklahoma State University, Stillwater, Oklahoma (1966).

77. Theeuwes, F. and R. J. Bearman, J. Chem. Thermo. 2, 171 (1970).

78. Theeuwes, F. and R. J. Bearman, Trans. Kansas Acad. Sci. 72 No. 3, 342 (1969).

79. Thomaes, G. and R. van Steenwinkel, Nature 187, 229 (1960).

80. Ibid., 193, 160 (1962).

81. Timoshenko, S. and S. Wornowsky-Krieger, "Theory of Plates and Shells," 2 Ed., McGraw Hill Book Co., New York.

82. Toxoaerd, S. and E. Praestgaard, Acta. Chem. Scand. 22, 1873 (1968).

83. Trappeniers, N. J., T. Wassenaar and G. S. Wolkers, Physica 32, 1503 (1966).

84. Varekamp, F. H. and J. J. M. Beenakker, Physica 24, 167 (1958).

85. Vogl, W. F. and K. R. Hall, Physica 59, 529 (1972).

86. Weir, R. D., Mol. Phys. 11, 97 (1966).

87. Weir, R. D., I. W. Jones, J. S. Rowlinson and G. Saville, Trans. Farraday Soc. 63, 1320 (1967).

88. Whalley, E., Y. Lupien and W. G. Schneider, Can. J. Chem. 31, 722 (1953).

89. Whally, E. and W. G. Schneider, Trans. ASME 76, 1001 (1954).

90. White, D., et al, J. Phys. Chem. 64, 1607 (1960).

91. Wiebe, R., V. L. Gaddy and C. Heins, Jr., J. Am. Chem. Soc. 60, 2300 (1938).

92. Wilde, D. J., "Optimum Seeking Methods," Prentice-Hall, Englewood Cliffs, N. J. (1964).

93. Witonsky, R. J. and J. G. Miller, J. Am. Chem. Soc. 85, 282 (1963).

94. Yntema, J. L. and W. G. Schneider, J. Chem. Phys. 18, 641 (1950).

95. Ziegler, J. G. and N. B. Nicholls, Trans. ASME 64, 759 (1942).

96. Values were taken from "Metallic Materials and Elements for Flight Vehicle Structures," Military Hardbook 5, Department of Defense, Washington, D. C. (1962).

APPENDIX A

ADDITIONAL EQUIPMENT SPECIFICATIONS

A description of the experimental apparatus used in this work was presented in Chapter III. In this section, supplemental information and equipment specifications will be given.

Equipment Used for Pressure Measurements

Ruska Dead Weight Testers

As discussed in Chapter III, two separate Ruska gauges were used in this work. Data on the 0^{o} C isotherm were taken utilizing Ruska model number 2400 HL piston gauge. The remaining data were taken with model number 2400.21, serial number 14203 Ruska gauge. Specifications and mass calibrations for the first gauge are given in Tables XLII and XLIII, respectively. Similarly, values for the second gauge are shown in Tables XLIV and XLV.

Ruska Differential Pressure Indicators

Two separate differential pressure indicators (DPI) were used in the pressure measuring equipment. The first (DPI1) was connected directly to the upper chamber of the Burnett cell while the second instrument (DPI2) was an integral part of an intermediate gas system. The use of two DPI instruments in conjunction with the intermediate

TABLE XLII

RUSKA PISTON GAUGE SPECIFICATIONS
(Model No. 2400 HL)

Accuracy:	1:10,000
Resolution:	5:1,000,000
Low Range Piston-Cylinder (No. LC-142):	
Area @ 25° C and 0 psig	0.130219 $in.^2$
Coefficient of thermal expansion	$1.7 \times 10^{-5}/°C$
Coefficient of distortion	-5.4×10^{-8}/psi
High Range Piston-Cylinder (No. HC-133):	
Area @ 25° C and 0 psig	0.0260416 $in.^2$
Coefficient of thermal expansion	$1.7 \times 10^{-5}/°C$
Coefficient of distortion	-3.6×10^{-8}/psi

TABLE XLIII

RUSKA MASS CALIBRATIONS
(Model No. 2400 HL)

Designation	Nominal Pressure, psig		Apparent Mass versus Brass Stds. (lb_m)
	High Range	Low Range	
Low tare	30	60	0.78107
High tare	30		0.78107
A	1000	200	26.03509
B	1000	200	26.03537
C	1000	200	26.03571
D	1000	200	26.03570
E	1000	200	26.03536
F	1000	200	26.03592
G	1000	200	26.03603
H	1000	200	26.03558
I	1000	200	26.03568
J	1000	200	26.03608
K	1000	200	26.03568
L	500	100	13.01794
M	200	40	5.20714
N	200	40	5.20715
O	100	20	2.60359
P	50	10	1.30181
Q	20	4	0.52072
R	20	4	0.52074
S	10	2	0.26035
T	5	1	0.13020
U	2	0.4	0.05208
V	2	0.4	0.05209
W	1	0.2	0.02604
X	0.5	0.1	0.01302

TABLE XLIV

RUSKA PISTON GAUGE SPECIFICATIONS
(Model No. 2400.21)

Accuracy:	1:10,000
Resolution:	5:1,000,000
Low Range Piston-Cylinder (No. LC-319):	
Area @ 25° C and 0 psig	0.1302097 $in.^2$
Coefficient of thermal expansion	-9.3×10^{-9}/psi
High Range Piston-Cylinder (No. HC-361):	
Area @ 25° C and 0 psig	0.0260335
Coefficient of thermal expansion	$9.1 \times 10^{-6}/^{\circ}C$
Coefficient of distortion	-8.7×10^{-9}/psi

TABLE XLV

RUSKA MASS CALIBRATIONS
(Model No. 2400.21)

Designation	Nominal Pressure, psig		Apparent Mass versus Brass Stds. (lb_m)
	High Range	Low Range	
Low tare	30	60	0.781067
High tare	30		0.781085
A	1000	200	26.03523
B	1000	200	26.03558
C	1000	200	26.03462
D	1000	200	26.03529
E	1000	200	26.03541
F	1000	200	26.03518
G	1000	200	26.03548
H	1000	200	26.03551
I	1000	200	26.03550
J	1000	200	26.03545
K	1000	200	26.03580
L	500	100	13.01735
M	200	40	5.20726
N	200	40	5.20717
O	100	20	2.60353
P	50	10	1.30173
Q	20	4	0.520692
R	20	4	0.520723
S	10	2	0.260364
T	5	1	0.130219
U	2	0.4	0.052085
V	2	0.4	0.052080
W	1	0.2	0.026045
X	0.5	0.1	0.013028

gas system associated with the dead weight tester from the Burnett cell temperature bath.

A general characteristic of the Ruska DPI cells is a slight null shift as a function of applied pressure. A calibration curve was supplied by Ruska for each instrument which allowed calculation of the pressure across the instrument at apparent null. This information was sufficient for successful use of the intermediate gas DPI since this instrument was housed in a temperature bath maintained at a temperature near that for which the calibration was made by Ruska. Also, and more importantly, the slight flexure of the diaphragm at apparent null did not affect the volume of the Burnett cell. However, the DPI connected directly to the Burnett cell caused the volume of the upper Burnett chamber to vary with changing position of the diaphragm. Thus corrections must be made to compensate for this factor. Since these corrections are quite involved, Appendix B and C are devoted to this and other relevant correction factors.

The calibration curve for the intermediate gas DPI is shown in Figure 19. Instrument specifications for DPI1 and DPI2 are presented in Table XLVI. The specification for sensitivity of DPI1 will be superseded by actual experimental measurements as outlined in Appendix B.

Temperature Measurements

A Leeds and Northrup G-2, Model 8069B, Mueller bridge was used in conjunction with a Leeds and Northrup Model 2284-D ballistic type galvanometer to measure the resistance of the platinum resistance thermometers. The ballistic galvanometer was supported by a Leeds

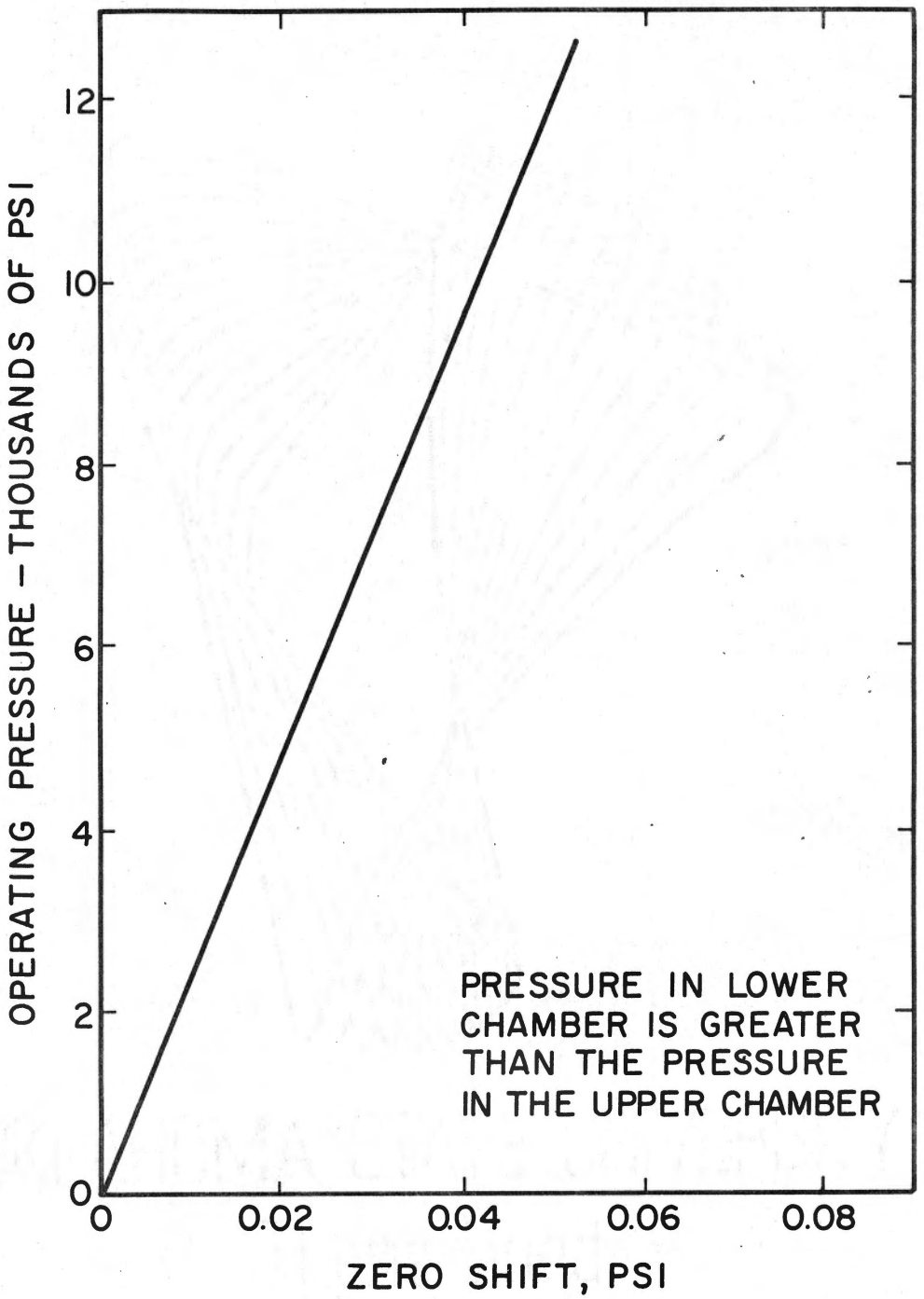

Figure 19. Effect of Pressure on the Null Point of the Intermediate Gas DPI

TABLE XLVI

SPECIFICATIONS FOR RUSKA DIFFERENTIAL PRESSURE INDICATORS

	Model 2416.1 Ser. No. 10091	Model 2437.5 Ser. No. 14739
Accuracy, psi	0.01	0.01
Sensitivity, psi	1×10^{-4}	2×10^{-4}
Max. Operating Pressure, psi	15000	15000
Temperature Range, ^{o}F	40 to 130	40 to 160
Thickness of Diaphragm, in.	0.002	0.002

and Northrup Model 2162 Julius Suspension apparatus. The Mueller bridge had been calibrated by Leeds and Northrup. The calibration is shown in Table XLVII.

Three different platinum resistance thermometers were used during the course of this work. During the equipment check out phase and for the first two runs on pure helium (0^{o} C isotherm) a Leeds and Northrup Model 8163, Serial No. 1576919, was used. This thermometer was housed in a glass sheath which was inadvertantly broken during a downtime for equipment repairs. The remaining data on the 0^{o} C isotherm were taken with a Leeds and Northrup Model 8164, Serial No. 1612800, thermometer. The remaining experimental work was completed with Model 8164, Serial No. 1697602.

All thermometers were constructed from strain-free, high-purity platinum and were calibrated by the National Bureau of Standards (NBS). The calibrations supplied by NBS were in both tabular and equation form. The equation form of the calibrations was used in this work.

$$T = \frac{R_t - R_0}{aR_0} + b\left[\frac{T}{100} - 1\right]\frac{T}{100} + C\left[\frac{T}{100} - 1\right]\left[\frac{T}{100}\right]^3 \quad \text{(A-1)}$$

where

T = ^{o}Celsius at outside surface of protective sheath

R_t = Resistance at T ^{o}C, abs. ohms

R_0 = Resistance at 0^{o} C, abs. ohms

a, b, c = Constants of calibration

The resistance at T^{o} C is measured with the Mueller bridge with first normal and then reverse flow of current (2 milliamps) through the thermometer. The normal and reverse reading are designated N and R,

TABLE XLVII

G-2 MUELLER BRIDGE CALIBRATION
(Serial No. 1550042)*

Reading	Correction, ohms	Reading	Correction, ohms
	10 Dial		1 Dial
0	0.0000	0	0.00000
10	0.0000	1	0.00001
20	0.0002	2	0.00002
20.5	0.0001	3	0.00002
30	0.0003	4	0.00002
40	0.0003	5	0.00003
50	0.0003	6	0.00004
60	0.0004	7	0.00005
70	0.0005	8	0.00006
80	0.0006	9	0.00006
90	0.0007	X	0.00006
X	0.0007		
	0.1 Dial		0.01 Dial
0.0	0.00000	0.00	0.00000
0.1	0.00000	0.01	0.00000
0.2	0.00000	0.02	0.00000
0.3	0.00001	0.03	0.00000
0.4	0.00001	0.04	0.00001
0.5	0.00002	0.05	0.00001
0.6	0.00002	0.06	0.00001
0.7	0.00002	0.07	0.00001
0.8	0.00002	0.08	0.00001
0.9	0.00003	0.09	0.00001
X	0.00003	X	0.00001

* Note: No correction for 0.001 and 0.0001 dial settings.

respectively. R_t is then given by $(N + R)/2$.

The constants for use with Equation (A-1) are as follows:

	Serial No. 1612800	Serial No. 1697602
a =	0.003926375	0.003926208
b =	1.49241	1.4915154
$T < 0^{\circ}C$, c =	0.11027	0.1105781
$T > 0^{\circ}C$, c =	0	0
R_0 =	25.5475	25.531583

As discussed in Chapter III, the temperature measuring equipment was checked before data aquisition started on each isotherm with a Trans-Sonics, Inc., triple-point-of-water cell. The triple point cell was guaranteed to reproduce the triple point of water (0.01° C) with an accuracy of $\pm 0.0005^{\circ}$ C. This check served as an important function since all associated equipment as well as the resistance of the thermometer could be validated.

APPENDIX B

EFFECT OF PRESSURE ON NULL POINT AND SENSITIVITY OF THE CRYOGENIC DIFFERENTIAL PRESSURE INDICATOR

As described in Chapter III, the lower chamber of the cryogenic DPI was connected directly to the upper chamber of the Burnett cell. An inherent characteristic of this instrument is a slight null shift with pressure. That is, when equal pressures are applied to both sides of the diaphragm, the DPI read-out varies from the initial zero reading as the applied pressure is increased. Thus if pressure determinations are made at zero DPI readings, a pressure difference actually exists across the diaphragm. This pressure difference causes a slight flexure of the diaphragm and a corresponding change in the volume of the Burnett cell. Therefore, a means must be provided to correct for both the pressure difference and the volume change due to the null shifts of the DPI.

After data acquisition had been completed, an experiment was designed to yield the necessary information for the above mentioned corrections. Figure 20 shows a schematic representation of the equipment as used in these determinations. The only change from the original configuration is that the expansion valve was repiped to the upper chamber of the DPI rather than the second volume of the Burnett cell. With this configuration, the null shift could be monitored as a

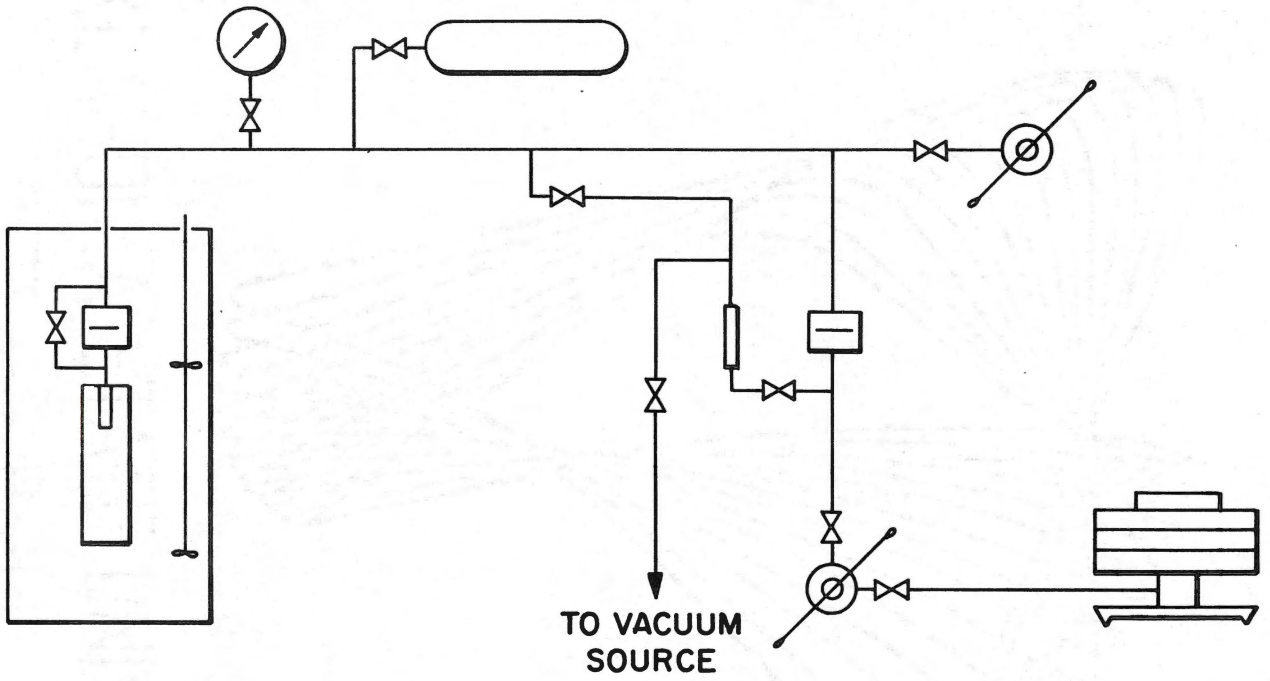

Figure 20. Schematic Representation of Equipment Configuration

function of pressure with the assurance that the pressures in the upper and lower chambers of the DPI were identical. However, some means had to be developed to determine the pressure difference required to bring the DPI reading back to its original zero setting. The necessary experimental measurements were made according to the procedure described below.

The first step was to establish temperature control. This was accomplished in accord with the procedure discussed in Chapter IV. This task accomplished, both the cryogenic and intermediate DPI, denoted hereafter as DPI1 and DPI2, respectively, were overpressured from the one side by approximately 100 psi. This helped to enhance the stability of the instruments providing that any overpressure during the course of measurements occurred only from this side. With reasonable precaution and perserverance this prerequisite could be met. After several minutes, the overpressure was slowly relieved and both DPI1 and DPI2 were zeroed after waiting about one hour for any thermal effects to equilibrate. The procedure for zeroing these instruments is discussed fully in Chapter IV. Next, with the by-pass valve open, the system was charged to highest pressure used for the compressibility measurements (about 2000 psig). While waiting for temperature equilibration, the dead weight tester was turned on and balanced to the system pressure according to the procedure discussed in Chapter IV. After approximately one hour, the reading for DPI1 was recorded and the by-pass valve slowly closed so as not to cause any change in the reading. Closing the valve changed the system pressure slightly making it necessary to add weights to the dead weight tester in order to restore a null reading on DPI2. At this point, the diaphragm of

DPI1 was unflexed and the system pressure precisely known. Using the gas pump, the pressure in the upper chamber of DPI1 was varied to yield a null reading. Then sufficient mass was added or subtracted from the dead weight tester to restore the DPI2 reading to null. When converted to pressure difference, this mass change was a direct measure of the apparent null shift of DPI1. Next, the gas pump was used to vary DPI1 reading full scale and one-half scale deflections with similar pressure difference measurements being made. These measurements constituted apparent sensitivity determinations. The above procedure was repeated at successively lower pressures at increments usually of 100 psi. For cases where the null shift was very small, such as at low pressure, no direct measure of the null shift was attempted. Rather, the apparent DPI sensitivity was measured and the DPI reading for the null shift assumed to be a linear fraction of the pressure difference measured for one-half scale deflection.

The determinations as described above were not direct measurements of null shift and sensitivity since as the pressure is varied in the upper chamber of DPI1 the diaphragm is flexed thus causing a corresponding pressure change below the diaphragm. Thus the actual pressure difference across the diaphragm must be calculated by combining the above measurements with strength of materials calculations, specifically the theory of thin plates and shells (81).

Applying the theory of thin plates and shells, the deflection (δ) of the center of the diaphragm can be expressed as

$$\delta + 0.583 \frac{\delta^3}{h^2} = 0.176 \frac{qa^4}{Eh^3} \qquad \text{(B-1)}$$

where

a = radius of diaphragm = 0.95 in.

E = modulus of elasticity

h = diaphragm thickness = 0.002 in.

q = load, psi

Assuming the geometry of the diaphragm to be spherical, the volume change for a given deflection is

$$V = \frac{1}{6} \Pi \delta \ (3a^2 + \delta^2) \tag{B-2}$$

or to a close approximation, since δ is quite small

$$V = \frac{1}{2} \Pi \ a^2 \ \delta \tag{B-2a}$$

For isothermal compression, the pressure change below the diaphragm is

$$\Delta P_{lc} = P_i \Delta V / V_i \tag{B-3}$$

where the subscripts lc and i indicate lower chamber and initial value, respectively. Subtracting the pressure change below the diaphragm from the experimentally measured change that occurs in the upper chamber gives the net diaphragm load, q.

$$q = \Delta P_{uc} - \Delta P_{lc} \tag{B-4}$$

Substituting (B-3) into (B-4) gives

$$q = \Delta P_{uc} - P_i \Delta V / V_i \tag{B-5}$$

and (B-2) into (B-5) yields

$$Q = \Delta P_{uc} - \frac{P_i}{V_i} \left(\frac{1}{2} \Pi \ a^2 \ \delta\right) \tag{B-6}$$

Finally, an important result is given by substituting (B-6) into (B-1)

$$\delta + 0.583 \frac{\delta^3}{h^2} = \frac{0.176a^4}{Eh^3} \left[\Delta P_{uc} - \frac{P_i}{V_i} \left(\frac{1}{2} \pi a^2 \delta\right)\right] \qquad \text{(B-7)}$$

Equation (B-7) expresses the unknown deflection, δ, in terms of the measured pressure change in the upper chamber of the DPI, the system pressure, dimensions of the diaphragm, volume of the upper Burnett chamber and the modulus of elasticity of the diaphragm. The modulus of elasticity is a function of temperature, and this information is not readily available for stainless steel. However, sufficient data were available (96) for 301 half-hard stainless (the diaphragm was 302 SS of unknown hardness) and the calculations were made using this information. The temperature dependence was available only for room temperature and above, but the relationship was quite linear over a range of 900° F. Thus extrapolation to 0 and -50° C could be made with relatively high confidence. The values used were 30.1, 29.3 and 28.9×10^6 psi for -50, 0 and 50° C, respectively.

After the deflection is obtained from Equation (B-7), the diaphragm load follows directly from Equation (B-6). This corresponds to the actual null shift or sensitivity for one-half scale deflection, depending on the type of experimental pressure change, ΔP_{uc}, measured.

The results of the foregoing analysis are shown in Figures 21 and 22. Figure 21 shows the relationship between the system pressure, P_i, and the sensitivity for one-half scale deflection. Figure 21 indicates essentially no dependence of sensitivity on temperature. For -50 and +50° C, the pressure dependence follows a rational trend, but the 0° C data exhibit near randomness. However, the important

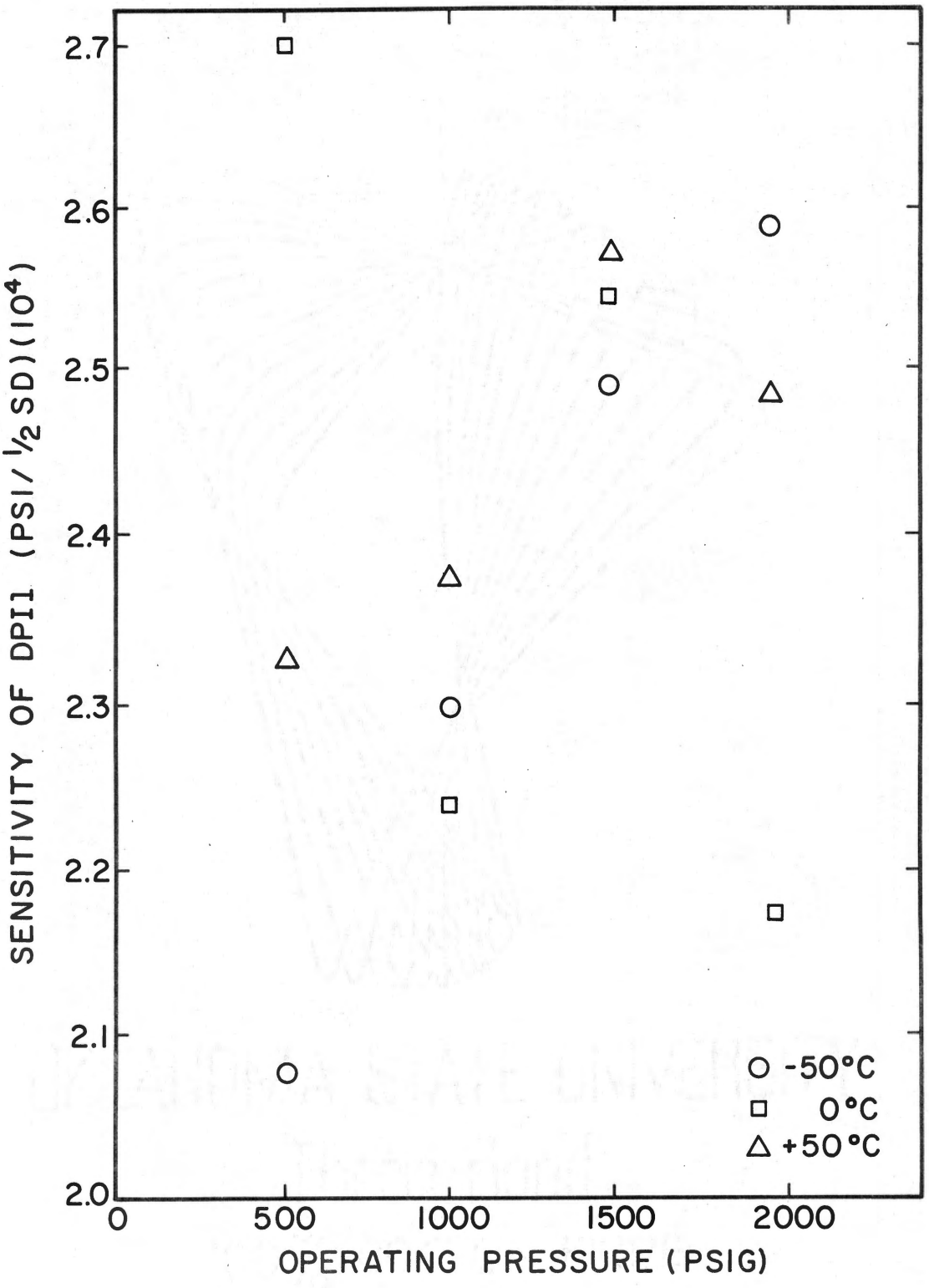

Figure 21. Sensitivity of the Cryogenic DPI

conclusion to be drawn is the relatively small range of sensitivity (2.0 to 2.7×10^{-4} psi) over the entire temperature and pressure range used in the course of experimental compressibility determinations. Figure 22 depicts the null shift as a function of pressure. The dependence of null shift on the temperature and pressure is quite evident and can be correlated with confidence.

Since the information contained in Figure 22 was needed in the computer calculations used to convert the dead weight tester readings to pressures, the information was put into equation form using linear regression techniques. The resulting equations were

$$\text{For } 50^{\circ}\text{ C}, \quad \Delta P = 0.195 \times 10^{-6} P - 2.85(10^{-6}) \tag{B-8}$$

$$\text{For } 0^{\circ}\text{ C}, \quad \Delta P = 0.40377(10^{-6}) - 0.26866(10^{-7})P + 0.16711(10^{-9})P^2 - 0.14140(10^{-12})P^3 + 0.52451(10^{-16})P^4 - 0.66897(10^{-20})P^5 \tag{B-9}$$

$$\text{For } -50^{\circ}\text{ C}, \quad \Delta P = 0.78911(10^{-6}) - 0.95746(10^{-7})P + 0.24800(10^{-9})P^2 - 0.20366(10^{-12})P^3 + 0.80889(10^{-16})P^4 - 0.12030(10^{-19})P^5 \tag{B-10}$$

where pressure is expressed in psi.

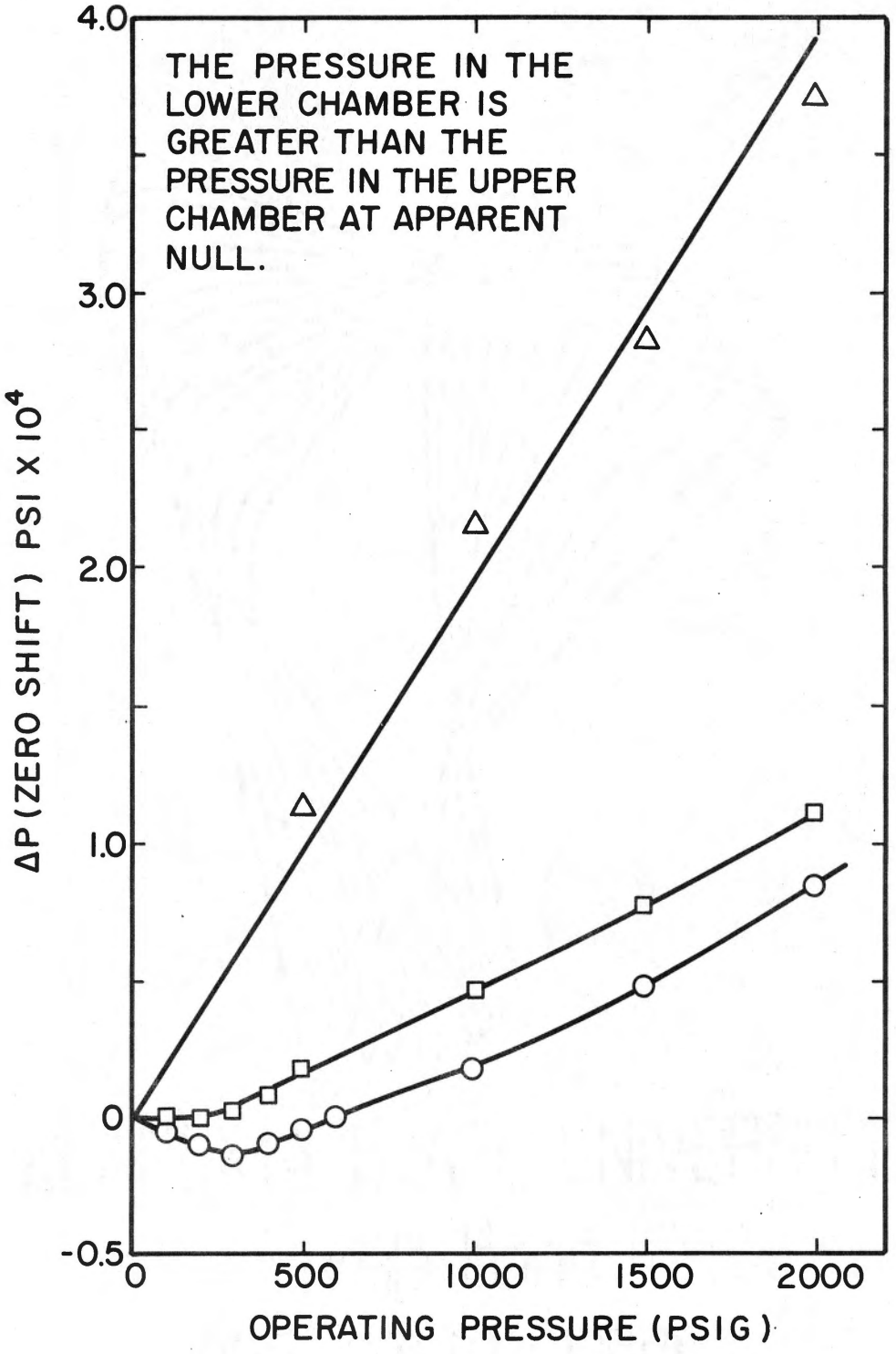

Figure 22. Effect of Pressure on the Null Point of the Cryogenic DPI

APPENDIX C

EFFECT OF PRESSURE ON THE APPARATUS VOLUME RATIO

Successful application of the Burnett method requires an accurate knowledge of the apparatus volume ratio as a function of pressure. The apparatus volume ratio is defined by

$$N_j = \frac{(V_a + V_b)_j}{(V_a)_{j-1}} \qquad \text{(C-1)}$$

The denominator of Equation (C-1) is the volume occupied by the sample before an expansion. This volume includes the volume of the upper chamber of the Burnett cell, all fittings used to connect the cell to the DPI, the seat side of the expansion valve and all interconnecting tubing between the charge and expansion valve. The numerator is the total volume after an expansion and this term includes all of the above plus the volume contributed by the lower chamber of the Burnett cell, the packing side of the expansion valve, the seat side of the exhaust valve, and all interconnecting fittings and tubing between these valves. Equation (C-1) can be written in terms of the volume at zero pressure and the change in volume due to pressure distortion as follows

$$N_j = \frac{(V_a)_{00} + (\Delta V_a)_j + (V_b)_{00} + (\Delta V_b)_j}{(V_a)_{00} + (\Delta V_a)_{j-1}} \qquad \text{(C-2)}$$

where the subscript ∞ denotes values at zero pressure and the delta quantities are the volume changes due to pressure. Dividing (C-2) by $(V_a)_\infty$ gives

$$N_j = \frac{\frac{(V_a)_\infty + (V_b)_\infty}{(V_a)_\infty} + \frac{(\Delta V_a + V_b)_j}{(V_a)_\infty}}{1 + \frac{(\Delta V_a)_{j-1}}{(V_a)_\infty}} \qquad \text{(C-3)}$$

or

$$N_j = N_\infty \frac{1 + \frac{(\Delta V_a + \Delta V_b)_j}{(V_a + V_b)_\infty}}{1 + \frac{(\Delta V_a)_{j-1}}{(V_a)_\infty}} \qquad \text{(C-4)}$$

where N_∞ is the apparatus volume ratio at zero pressure and by Burnett convention is defined as the cell or apparatus constant. The cell constant is determined from treatment of the Burnett data. Thus the problem of calculating the volume ratios at the various experimental pressures is dependent only on successful determination of the cell constant and the effect of pressure on the elements of the Burnett cell.

The pressure effect on the volume of several of the individual components can be calculated by employing the theory for closed-end thick walled cylinders. As presented by Love (54), the pressure effect for this case can be expressed as

$$\frac{\Delta V}{V} = \frac{P_0}{E(R_1^2 - R_0^2)} \left[2(1-\mu)R_1^2 + 3(1-2\mu)R_0^2\right] \qquad \text{(C-5)}$$

where

R_0 = internal diameter

R_1 = external diameter

E = modulus of elasticity

μ = Poisson's ratio

P_0 = internal pressure

Burnett Cells

The Burnett chambers were identical in size and the appropriate values for application of Equation (C-5) are

$R_0 = 0.591$ inches

$R_1 = 3.0$ inches

$E = 3X10^7$ psi

$\mu = 0.4$

$V = 1.235 in^3$

Thus the pressure effect for the chambers is

$$\frac{\Delta V}{V} = 2.24X10^{-8}P_0 \qquad (C-6)$$

or

$$\Delta V = 2.78X10^{-8}P_0 \qquad (C-7)$$

where

P_0 is expressed in pounds per square inch.

A cylinder (9/16 O.D.X2 1/4 inch long) was inserted into the second, or expansion, Burnett chamber in order to achieve the desired volume ratio. Any deformation of this cylinder would represent an

increase in V_b and thus must be taken into account. The compressibility of metals can be expressed as

$$\frac{\Delta V}{V} = KP_0 \qquad \text{(C-8)}$$

where K is the bulk modulus of the metal. For stainless steel K is approximately $1.09X10^{-7}$/psi. Then

$$\Delta V = 6.1X10^{-8}(P_0) \qquad \text{(C-9)}$$

The total deformation of the expansion chamber is the sum of (C-7) and (C-9)

$$\Delta V = 8.88X10^{-8}P_0 \qquad \text{(C-10)}$$

Tubing, Valves and Fittings

The tubing and fittings can be treated as thick walled cylinders. Thus the pressure effect for these items can be calculated by straightforward application of Equation (C-5). The valves however, because of their complicated geometry, cannot be expected to conform to the theory of closed-end thick walled cylinders. Since the contribution of these items is such a small fraction of the total volume, the deformation will be assumed negligible in comparison with the other items involved.

The effect of pressure on the tubing and fittings associated with the first and second chambers of the Burnett cell is shown in Tables XLVIII and XLVIX, respectively.

TABLE XLVIII

THE EFFECT OF PRESSURE ON TUBING AND FITTINGS ASSOCIATED WITH THE FIRST CHAMBER OF THE BURNETT CELL

Item	Effective Dimensions (In.) I.D.	O.D.	Length	Vol.	$\Delta V/P$ (In^3/Psi)
Tubing	0.06	0.125	12	0.034	$1.97(10^{-9})$
Connector, 3/16"RIC* to 1/8"NPT	0.0767	0.327	1.606	0.00741	$0.32(10^{-9})$
Cross, 1/8"FNPT X 3 - 1/8"RIC					
1/8"FNPT	0.330	0.590	0.50	0.0427	$2.44(10^{-9})$
3 - 1/8"RIC	0.055	0.319	2.77	0.00802	$0.37(10^{-9})$
Connector, 1/8"FRIC to 1/8"NPT	0.122	0.395	0.687	0.00802	$0.37(10^{-9})$
Bushing, 1/8FNPT to 3/8"NPT	0.343	0.638	0.50	0.0462	$4.00(10^{-9})$
Total				0.1449	$7.1\ (10^{-9})$

* Ruska Instrument Corporation

TABLE XLVIX

THE EFFECT OF PRESSURE ON TUBING AND FITTINGS ASSOCIATED WITH THE SECOND CHAMBER OF THE BURNETT CELL

Item	Effective Dimensions (In.) I.D.	O.D.	Length	Vol.	$\Delta V/P$ (In^3/Psi)
Tubing	0.06	0.125	20	0.057	$3.28(10^{-9})$
Bushing, 1/8"FNPT to 3/8"NPT	0.343	0.638	0.50	0.0462	$4.00(10^{-9})$
Tee, 1/8"NPT X 2 - 1/8"RIC					
1/8"NPT	0.109	0.406	0.75	0.00700	$0.31(10^{-9})$
2 - 1/8"RIC	0.055	0.319	1.875	0.00445	$0.21(10^{-9})$
Total				0.1147	$7.80(10^{-9})$

Differential Pressure Indicator

The experimental pressure readings were made when the DPI read-out was on zero. However, due to the slight null shift with pressure which is an inherent characteristic of this type instrument, a very small pressure difference across the diaphragm existed. This, of course, causes a slight flexure of the diaphragm and a corresponding change in the volume of the upper Burnett chamber. As described earlier, this volume change can be expressed as a function of the pressure difference, q, across the diaphragm.

$$\Delta V = \frac{0.088\Pi a^6 q}{Eh^3} \qquad \text{(C-11)}$$

where

a = diaphragm radius = 0.95 inches

E = modulus of elasticity = $3X10^7$ psi

h = diaphragm thickness = 0.002 inches

q = load, psi

since q is a function of pressure, Equation (C-11) can be combined with pressure versus q relationships to give the volume change as a function of pressure. The resulting equations are listed below.

For 50^o C, $\Delta V = \beta(10^{-6})(-2.85+0.195P)$ (C-12a)

For -50^o C,

$$\Delta V = \beta[0.78911(10^{-6})-0.95746(10^{-7})P+0.24800(10^{-9})P^2 -0.20366(10^{-12})P^3+0.80889(10^{-16})P^4 -0.12030(10^{-19})P^5] \qquad \text{(C-12b)}$$

For 0^{o} C, $\Delta V = \beta[0.40377(10^{-6})-0.26866(10^{-7})P+0.16711(10^{-9})P^2$

$$-0.14140(10^{-12})P^3+0.52451(10^{-16})P^4$$

$$-0.66897(10^{-20})P^5] \qquad \text{(C-12c)}$$

where

$$\beta = 0.088\pi a^6/Eh^3$$

In addition to the volume change caused by the null shift, slight deformation of the DPI cell occurs. However, its geometry is such that any attempt to estimate the deformation would probably be fruitless. Since the volume of that portion of the DPI cell under the disphragm is only about 1.5cc, the deformation probably is not significant.

Combining the foregoing results yields the necessary quantity for evaluation of N_j from Equation (C-4). The results of this combination are as follows

$$(\Delta V_a)_j = 3.49(10^{-8})P_j+F(P_j) \qquad \text{(C-13)}$$

$$(V_a)_{\infty} = 1.47 \text{ in}^3 \qquad \text{(C-14)}$$

$$(\Delta V_b)_j = 9.66(10^{-8})P_j \qquad \text{(C-15)}$$

$$(V_b)_{\infty} = 0.79 \text{ in}^3 \qquad \text{(C-16)}$$

where

$F(P_j)$ is the volume change due to the null shift of the DPI and is calculated from Equation (C-12).

APPENDIX D

COMPOSITION OF SAMPLE GASES

The composition of the sample gases used in this study will be presented in detail in this Appendix. The composition of the samples is an important parameter since the compressibility can be a strong function of composition. As discussed previously, the experimental procedure used for data aquisition was designed to minimize the potential for contamination from one run to the next.

The pure helium used in this work was donated by the Bureau of Mines, Helium Research Center. The helium was ultra pure and an analysis by the Helium Research Center of the gas from the cylinder supplied indicated 4.7 molar ppm impurities. The pure krypton gas was research grade and was supplied by Air Products, Inc. The analysis of the pure krypton (analysis by Air Products, Inc.) indicated 80 molar ppm impurities. The helium-krypton mixture samples were also supplied by Air Products, Inc. The mixtures were prepared from ultra pure grade helium and the same krypton as that supplied for the pure krypton sample. A summary of the analyses for the pure gases is presented in Table L.

The helium-krypton mixture compositions were specified by Air Products, Inc. The method of analysis was gas chromatography. For the purpose of an independent check, samples of the mixtures were shipped to the Helium Research Center for analyses via mass spectrometer. The analyses of the helium-krypton samples are shown in Table LI.

TABLE L

ANALYSIS OF THE HELIUM AND KRYPTON
PURE GAS SAMPLES

Component	Analytical Result, Molar ppm		
	Pure Helium		Krypton
	Sample Gas	Mixture Gas	
Nitrogen	0.9	< 5.0	29.0
Hydrogen	0.0		< 2.0
Oxygen & Argon	0.3	0.5	20.0
Neon	0.9		
Xenon	-		25.0
Water	2.5	0.2	0.2
Hydrocarbon	0.0	< 1.0	2.8
Carbon Dioxide	0.1		

TABLE LI

COMPOSITION ANALYSIS OF HELIUM-KRYPTON
SAMPLE GASES

Nominal Composition	Composition, Mole % He in Kr	
	Gas Chromatograph	Mass Spectrometer
25% He	24.4	24.8
50% He	48.9	49.7
75% He	74.6	74.6
Krypton	100.0	--

APPENDIX E

CONVERSION FACTORS

The virial equation of state, in the fundamental form, is an infinite series in reciprocal volume. However, other forms of the equation are useful and virial coefficients are often expressed and reported in units other than the centimeter, gram, second (metric) system. The functional relationships between the virial coefficients along with the basic constants used in reduction of the data from the work as presented in this section.

Basic Constants

The volume of an ideal gas at standard conditions was taken as 22413.6 cc/mole. Standard conditions are defined as follows:

Pressure = 1 atm = 14.69 psi

Temperature = 273.15° K = 0° C

Other basic values used are as follows:

Avogadros constant, N_0 = 6.0229×10^{23}/mole

Boltzmann constant, k, = 1.38044×10^{-16} erg/deg

Molecular weight, He = 4.003
Kr = 83.80

Ionization potential, He = 24.5 ev
Kr = 14.0 ev

Critical temperature, He = -268° C
Kr = -63.6° C

Critical pressure, He = 33.2 psia
Kr = 796.2 psia

Virial Coefficient Relationships

The three commonly used forms of the virial equation of state can be written as follows:

$$PV = RT \left[1 + B_v/V + C_v/V^2 + \ldots \right] \qquad \text{(E-1)}$$

or

$$PV + RT \left[1 + B_p P + C_p P^2 + \ldots \right] \qquad \text{(E-2)}$$

and

$$PV_a = A_a + B_a/V_a + C_a/V_a^2 + \ldots \qquad \text{(E-3)}$$

The first expansion is the fundamental form since the various coefficients can be related to the intermolecular potential energy of interaction. In this form, volume is expressed in the c-g-s system, i.e., cc/mole. Since this is the fundamental form of the virial equation, the virial coefficients shown in for the purpose of comparisons in Chapter VI were expressed in c-g-s units.

The expansion in the pressure series is convenient since pressure is more readily measured than volume. However, the pressure series normally converges slower than the volume series and the coefficient must of course, be converted to the equivalent volume series coefficients for use in molecular interaction studies.

The expansion shown in Equation (E-3) has volume expressed in the amagat unit. Volume in Agagat units is the ratio of the actual volume of gas to the volume of the gas at 0° C and 1 atm.

Determination of the relationship between the coefficients from the pressure series and the volume series can be established by simple substitutions of Equation (E-2) into Equation (E-1) and then collecting similar terms. Carrying out this exercise gives

$$B_p = B_v/RT \tag{E-4}$$

and

$$C_p = (C_v - B_v^2)/(RT)^2 \tag{E-5}$$

Conversion from Amagat units to the corresponding units in the volume expansion requires knowledge of the volumetric properties of the gas in question at standard conditions. Assuming that the volume of one mole of the gas is known for 0^o C and 1 atm and defining this volume as V_n, Equation (E-3) can be rewritten

$$P(V/V_n) = A_a + B_a/(V/V_n) + Ca\ (V/Vn)^2 + \ldots \tag{E-6}$$

Multiplying both sides of Equation (E-6) by V_n and rearranging slightly gives

$$PV = A_a V_n + B_a V_n^2/V + C_a V_n^3/V^2 + \ldots \tag{E-7}$$

or

$$PV = A_a V_n\ [\ 1 + (B_a/A_a)V_n/V + (C_a/A_a)V_n^2/V^2 + \ldots \tag{E-8}$$

By inspection, the relationships between the coefficients in Equation (E-8) and (E-1) are:

$$A_a V_n = RT \tag{E-9}$$

$$(B_a/A_a)V_n = B_v \tag{E-10}$$

$$(C_a/A_a)V_n^2 = C_v \tag{E-11}$$

APPENDIX F

ESTIMATED UNCERTAINTIES DUE TO SYSTEMATIC AND RANDOM ERRORS

Each of the factors affecting the uncertainty of the results of this study are analyzed in detail in this Appendix. In general, the random errors will be analyzed via maximum propagation or errors calculation. Systematic errors will, by necessity, be estimated from qualitative considerations.

Errors Associated with Pressure Determination

The uncertainty in the pressure determination is a function of the following factors:

1. Ruska dead-weight tester
2. Head corrections
3. Differential pressure indicators
4. Barometric pressure determination
5. Acceleration of gravity

Ruska Dead-Weight Tester

As mentioned earlier, two different Ruska piston gauges were used at different times during the course of the experimental work. Complete specifications are shown for both instruments in Appendix A. Since the gauges were essentially identical, the error analysis will

only be carried out for one of the gauges. The gauge used for the largest number of runs was selected for analysis. The model and serial numbers for this gauge are 2400.21 and 14203, respectively.

Each dead-weight gauge manufactured by Ruska Instrument Corporation is calibrated by intercomparison with Ruska Instrument Corporation Laboratory Master Dead-Weight Gauge No. 8965. This standard gauge has been calibrated by the National Bureau of Standards. The piston area for the master gauge is reported by the National Bureau of Standards to be correct to one part in 10,000 at 25^{o} C.

The primary purpose of the calibration, as performed by Ruska, is to determine values for the piston area at 25^{o} C, the effect of pressure on the piston area, the effect of temperature on the piston area, and the plane of reference for the instrument. For the sake of simplicity, any systematic uncertainties resulting from this calibration will be pooled in the value for the piston area at 25^{o} C. Thus, the piston area at 25^{o} C is estimated to be known within 1 part in 10,000. The resulting possible systematic error is calculated as follows:

$$P = W/A \tag{F-1}$$

where

P = pressure, psig

W = weight, lb_f

A = area, in^2

Then,

$$\frac{\partial P}{\partial A} = -W/A^2 \tag{F-2}$$

Or, to a close approximation,

$$\Delta P = \left(\frac{W}{A}\right) \frac{\Delta A}{A} = P \frac{\Delta A}{A} \qquad \text{(F-3)}$$

Inserting 0.1302097 $in.^2$ for A and 1.302×10^{-5} for ΔA gives

$$\Delta P = \pm 10^{-4} P \qquad \text{(F-4)}$$

Another possible source of systematic error is the values used for the masses of the various weights used with the dead-weight tester. The mass of each weight was calibrated by Ruska Instrument Corporation and specified not to exceed deviations from the true values by more than one milligram, 0.002%, and 0.001% for weights corresponding to pressure ranges of 0. to 0.1, 0.1 to 1.0, and 1.0 to 200 psi, respectively.

The uncertainty associated with errors associated with the various weights could be argued to be random. However, the weights were always used in a designated sequential order such that the randomness was minimized. Only the weights corresponding to approximately the last 5% of the pressure reading were ever used out of sequence. Therefore, the total uncertainty due to this factor will be split, i.e., 95% systematic and 5% random.

Breaking the calculation for pressure into three segments corresponding to the three calibaration ranges gives

$$P = \frac{W_1}{A} + \frac{W_2}{A} + \frac{W_3}{A} \qquad \text{(F-5)}$$

where

W_1 corresponds to the range 0 to 0.1 psig,

W_2 corresponds to the range 0.1 to 1.0 psig,

and W_3 corresponds to the range 1.0 to 2400 psig.

By inspection,

$$\pm\Delta P = \left| \frac{\Delta W_1}{A} \right| + \left| \frac{\Delta W_2}{A} \right| + \left| \frac{\Delta W_3}{A} \right| \qquad \text{(F-6)}$$

and, since $\Delta W_3 >> \Delta W_2 >> \Delta W_1$,

$$\Delta P \simeq \pm \Delta W_3/A \qquad \text{(F-7)}$$

or, substituting 0.001% for ΔW_3,

$$\Delta P = \pm 10^{-5} P \qquad \text{(F-8)}$$

The remaining factors that are required for a pressure determination (at the reference plane of the dead-weight tester) are the corrections for the effect of temperature and pressure on the piston area. The latter factor is a straightforward calculation and any uncertainties would be systematic, and, as mentioned earlier, this uncertainty was included in the systematic error for the total piston area. However, the temperature correction requires the experimental determination of the piston temperature and is, therefore, subject to random uncertainty. The thermometer used for this purpose was graduated in $1/2^{\circ}$ C increments. Estimating the uncertainty in the reading to be $\pm 0.1^{\circ}$ C, the following error in pressure would result.

$$P = \frac{W}{A_T} = W/[A_0(1+CX)] \qquad \text{(F-9)}$$

where

A_t = Piston area @ actual temperature

A_0 = Piston area @ 25° C

C = Thermal expansion factor, $9.1 \times 10^{-6}/^{\circ}C$

X = Piston temperature -25^{o} C

Differentiating,

$$\frac{\partial P}{\partial X} = \frac{\partial P}{\partial A_T} \frac{\partial A_T}{\partial X} = - \frac{W}{A_T^2} C A_0 \qquad \text{(F-10)}$$

or, using $A_T \simeq A_0$

$$\Delta P = \pm CP\Delta X \qquad \text{(F-11)}$$

and, with $\Delta X = 0.1^{o}$ C,

$$\Delta P = 0.91P \times 10^{-6} \qquad \text{(F-12)}$$

Summarizing the above results, the maximum systematic and random error associated with the dead-weight tester is $1.095 \times 10^{-4}P$ and $0.141 \times 10^{-5}P$, respectively.

One remaining factor must be evaluated to assure that the above results are meaningful. This factor is the sensitivity or resolution of the dead-weight tester. The reported resolution for the gauge was 5 PPM which is about an order-of-magnitude better than the maximum possible random error. During the course of the experimental phase of this work, the sensitivity of the gauge was found to be better than the indicated value as reported by the manufacturer. Mass changes of 100 milligrams were used with good success in the final adjustments to the total mass before a pressure determination was recorded. Even at the lowest experimantal pressure, say 100 psig, 100 milligrams would correspond to less than 2 PPM. Thus, the sensitivity of the gauge is compatible with the precision indicated by the maximum possible random error of $0.14 \times 10^{-5}P$.

Head Corrections

When a pressure determination is made with a dead-weight gauge, the value obtained is valid only at the reference plane of the instrument. Further, the instrument reference plane is variable due to the fact that the position of the piston in the gauge is a function of the volume of oil in the chamber below the piston. This volume can be changed with the oil pump provided for this service and also changes due to the small leakage of oil past the piston when the gauge is in operation. However, the instrument is provided with suitable marks on the weights to determine the piston location relative to a preselected datum plane. In the present work, a score on an oil manometer at a height equal to the unflexed position of the ambient DPI was selected as the datum plane. This, along with other pertinent information needed for calculation of the head corrections, is shown schematically in Figure 23.

Examining Figure 23, the value of pressure at the mid-point of the Burnett cell is

$$P - P_R - P_H \tag{F-13}$$

where

P = Pressure @ mid-point of Burnett cell, psig.

P_R = Pressure @ piston gauge reference plane, psig.

P_H = Head corrections, psig.

Expanding the head correction into the component parts gives

$$P_H = K\, g/g_c\, [h_1\rho_1+h_2\rho_2+(h_3-h_4)\rho_3-h_6\rho_4-(h_5-h_6)\rho_5] \tag{F-14}$$

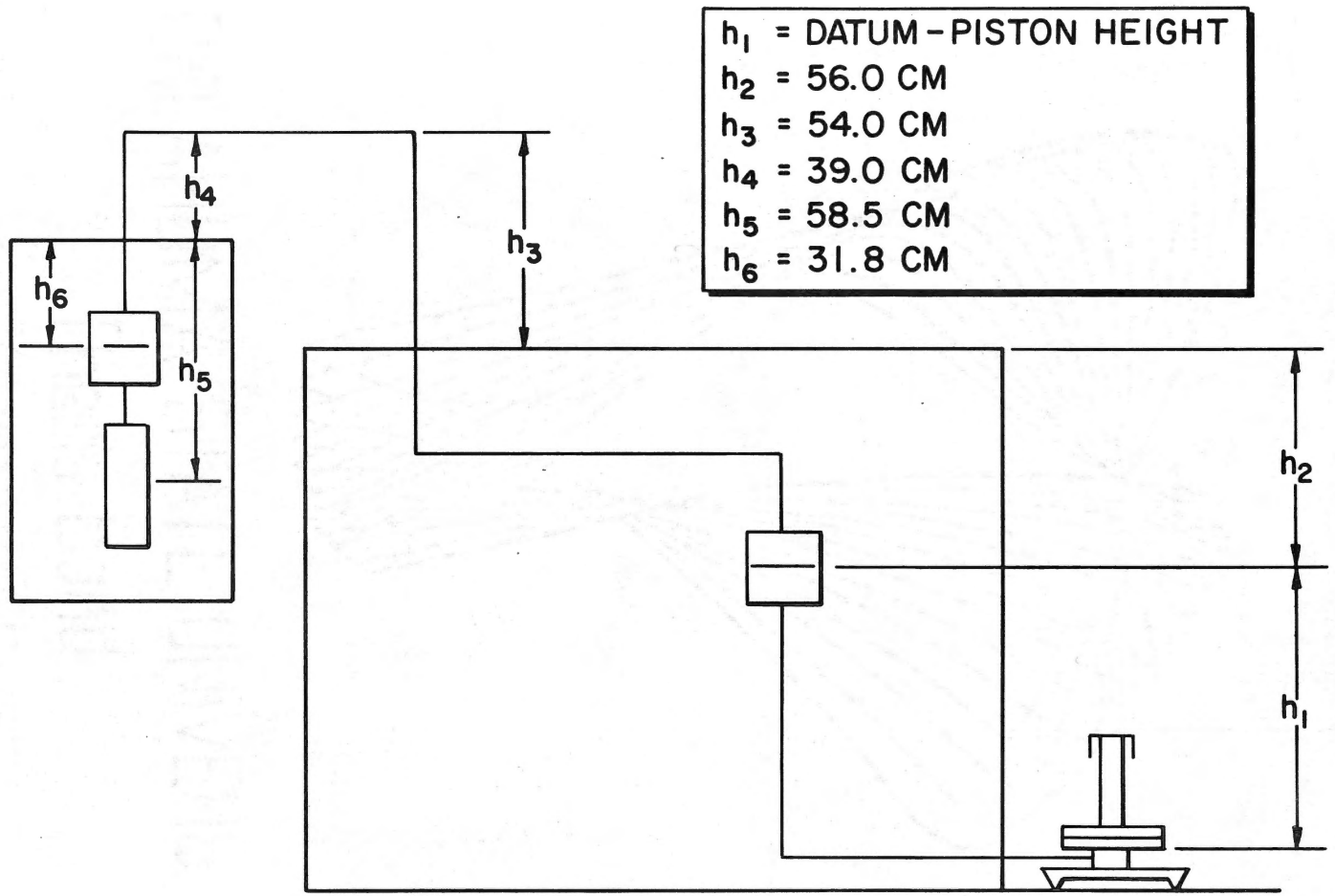

Figure 23. Schematic Representation of Equipment Heights Relative to Datum Plane

where

ρ_1 = Density of Ruska oil, @ instrument air bath temperature, lb_m/ft^3

ρ_2 = Density of helium @ instrument air bath temperature and run pressure, lb_m/ft^3

ρ_3 = Density of helium @ room temperature and run pressure, lb_m/ft^3

ρ_4 = Density of helium at run temperature and run pressure, lb_m/ft^3

ρ_5 = Density of system gas at run temperature and run pressure, lb_m/ft^3

g = Acceleration of gravity @ Stillwater, Oklahoma, ft/Sec^2

g_c = Gravitional constant, lb_m ft/lb_f Sec^2

K = Conversion factor for lb_f/ft^2 to lb_f/in^2

Examining the various items in Equation (14) reveals that the only term requiring experimental determination before its contribution can be calculated is the oil head. The vertical height of the oil head was measured with a cathetometer which, with the aid of a vernier device, could be read to the nearest 0.1 mm and estimated to within $\pm$0.02 mm. Since two readings were required for the vertical height, the random uncertainty is estimated to be approximately $\pm$0.04mm. This corresponds to a random error in pressure of $\pm$0.000478 psi.

Differential Pressure Indicators

As discussed previously, the experimental method used in this study required simultaneous balancing of two separate differential pressure indicators. The cryogenic indicator (DPI1) operated at the experimental temperature while the ambient indicator (DPI2) was housed

in an air bath which was contolled at 29 $\pm$ 1^{o} C. Obviously, the sensitivity and null shift as a function of applied pressure are prerequisites to precise pressure determinations. These parameters were reported by the manufacturer for approximately 25^{o} C. In the case of the ambient DPI, this condition was not restrictive and the parameters were used as reported. However, due to the temperature range over which the cryogenic DPI was used, these parameters were evaluated at temperatures corresponding to the three isotherms for which experimental measurements were made, i.e., -50, 0, and +50^{o} C. The details of these calibrations are reported in Appendix B.

The sensitivity of the ambient DPI, as reported by the manufacturer was 0.00001 psi. The sensitivity of the cryogenic DPI was better than 6 x 10^{-4} psi for a full scale deflection over the total pressure-temperature range of the study. This corresponds to a discernable meter deflection for a pressure difference of less than 0.00001 psi. Thus, the sensitivity of these instruments was at least an order of magnitude better than the ultimate precision attainable with the basic measurement device (Ruska piston gauge). Therefore, any uncertainty in the results due to DPI sensitivity was judged to be negligible.

The null-shift for the ambient DPI, as reported by the manufacturer-was a linear function of applied pressure. The equation for the relationship is

$$P_{LC} = P_{UC} + \Delta P \qquad \text{(F-15)}$$

and

$$\Delta P = 4.286 \times 10^{-6} P \qquad \text{(F-16)}$$

where

P_{LC} = Pressure in lower chamber of DPI,

P_{UC} = Pressure in upper chamber of DPI,

P = Applied pressure, psi

Thus, for a maximum run pressure of 2400 psi, the total correction necessary to compensate for the shift in the null point of the ambient DPI would be approximately 0.01 psi.

As mentioned earlier, the null-shift as a function of temperature and pressure was determined experimentally for the cryogenic DPI and the results of these determinations were shown in Figure 22 in Appendix B. The experimental measurements required for the null-shift calibrations were very reproducible and any uncertainty due to random errors in these measurements would be very small. However, the experimental measurements were used in conjunction with strength-of-materials calculation, and this introduces the possibility of systemati uncertainty.

As indicated in Figure 22, the largest correction due to null-shift was necessary for the $+50^{o}$ C isotherm. The null-shift as a function of pressure for the cryogenic DPI at $+50^{o}$ C can be expressed as

$$P_{LC} = P_{UC} + \Delta P \qquad \text{(F-17)}$$

and

$$\Delta P = 0.195 \times 10^{-6} P \qquad \text{(F-18)}$$

Using Equation (17), the maximum correction, for the cryogenic DPI corresponding to a run pressure of 2400 psi, would be approximately .0005 psi.

As indicated by the maximum magnitude of the correction terms, 0.01 and 0.0005 psi for the ambient DPI and the cryogneic DPI, respectively, the uncertainty due to any systematic or random uncertainty in the calibrations for these instruments would be quite small. For the purpose of estimating the uncertainty due to this factor, the calibrations were assumed to be accurate to within $\pm$ 10% of the calculated correction. This translates to a systematic uncertainty in the system pressure determinations of $\pm$0.00105 psi.

Another factor which affects the precision and accuracy of the DPI instruments is the stability of the null-point as a function of time. The DPI's were zeroed prior to the beginning of each run and the total time required to complete a run was often in excess of 24 hours. To check the possibility of a zero-shift during each run, null point of the DPI's was always evaluated as the last step in the run procedure. This evaluation was carried out by the same procedure as used to zero the DPI's prior to a run, i.e., applying equal pressures across the instrument. A very small, but decernable, zero shift was usually noted. However, occasionally the shift would be as much as 50% of full scale. Using the sensitivities of the respective instruments, 50% of full scale corresponds to a maximum combined random uncertainty of 5.5×10^{-4} psi. Thus, the total uncertainty in the pressure determination due to the differential pressure indication is estimated to be no more than $\pm$0.00105 psi systematic and $\pm$0.00055 psi random.

Barometric Pressure

In order to convert the pressure measurements taken with the Ruska piston gauge and associated instruments to absolute pressure, the gauge readings were combined with barometric pressure determination. Two methods were used to measure barometric pressure. For the majority of the experimental runs, a Texas Instrument gauge was used. The repeatability and accuracy of this instrument was as reported by the manufacturer, ± 0.015 mm Hg or $\pm 2.9 \times 10^{-4}$ psi. The remaining data were taken using a standard mercury barometer. This instrument was equipped with a vernier device which could be read quite precisely. However, the readings with this device required judging the location of the mercury meniscus as well as the level in the mercury reservoir. These were the limiting factors in the determinations. The precision of the determinations with the standard barometer is estimated to be ± 0.10 mm Hg or 1.93×10^{-3} psi.

Acceleration of Gravity

The localized value for the acceleration of gravity can be calculated from the knowledge of the latitude, longitude and height above sea level. The value, as calculated and reported by A. N. Stuckey (76) is 979.777 cm/sec^2. Combining this value with the standard acceleration value of 980.665 yields g/g_c value of 0.999094 lb_f/lb_m. The values, as calculated, are sufficiently precise to assume negligible contribution on the total uncertainty of the pressure determinations.

Combined Factors

For convenience, the factors affecting the precision and accurcay of the pressure determinations are summarized in Table LII. The values of uncertainty as reported in Table LII are the anticipated maximum errors associated with the measurements and calculations required to determine the system pressure. In all cases, the errors reported are greater than the expected, or probable, values. Combining the values in Table LII with a maximum run pressure of 2400 psia, gives a maximum uncertainty of $\pm$0.26 psi systematic and $\pm$0.0095 psi random.

Errors Associated with Temperature Determinations

The platinum resistance thermometers, resistance bridge, and galvanometer used for temperature measurement are described in detail in Appendix A. The thermometers had been calibrated by the National Bureau of Standards and were certified to reproduce the International Practical Temperature Scale within $\pm 0.01^{\circ}$ C. The accuracy and stability of the combined components of the measuring system was checked at the beginning of data acquisition on each isotherm with the use of a triple point of water cell. The triple point cell was certified by the manufacturer to reproduce the triple point of water (defined as 0.0100° C) with an accuracy of better than $\pm 0.0005^{\circ}$ C. A typical calibration of the system using the triple point cell is shown in Table LIII. A more complete description of the temperatue calibration information is given in Appendix A.

TABLE LII

MAXIMUM UNCERTAINTY IN EXPERIMENTAL PRESSURE DETERMINATIONS

Factor	Uncertainties, psi	
	Systematic	Random
Dead Weight Tester		
Piston Area	$\pm 1.0 \times 10^{-4} P$	--
Mass of Weights	$\pm 9.5 \times 10^{-6} P$	$\pm 5.0 \times 10^{-7} P$
Piston Temperature	--	$\pm 9.1 \times 10^{-7} P$
Head Corrections	--	$\pm 4.78 \times 10^{-4}$
Differential Pressure Indicators	$\pm 1.05 \times 10^{-3}$	$\pm 5.5 \times 10^{-4}$
Barometric Pressure	--	$\pm 1.93 \times 10^{-3}$
TOTAL	$\pm (1.05 + 0.1095P) \times 10^{-3}$	$\pm (2.96 + 0.00141P) \times 10^{-3}$

TABLE LIII

MEASUREMENT OF THE TRIPLE POINT OF WATER

Reading No.	N (ohms)	R (ohms)	Average Reading (ohms)
1	25.5311	25.5341	25.53260
2	25.5312	25.5340	25.53260
3	25.5311	25.5340	25.53255
4	25.5312	25.5341	25.53265
5	25.5311	25.5340	25.53255
6	25.5311	25.5340	25.53255
7	25.5311	25.5340	25.53255
8	25.5311	25.5340	25.53255
9	25.5311	25.5340	25.53255
	(20 minute wait)		
10	25.5311	25.5340	25.53255

As indicated by the reading in Table LIII, the total variation across 10 readings was 0.0001 ohms. This variation in resistance translate to approximately 0.001^{o} C. Combining the results of the triple point of water measurements with stability of temperature control observed during data acquisition, the maximum random uncertainty in the temperature measurements is estimated to be $\pm 0.002^{o}$ C.

Uncertainty in the Apparatus Volume Ratio

The apparatus volume ratio, N_j, is a function of pressure due to the effect of pressure on teh components of the Burnett cells and due to the inherent nature of the differential pressure indicator which is an integral part of the upper cell. The null point is a function of pressure. Since all pressure measurements were made at apparent null, there was actually a slight load on the diaphragm of the DPI. The effect of pressure on the apparatus volume ratio is discussed in detail in Appendix C.

For the purpose of estimating the uncertainty in the apparatus volume ratio, the effect of the previously estimated maximum uncertainty in the pressure measurements due to null shift will first be calculated. These results will then be combined with estimates of possible uncertainty due to systematic errors in the caluclations presented in Appendix C.

Null-Shift

The maximum error in pressure due to null-shift in the cryogenic DPI was 5×10^{-5} psi systematic and 3×10^{-4} psi random. The uncertainty

in the apparatus volume ratio resulting from the possible errors in pressure can be calculated by using Equation (C-11).

$$\Delta V = 0.088\pi a^6 q/Eh^3 \qquad \text{(F-19)}$$

where

ΔV = Volume change due to flexure of the diaphragm, in^3

a = Diaphragm radius = 0.95 in.

E = Modulus of elasticity = 3×10^7 psi

h = Diaphragm thickness = 0.002 in.

q = load, psi.

Since Equation (C-11) was used to calculate the correction factor to be applied to the apparatus volume ratio, the error in the calculation can be expressed as

$$\varepsilon_{\Delta V} = 0.088\pi a^6 \varepsilon_q/Eh^3 \qquad \text{(F-20)}$$

where

ε_q = Error in pressure due to null shift, psi

$\varepsilon_{\Delta V}$ = Resulting error in volume correction, in^3

Inserting the appropriate values in Equation (F-20) gives

$$\varepsilon_{\Delta V} = 0.847\varepsilon_q$$

Then, the systematic error in ΔV is approximately $\pm 4.23 \times 10^{-5}$ in^3, and the random error is approximately $\pm 2.54 \times 10^{-4}$ in^3.

Since the volume of the upper chamber of the Burnett cell was approximately 1.235 in^3 and the nominal value of the apparatus volume

ratio was 1.588, the maximum systematic error in N_j would be $\pm$0.0000544 or $\pm$0.0034%. The maximum random error in N_j is $\pm$0.000327 or $\pm$0.021%.

Calculational Errors

While the calculated correction factors as a function of pressure (as per Appendix C) were somewhat involved, the assumptions made during the development were not restrictive. Thus, the calculations are estimated to be accurate to within $\pm$5%. The largest value calculated corresponds to the maximum run pressure on the +50° C isotherm. For this case, ΔV is given by Equation (C-12a)

$$\Delta V = \left[\frac{0.088\Pi a^6}{Eh^3}\right] [-2.85+0.195P]X10^{-6} \qquad \text{(F-21)}$$

Substituting 2400 psi into Equation (F-21), along with the appropriate values for the other parameters, gives a value for ΔV of approximately $\pm 4.0 \times 10^{-4}$ in.^{3}. Taking 5% of this value as the maximum systematic uncertainty due to calculational errors yields $\pm$.00002 in^3. This corresponds to an error in N_j of $\pm$0.0000257 or $\pm$0.0016%.

Combining the above results, the maximum systematic and random uncertainty in the apparatus volume ratio is $\pm$0.0050% and 0.021%, respectively.

Errors Related to Composition

The pure component gases contained impurities of no more than a few parts per million. Thus, the results for the pure components are essentially free of composition related errors.

The composition of the helium-krypton mixtures was reported by the supplier (Air Products, Inc.). A separate composition analysis

was provided by the U. S. Bureau of Mines Helium Research Center. For the nominal compositions of 25, 50 and 75 mole % He in Kr mixtures, the analysis by Air Products, Inc. indicated values of 24.8, 49.7 and 74.6 mole % while the results from the Helium Research Center were reported as 24.4, 48.9 and 74.6 mole % He in Kr. Thus, the maximum difference via the two analyses was 0.8 mole % for nominal 50 mole % He in Kr mixture.

Since three mixtures were studied on each isotherm, three values for the interaction virial coefficient can be calculated for each isotherm. Also, a least squares analysis can be used to condense all available information into a single best estimate for the interaction virial coefficient for each isotherm. The interaction virial coefficient can be expresses as

$$B_{12} = \frac{B_m - Y_1^2 B_{11} - Y_2^2 B_{22}}{2Y_1 Y_2} \qquad \text{(F-22)}$$

where

B_{12} = Interaction second virial coefficient

B_{11} = Helium second virial coefficient

B_{22} = Krypton second virial coefficient

Y_1 = Mole fraction helium

Y_2 = Mole fraction krypton

The expression for the least squares estimate for B_{12} is

$$B_{12} = \frac{\sum_{i=1}^{3} [B^*_{mi} - Y_{1i}^2 B_{11} - Y_{2i}^2 B_{22}]}{2 \sum_{i=1}^{3} Y_{1i} Y_{2i}} \qquad \text{(F-23)}$$

where

B^*_{mi} = experimental value for the mixture virial coefficient and the subscript i denotes the three compositions.

Using the above equations, values for the interaction virial coefficient were calculated for each composition on each isotherm as well as the least squares estimate for each isotherm. The calculations were carried out separately for the two composition analyzes. The results of these calculations are shown in Table LIV.

The total sum of squares associated with the least squares estimates for the interaction virial coefficient was calculated from

$$\sum_{j=1}^{3} \sum_{i=1}^{3} (B_{mij} - B^*_{mij}) \qquad \text{(F-24)}$$

where i denotes composition, j denotes temperature, and B_m values are the calculated and experimental (superscript*) mixture viaial coefficients. Using Equation (22) the total sum of squares was 1.15 and 1.30 for the Air Products and Helium Research Center analysis, respectively. Thus, the analysis as supplied by Air Products, Inc. was judged to be preferable and the least-squares estimates for the interaction virial coefficients calculated via this analysis are reported as final results.

A cursory analysis of the results in Table LIV indicates the critical dependency of the interaction virial coefficients on the accuracy of the composition analysis. The maximum uncertainty in B_{12} due to a given uncertainty in composition can be calculated using Equation (F-22). Rewriting Equation (F-22) with $Y_2 = 1-Y_1$ gives:

TABLE LIV

CALCULATED VALUES FOR THE INTERACTION VIRIAL COEFFICIENT

Composition, mole % He in Kr		Interaction Virial Coefficient, cc/mole		
Nominal	Reported	-50°C	0°C	50°C
----------Composition Analysis per Air Products, Inc.----------				
25	24.8	19.0	22.1	24.2
50	49.7	19.2	21.6	23.1
75	74.6	20.2	21.0	22.0
Least-Squares Estimate		19.5	21.5	23.1
----------Composition Analysis per Helium Research Center----------				
25	24.4	20.8	23.4	25.1
50	48.9	21.0	22.8	23.9
75	74.6	20.2	21.0	22.0
Least-Squares Estimate		20.7	22.3	23.7

$$B_{12} = \frac{B_m - Y_1^2 B_{11} - (1-Y_1)^2 B_{22}}{2Y_1(1-Y_1)} \qquad \text{(F-25)}$$

or

$$\frac{\partial B_{12}}{\partial Y_1} = \frac{-2Y_1 B_{11} + 2(1-Y_1)B_{22}}{2Y(1-Y_1)} + \qquad \text{(F-26)}$$

$$\frac{[B_m - Y_1^2 B_{11} - (1-Y_1)^2 B_{22}][4Y_1-2]}{4Y_1^2(1-y_1)^2}$$

Using the results of this study for values for the virial coefficient, Equation (F-26) can be used to evaluate the effect of composition on the interaction virial coefficient. As would be expected, the results of the calculations show a strong dependency on the various levels of Kr in the mixtures. For the -50° C isotherm, Equation (F-26) yields numerical values of ±447, ±213 and ±121 for 25, 50 and 75% helium in krypton. Thus, an error of 0.01 mole fraction would result in an error varying from 4.5 to 1.2 cc/mole depending on the level of keypton in the mixture.

The primary factor considered in estimating the maximum uncertainty in the composition analysis for the helium-krypton mixtures was the comparison of the two separate analyzes as reported by Air Products, Inc. and the Helium Research Center. The maximum uncertainty in composition was subjectively estimated to be 50% of the difference

in the reported compositions or ± 0.001 mole fraction, whichever was greatest. Thus, for the 25, 50 and 75 nominal mole % He levels, the composition error was estimated to be ± 0.002, ± 0.004 and ± 0.001 mole fraction, respectively.

Using the $(\partial B_{12}/\partial Y)$ values calculated from Equation (F-26), the error in the interaction virial coefficient for 25, 50 and 75% He would be ± 0.89, $\pm .85$ and ± 0.12 cc/mole, respectively. This corresponds to an average of ± 0.62 cc/mole. Since the results reported for the final values of the interaction virial coefficient were the least-squares estimates using simultaneous regression of the three measurements on each isotherm, the maximum error resulting from uncertainties in composition in the reported values for the interaction virial coefficients is estimated to be no greater than ± 0.62 cc/mole.

APPENDIX G

REGRESSION ANALYSIS UTILIZING THE REDLICH-KWONG EQUATION OF STATE

In Chapter VI, the techniques used to reduce the volumetric data generated in this study were presented. Briefly, graphical regression was used for determination of starting valves for the cell constant (N_{∞}), the initial compressibility factors (Z_0), the second virial coefficient, and the third virial coefficient. The second step was to use non-linear regression to improve the starting values and also to determine approximations for higher order virial coefficients. The final step was to use these values as starting values in an improved non-linear regression technique as developed by Hall (30).

While the above methods were effective, they required a large expediture of time and computational cost (computer time). The second step was particularly tedious due to the difficulty in estimating starting guesses for the higher order virial coefficients. Subsequent to completion of the data reduction phase of the study, a method was developed to supplant the second step of the procedure. The method proposed is presented below.

The method consists of a substitution of an analytically closed equation of state in place of the virial equation of state in the non-linear regression analysis. The Redlich-Kwong (R-K) equation of state (68) was selected for this purpose. The R-K equation of

state is an empirical two-constant equation of the form

$$P = \frac{RT}{V-b} - \frac{a}{T^{1/2}\, V(V-b)} \qquad \text{(G-1)}$$

The two constants can be expressed in terms of the critical temperature (T_c) and critical pressure (P_c),

$$a = 0.4278\, R^2 T_c^{2.5}/P_c \qquad \text{(G-2)}$$

and

$$b = 0.00867 RT_c/P_c \qquad \text{(G-3)}$$

The R-K equation can be applied to multicomponent mixture by the use of the following combination rules (68):

$$\sqrt{a} = \sum_i Y_i \sqrt{a_i} \qquad \text{(G-4)}$$

$$b = \sum_i Y_i b_i \qquad \text{(G-5)}$$

Using the critical properties of helium and krypton along with the above combination rules, initial values were for the two constants were generated for the sample gases used in this work. These values were then used in starting value for the non-linear regression runs. The regression method generated optimal values (in a least-squares sense) for the two constants corresponding to each of the gas compositions.

Having established the constants for the R-K equation, approximations for the virial coefficients can be calculated by the method shown below.

Rearranging Equation (G-1)

$$\frac{PV}{RT} = Z = \frac{V}{V-b} - \frac{a}{RT^{1.5}(V-b)} \qquad \text{(G-6)}$$

or

$$Z = (V-b)^{-1}\left[V - \frac{a}{RT^{1.5}}\right] \qquad \text{(G-7)}$$

Next, the term $(V-b)^{-1}$ is expanded via the binominal formula. That is,

$$(V-b)^{-1} = V^{-1} + V^{-2}b + V^{-3}b^2 + V^{-4}b^3 + \text{---} \qquad \text{(G-8)}$$

Combining Equations (G-7) and (B-8) and collecting similar terms,

$$Z = 1 + (b-a/RT^{1.5})/V + (b^2-ab/RT^{1.5})/V^2$$

$$+ (b^3 - ab^2/RT^{1.5})/V^3 + \text{---} \qquad \text{(G-9)}$$

or, in general,

$$Z = 1 + \sum_i [(b^i - ab^{i-1}/RT^{1.5})/V^i] \qquad \text{(G-10)}$$

The various virial coefficients can be extracted from Equation (G-10) by inspection.

In Table LV selected values for the various regression parameters estimated via the above procedure are compared to the final results for the corresponding parameters. The results from the analysis using the R-K equation represent a single computer run. A cursory analysis of the results in Table LV indicates that the R-K method compares well with the final results except in one instance. The

TABLE LV

APPLICABILITY OF THE REDLICH-KWONG EQUATION OF STATE FOR REDUCTION OF BURNETT DATA

Composition	Second Virial Coefficient (cc/mol)		Third Virial Coefficient $(cc/mol)^2 \times 10^3$		Sum of Squares	
	R-K	Final	R-K	Final	R-K	Final
			-50° C			
He	11.4	11.7	0.13	0.10	2×10^{-8}	2×10^{-9}
25% Kr	--	12.1	--	0.33	--	3×10^{-10}
50% Kr	3.4	3.8	0.69	0.60	3×10^{-9}	2×10^{-9}
75% Kr	-14.8	-14.1	1.34	1.12	1×10^{-7}	1×10^{-7}
Kr	-42.5	-42.1	2.33	2.16	3×10^{-7}	3×10^{-7}
			0° C			
He	11.6	11.8	0.14	0.12	4×10^{-8}	3×10^{-8}
25% Kr	10.7	10.5	0.33	0.37	3×10^{-8}	3×10^{-8}
50% Kr	- 2.3	- 1.9	0.82	0.70	8×10^{-9}	5×10^{-9}
75% Kr	-27.1	-25.9	1.66	1.34	4×10^{-8}	6×10^{-9}
Kr	-62.6	-61.6	2.87	2.55	3×10^{-8}	1×10^{-8}
			-50° C			
He	11.7	12.0	0.14	0.13	5×10^{-8}	5×10^{-9}
25% Kr	8.6	8.3	0.33	0.38	8×10^{-7}	8×10^{-9}
50% Kr	-11.5	-11.2	1.00	0.93	2×10^{-8}	2×10^{-8}
75% Kr	-46.6	-45.4	2.21	1.83	3×10^{-6}	2×10^{-7}
Kr	-94.3	-94.1	3.85	3.42	4×10^{-6}	3×10^{-7}

R-K method did not converge for the 25% Kr in He sample at 50° C. Since the results of the R-K analysis are presented only as an example to support the applicability of the method, further attempts to generate a converged solution for this sample were not taken.

VITA

Donald Dwayne Dillard

Candidate for the Degree of

Doctor of Philosophy

Thesis: THE VOLUMETRIC PROPERTIES OF THE HELIUM-KRYPTON SYSTEM AT MODERATE TEMPERATURES AND PRESSURES

Major Field: Chemical Engineering

Biographical:

Personal Data: Born in Plainview, Texas, September 10, 1940, the son of John Wesley and Elma M. Dillard.

Education: Attended elementary school in Silverton, Texas and Gentry, Arkansas; graduated in 1959 from Gentry High School; received the Bachelor of Science degree in Chemical Engineering from the University of Arkansas, Fayetteville, in January, 1965; received the Master of Science degree in Chemical Engineering from Oklahoma State University in July, 1966; completed the requirements for the Doctor of Philosophy degree in July, 1975.

Professional Experience: Employed as a Process Engineer by Continental Oil Company during the summers of 1964 and 1965. Presently employed by Exxon Company, U.S.A. as Head, Project Development Section, Baton Rouge Refinery.